

TA7

C6

CER-68-69-41

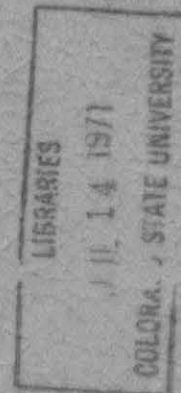
LIBRARIES
COLORADO STATE UNIVERSITY
FORT COLLINS, COLORADO

U. S. GEOLOGICAL SURVEY

TURBULENCE MEASUREMENT WITH A PROPELLER FLOW METER

By

James P. Bennett



Open-file Report

September 1968

CER68-69-JPB-41

U.S. GEOLOGICAL SURVEY

TURBULENCE MEASUREMENT WITH A PROPELLER FLOW METER

By

James P. Bennett

Open-file Report

September 1968

TABLE OF CONTENTS

<u>Chapter</u>	<u>Page</u>
LIST OF TABLES	iv
LIST OF FIGURES	v
ABSTRACT	viii
ACKNOWLEDGMENTS	x
LIST OF SYMBOLS	xi
I INTRODUCTION.	1
II TURBULENCE MEASUREMENTS IN WATER.	4
A. Hot-Film Anemometer.	4
B. Flow Visualization	6
C. Electrokinetic Transducer.	8
D. Electromagnetic Induction.	9
E. Impact Tube.	10
F. Miscellaneous Techniques	11
G. Propeller Flow Meter	11
III PROPELLER RESPONSE THEORY	14
A. Effect of Lateral Velocity Components.	14
B. Propeller Equation of Motion	15
1. Lift and Drag on a Blade.	16
2. Propeller Blade Equation of Motion.	18
C. Frequency Response of the Propeller.	21
D. Spatial Averaging.	27
IV EXPERIMENTAL EQUIPMENT AND PROCEDURES	31
A. Flow Meter and Associated Electronics.	32
B. Propeller Mean Velocity Calibration.	35
C. Determination of the System Function	35
1. Sinusoidal Excitation Experiments	36
2. Step Input Experiments.	42
3. Effect of Velocity Fluctuations on Output Mean Velocity	44

TABLE OF CONTENTS (cont'd)

<u>Chapter</u>	<u>Page</u>
D. Spectral Recovery Efficiency	47
1. The Hot-Film Anemometer	49
2. Power Spectral Density Computation.	51
3. Computation of Spectral Recovery Efficiency.	56
4. Flow Parameter Dependency of Spectral Recovery Efficiency.	57
E. Conversion of Voltage Fluctuations to Velocity Fluctuations	60
V EXPERIMENTAL RESULTS AND FIELD MEASUREMENTS.	64
A. Dynamic Behavior of the Propeller--Flow System.	64
1. Sinusoidal Excitation Experiments	65
2. Step-Input Experiments.	72
3. Effect of Velocity Fluctuations on Output Mean Velocity	74
4. Generalized System Description and Propeller Design.	78
B. Correction for Spatial Averaging	85
1. Spectral Recovery Efficiency.	86
2. Empirical Power Spectral Density Curves.	91
C. Turbulent Intensity Recovery	96
D. Field Measurements of Turbulence	97
1. Power Spectral Densities.	97
2. Turbulent Intensities	102
VI SUMMARY AND CONCLUSIONS	110
VII SUGGESTIONS FOR FURTHER RESEARCH.	115
LITERATURE CITED.	117
APPENDIX I: Tables.	123
APPENDIX II: Figures.	130

LIST OF TABLES

<u>Table</u>	<u>Page</u>
1	Important terms in the calculation of the complex natural frequency M_2 124
2	Flow parameters of spectral recovery runs 125
3	Length scales from the power spectral densities of runs 12, 16, 17, and 18. 125
4	Calculated turbulent intensity recovery ratios. . 126
5	Computation of frequency response correction for $\bar{U} = 1.68$ ft/sec, 1-3 propeller. 127
6	Energy distribution coefficients and propeller diameter-length scale ratios for figures 39 and 40 128
7	Turbulent relative intensities from a rms voltmeter, flume runs 128
8	Propeller-rms meter turbulent intensities behind a trashrack, Gavins Point Dam 129

LIST OF FIGURES

<u>Figure</u>		<u>Page</u>
1	Flow situation at a propeller blade element. . .	131
2	Flow situation at a propeller blade element with a transverse velocity of $2\pi n_0 r$ superimposed	131
3	Meter body	132
4	Propellers and meter body.	133
5	Propeller mean velocity calibration curves . . .	134
6	Schematic of the sine motion generator	135
7	Bottom view of sine motion generator	136
8	Side view of sine motion generator	136
9	Towing tank and instrument cart.	137
10	Typical sine excitation output velocity- position record	138
11	Typical step-input excitation output record. . .	139
12	Simplified flow chart of computer program for spectral recovery efficiency data analysis . . .	140
13	Example of graphical construction of $\eta(f)$	141
14	Absolute value of the system function $ H(\omega) $ as a function of angular frequency ω , 1 propeller .	142
15	Absolute value of the system function $ H(\omega) $ as a function of angular frequency ω , 1-3 propeller.	143
16	Absolute value of the system function $ H(\omega) $ as a function of angular frequency ω , 2-3 propeller.	144
17	Absolute value of the system function $ H(\omega) $ as a function of frequency ratio ω/ω_n , all propellers	145
18	Phase shift ϕ as a function of angular frequency ω , 1 propeller	146

LIST OF FIGURES (cont'd)

<u>Figure</u>	<u>Page</u>
19 Phase shift ϕ as a function of angular frequency ω , 1-3 propeller	147
20 Phase shift ϕ as a function of angular frequency ω , 2-3 propeller	148
21 Phase shift ϕ as a function of angular frequency ω , all propellers.	149
22 Natural frequency ω_n as a function of mean velocity \bar{U}	150
23 $ M_2 $ as a function of angular frequency ω	151
24 Phase shift of the complex natural frequency γ as a function of angular frequency ω , 1-3 propeller.	152
25 Response of the propeller-flow system to a step input.	153
26 D the output velocity percent deviation from true mean velocity as a function of the relative intensity v'/\bar{U}	154
27 Mean velocity misregistration function $g(\omega) = (\bar{U}/v')^2 (n_o - n_c)/n_c$ as a function of angular frequency ω	155
28 Generalized magnitude function $ M_2 /\bar{U}^{1/2}$ as a function of ω/\bar{U}	156
29 Generalized phase function $\cos\gamma$ as a function of angular frequency ω	157
30 Power spectral densities $S(f)$ and $S_{oo}(f)$ as functions of frequency f , run 12	158
31 Power spectral densities $S(f)$ and $S_{oo}(f)$ as functions of frequency f , run 16.	159
32 Power spectral densities $S(f)$ and $S_{oo}(f)$ as functions of frequency f , run 17.	160
33 Power spectral densities $S(f)$ and $S_{oo}(f)$ as functions of frequency f , run 18.	161

LIST OF FIGURES (cont'd)

<u>Figure</u>	<u>Page</u>
34	Frequency response corrected power spectral densities $S_T(f)$ as functions of frequency f . . . 162
35	Lateral scale ratio L_y/Y and eddy shape factor L_y/L_x as functions of relative depth y/Y 163
36	Spectral recovery efficiency $\eta(f)$ as a function of frequency f 164
37	Generalized empirical power spectral density $S(f)/(4L_x/\bar{U}_{loc})$ as a function of nondimensionalized frequency P 165
38	Comparison of empirical power spectral densities with experimental power spectral densities. 166
39	Propeller output and frequency response corrected power spectral densities $S(f)$ as functions of frequency f , field measurements . . 167
40	Hot-film anemometer velocity power spectral densities $S(f)$ as functions of frequency f , field measurements 168
41	Comparison of normalized power spectral densities, field measurements. 169
42	Mean velocity \bar{U} and turbulent intensity \bar{u}'/\bar{U} as functions of relative depth y/Y , Atrisco runs 170

TURBULENCE MEASUREMENT WITH A PROPELLER FLOW METER

By James P. Bennett

Abstract

There is a pressing need in much of the current Hydraulic Engineering research being conducted today for an easy, reliable, and cheap method for measuring longitudinal turbulent velocity fluctuations in water flows. Hot-film anemometers can be used in clean water flows, however, drift problems, fragileness, and expensiveness sometimes prevent their use in sediment and debris laden streams.

The propeller flow meter is a rugged, portable, relatively inexpensive flow measuring device which can be used to measure turbulence in large scale flows. It has two drawbacks when used as a turbulence measuring device, however. These are 1) inertial averaging, and 2) spatial averaging of the turbulent velocity fluctuations. These factors can be corrected for in the power spectral density of a particular turbulent flow phenomenon if the propeller system function and spectral recovery efficiency are known.

In this study, a propeller equation of motion is developed which describes the inertial averaging characteristics of propellers. A correlation function is developed which describes the spatial averaging effect on a particular propeller in a particular flow field, if the required statistical properties of the flow field are known.

Due to the complexity of the coefficients in the differential equation of motion of a propeller, experimental means were used in determining these coefficients. Similarly, the spatial averaging

characteristics had to be determined experimentally for a particular type of turbulent flow, rough boundary open channel flow.

The experimentally determined system functions were used to correct field turbulence data for inertial averaging. It appears that propellers of the size used in this study can be used in open channel flows of three feet in depth with very little correction required.

ACKNOWLEDGMENTS

This study was a part of the U.S. Geological Survey Water Resources Division research program on the mechanics and measurement of turbulence in open channel flow. This report was prepared in partial fulfillment of the requirements for the degree of Doctor of Philosophy in Civil Engineering from Colorado State University, Fort Collins, Colorado.

The writer wishes to express his thanks to his major professor, Dr. E. V. Richardson for his advice and encouragement throughout the writer's Ph. D. program. He would also like to thank his committee members Dr. J. E. Cermak, Dr. Arne Magnus, Dr. H. W. Shen, and Dr. D. B. Simons for their helpful comments on this manuscript.

Special thanks are extended to Dr. E. J. Plate for his advice and comments throughout this study. Special thanks are also extended to the National Science Foundation and the U.S. Geological Survey for the monetary support that they provided the writer during his graduate study program.

LIST OF SYMBOLS

<u>Symbol</u>	<u>Definition</u>	<u>Dimensions</u>
A	Flow meter calibration constant	L/T
B	Flow meter calibration constant	L
B_e	Equivalent filter band width	1/T
$C(v)$	Complex lift coefficient	
$C_0(\bar{U}, \omega), C_1(\bar{U}, \omega), C_2(\bar{U}, \omega), C_3(\bar{U}, \omega)$	= Coefficients modifying lift equations	
$C_D(\bar{U}, \omega)$	Drag coefficient	
D	Percent deviation of output from true mean velocity	
d	Propeller diameter	L
d_f	Degrees of freedom	
E	Digital-to-analog converter output voltage	
E_i, E_o	Complex input and output amplitudes	
e	Fluctuating component of hot-film anemometer voltage	
\bar{e}'	Root mean square hot-film anemometer voltage	
e', e'', e'''	Propeller turbulent intensity recovery ratios	
$F(\omega)$	Fourier transform of a function $f(t)$	
f	Frequency	1/T
f_c	Cutoff frequency	1/T
$g(\omega)$	Mean velocity misregistration function	
$H(\omega)$	System function	
h	Time increment between points of a discrete series	T

<u>Symbol</u>	<u>Definition</u>	<u>Dimensions</u>
$h(t)$	Unit impulse response function	
i	$\sqrt{-1}$	
K	A proportionality constant	
L, L_{\max}, L_{\min}	Strip chart recorder distances	L
L_x, L_y, L_z	Turbulent macro length scales	L
L_o	Lift due to the average angle of attack	F
L_1, L_2, L_3	Portions of the oscillatory lift	F
ℓ	Airfoil chord	L
ℓ_w	Hot-wire length	L
$M_1, M_2, M_3, M_4, M_5, M_6, M_7, M_8$	Propeller equation of motion coefficients	
m	Total number of lags	
$m(v)$	Generalized magnitude function	$(1/LT)^{\frac{1}{2}}$
N	Total number of points in a discrete time series	
n	Fluctuating component of propeller rotational frequency	1/T
n_o	Mean component of propeller rotational frequency	1/T
n_c	Propeller rotational frequency corresponding to a given towing cart speed	1/T
$n(\omega)$	Generalized phase function	
P	Nondimensionalized frequency	
p	Airfoil velocity perpendicular to mean stream	L/T
R	Total flow velocity	L/T

<u>Symbol</u>	<u>Definition</u>	<u>Dimensions</u>
R_i, R_o	Propeller blade root and tip radii	L
$R(\tau)$	Time autocorrelation	
r	Radial position on a blade	L
r_1	Sine motion generator radius	L
S	Strip chart recorder chart speed	L/T
S_a	Acceleration sensitivity	
$S(\omega)$	Power spectral density	T
s	Number of propeller blades	
T	Sampling time	T
t	Time	T
U	Total longitudinal velocity at a point	L/T
\bar{U}	Mean longitudinal velocity at a point	L/T
\bar{U}_{loc}	Mean local stream velocity	L/T
u	Fluctuating component of the longitudinal velocity	L/T
\bar{u}'	Longitudinal turbulent velocity fluctuation intensity	L/T
$u'_o(t)$	Normalized flow meter output velocity	
v	Depthwise fluctuating velocity component	L/T
\bar{v}'	Longitudinal velocity fluctuation intensity due to the sine motion generator	L/T
w	Lateral fluctuating velocity component	L/T
x	Length coordinate in the flow direction	L
Y	Mean flow depth	L
y	Length coordinate in the depthwise direction	L

<u>Symbol</u>	<u>Definition</u>	<u>Dimensions</u>
z	Length coordinate in the lateral direction	L
α	Angle of attack	
β	Pitch angle	
γ	Phase shift of the coefficient M_2	
$\delta(t)$	Unit impulse function	
$\eta(\omega)$	Spectral recovery efficiency	
θ	Angle between propeller axis and effective direction of velocity at the blade	
λ_x, λ_y	Longitudinal and depthwise microscales	L
ν	Reduced frequency of oscillation	
ρ	Mass density	M/L^3
τ	Lag time	T
ϕ	Phase shift of the system function	
ω	Angular frequency of oscillation	1/T
ω_n	Angular natural frequency	1/T

Chapter I

INTRODUCTION

Understanding of the field of open channel hydraulics has progressed a great deal since the start of this century with only the ability to measure mean flow parameters. It is now possible, for example, to predict roughly the flow regime and sediment transport of a given river or canal if the pertinent mean flow parameters are known. A point has been reached, however, where it becomes increasingly desirable to be able to measure the fluctuating components of such flow parameters as velocity and pressure. A knowledge of these quantities would aid greatly in expanding the understanding of such current open channel flow research problems as sediment transport, bed form mechanics, pollutant dispersion, and reaeration of deoxygenated streams.

In the measurement of air flows, the hot-wire anemometer is "the" accepted instrument for making turbulence measurements. This is because the hot-wire combines such desirable measuring instrument characteristics as small size, high frequency response, and stability of calibration. Unfortunately, there is no universally acceptable instrument which can be used to measure turbulence in water flows. The hot-film anemometer, an instrument quite similar to the hot-wire anemometer, shows considerable promise; however, in flows containing suspended sediment or colloidal impurities,

unstable calibration problems have been encountered. In addition, hot-film anemometer probes are extremely fragile and expensive.

Another instrument which shows considerable promise toward being useful as a turbulence measuring device, at least in large scale flows, is the propeller flow meter. Its advantages are adequate ruggedness for use in field flow situations, stability of calibration, and relative cheapness and portability of the associated instrumentation system. In addition, concurrent turbulence and mean velocity measurements can be made with propeller flow meters, a feat which cannot be accomplished with presently available hot-film anemometers. The propeller flow meter does, however, have some serious faults when it is to be used as a turbulence sensor. First, the amplitude-frequency response of most propellers is not adequate to follow the higher frequency velocity fluctuations present in open channel turbulence. Second, the dimensions of the propeller are generally large with respect to the dimensions of the fine scale of the open channel turbulence; this causes the propeller to register a spatially averaged instantaneous velocity rather than the true velocity at a point.

The main objectives of this study are: a) to evaluate the system function of propellers subjected to rapidly varying, spatially uniform velocity fields; b) to evaluate the spatial averaging characteristics of propellers in a rough boundary open channel flow; and c) to make field flow

velocity measurements with a propeller flow meter to determine the usefulness of the results of the studies of parts a and b in evaluating turbulence in a large scale open channel flow.

The system function of the propeller-flow system can be determined from the differential equation of motion of the propeller when it has been excited using a sinusoidal input, however, the flow about the propeller blades is so complex that experimental means must finally be used to obtain the system frequency response. The spatial averaging effects can be accounted for using a complex correlation function derived from the equation of motion of the propeller, however, again experimental means must be resorted to in determining a spectral recovery efficiency, because the evaluation of the correlation function involves a presently unavailable knowledge of the statistical properties of the turbulence field being measured. The system function and the spectral recovery efficiency are necessary in order to correct experimentally determined power spectral densities for propeller frequency response and spatial averaging.

Chapter II

TURBULENCE MEASUREMENT IN WATER

There are two classes of methods for making measurements in turbulent fluid flows. The first class utilizes a tracer or indicator which is injected into the flow to make portions of it visible. The second class uses some physical device which is inserted into the flow and in which an incremental change in velocity produces a measurable change in some property of the transducer.

The primary instrument for making turbulence measurements in air flows is the hot-wire anemometer. This is because the hot-wire anemometer is a small, stable device with a high frequency response. Unfortunately, because of bubble formation, electrolysis effects, dirt and lint collection, and low strength, the hot-wire anemometer cannot be used to obtain good quantitative information on water flows.

There are several measurement techniques which are used in water flows; none of which can, at present, be considered entirely satisfactory. These are discussed in the following sections.

A. Hot-Film Anemometer

The hot-film anemometer is quite similar to the hot-wire anemometer used in air flows. The sensor generates heat which is convected away by the flow, the rate of convection being proportional to the flow velocity. The

circuitry consists essentially of a self-balancing Wheatstone bridge. For work in air flows with the hot-wire anemometer, the constant current method is generally used. In water, however, the constant temperature method is used. This is because this method has high uncompensated frequency response, sensitivity to low frequency fluctuations, simpler operation, and the ability to monitor both the D.C. and A.C. levels of the fluctuations. The hot-film anemometer is probably the best instrument for use in relatively clean laboratory water flows.

The pioneering work on the hot-film anemometer was done around 1955 by Ling and Hubbard (1956). The probe consists of a 50 to 100 Angstrom coating of platinum fused to the surface of a supporting glass head form. The head form may be a cylinder, wedge, cone, or strip (for use on a flat surface). The probe is constructed in this way because it must be strong for use in water, however, if the entire probe were constructed of metal, the resistance would be too low, as would the frequency response. For use in water, the platinum is generally coated with a thin quartz film.

The early hot film probes were not coated with quartz. Researchers using these probes encountered difficulties due to dirt contamination, bubble formation on the probe from gases dissolved in the water, chemical reaction with the film, electrolysis and conductivity through the water. The addition of the quartz film has alleviated the last three problems, but the first two still cause stability problems

(Raichlen, 1967; McQuivey, 1967). The collection of dirt or gases on the probe causes a decrease in the output voltage at a constant mean velocity.

Richardson and McQuivey (1968) have overcome some of the drift problems of the hot-film anemometer by cleaning the probe before each run. Another procedure used by McQuivey was to use a pitot tube as a mean velocity transducer and to assume that drift in the voltage-velocity relationship was equivalent to a change in overheat ratio. If the mean velocity and the output voltage are both known, the effective overheat ratio can be found. If the probe has been calibrated at several overheat ratios, the turbulence intensity etc. can be determined from the correct calibration curve. The parabolic wedge probes because of their shape seem to be the most drift free for use in dirty water.

The hot-film anemometer, then, is an ideal turbulence sensing device for use in relatively clean flows. There is, however, some question of its stability in flows with considerable suspended material, and of the ability of the probe to withstand the impact of sediment particles.

B. Flow Visualization

Flow visualization techniques may be used in clear-water laboratory situations. They are most useful for obtaining Lagrangian information, and three-dimensional information can be obtained if desired. The main disadvantages of these techniques are the tediousness of data reduction and the fact that they cannot be used in turbid waters.

One flow visualization technique is the use of discrete particles which are insoluble in the flowing fluid. These particles may be injected into the fluid or circulated with it. If they are of the same density as the fluid, and small with respect to the microscale, they behave as fluid particles. The positions of the particles may be recorded with a moving picture camera, or on short-flash photographs. Hinze (1959) states that for use in fluids, emulsions have been found to yield satisfactory results. Mixtures of benzene and carbon tetrachloride or of olive oil and ethylene dibromide are especially useful, because their density can be adjusted to equal that of water (Kalinske and Pien, 1944). If the particle density is not nearly equal to that of the fluid, appropriate corrections must be made. Quantities which may be measured using this technique are: (1) Lagrangian velocities and correlations; (2) Eulerian mean and fluctuating velocity components, and (3) Eulerian velocity correlations.

A second flow visualization technique which may be used is the continuous injection of a substance miscible with the flowing fluid, but detectible in it, such as ink or fluorescent dye. In this technique, conclusions about the flow properties are made from the dispersion pattern of the injected substance downstream of the source. Quantities which can be measured using this technique are: (1) lateral Lagrangian correlation, (2) eddy diffusion coefficient, (3) the Reynolds stresses, and (4) root mean square values of

the fluctuating velocity components. It should be pointed out that there is considerable uncertainty involved in obtaining the last two quantities from the centroid and the skewness of the diffusion pattern.

There are other flow visualization techniques available; some of these are mentioned by Hinze (1959). The hydrogen bubble technique used by Kemp and Grass (1967) is particularly useful in water flows (see also Schraube et al., 1964).

C. Electrokinetic Transducer

The electrokinetic transducer consists of two electrodes mounted flush on a surface such as the wall of a pipe or the tip or sides of a pitot tube-like probe. The electrodes measure the streaming potential fluctuations which are due to the turbulent velocity fluctuations at the surface. The component sensed is the one in a plane parallel to the surface and along the line of centers of the electrodes.

Chuang and Cermak (1964) conclude that the spectral distributions of turbulent energies and shearing stress are directly proportional to the corresponding energy spectral distributions of the electrokinetic-potential fluctuation difference. This means that there should be a constant of proportionality relating the root mean square values of the potential fluctuations and the velocity fluctuations. Cermak and Baldwin report that this constant is a function of the mean approach velocity. In the work reported so far (Chuang and Cermak, 1964; Cermak and Baldwin, 1964; and

Chuang and Cermak, 1965) the proportionality constant has been determined by equating the output quantity at some point on a suitable nondimensional plot to the corresponding output quantity from some published experimental investigation in air. This inability to calibrate the electrokinetic transducer directly limits its usefulness in evaluating the turbulence levels in less well understood flows.

D. Electromagnetic Induction

Electromagnetic induction is a method of component velocity fluctuation measurement in turbulent liquid flows which is based on the induction of an electrical potential field in a conducting fluid moving relative to a stationary uniform magnetic field. The basic principle is Faraday's law of electromagnetic induction, that is, an electromotive force is generated which is perpendicular to both the instantaneous velocity component and the direction of the magnetic field. The magnitude of the electric field strength at a point is directly proportional to the magnitude of the velocity at that point. The sensor used in the flow is a pair of electrodes to measure the voltage difference between two points in the flow field. The frequency response is limited only by that of the amplifier used, and the lower limit of the size resolution is the gap between the electrodes.

Grossman et al., (1957) report on a study of turbulence in a pipe flow in which the entire flow field passed through the magnetic field. A difficulty was encountered here in

the interpretation of the voltage signal due to the fact that induced currents due to the mean velocity profile cannot be differentiated from the voltages due to the local velocity fluctuations. The size of the flow field which can be investigated in this way is, of course, limited by the size of the magnet which can be used.

A second approach which can be used is pointed out by both Grossman et al., (1957) and Hinze (1959). This is to affix small magnets to the voltage probe and immerse both in the flow. This method avoids the induced current problem, but the probes are too large to sense all but the largest scale turbulence.

E. Impact Tube

The impact tube is a sensor which samples the total head of the flow at a point. It may consist of a total head tube and capacitance transducer as used by Ippen and Raichlen (1957) or of a small piezoelectric ceramic pressure transducer installed in the tip of a total head tube as used by Eagleson and Perkins (1961). The high frequency response of these devices is adequate for water flows, as Ippen and Raichlen report a natural frequency of 240 Hz and Eagleson and Perkins a high frequency cutoff of 1150 Hz. The low frequency cutoff of Eagleson and Perkins device is 1 Hz, however, and this could be a problem in some water flows.

This type of sensor is tough enough to be used in almost any flow situation. It is, however, sensitive to

pressure fluctuations as well as to velocity fluctuations, and this limits the usefulness of the device, as does the fact that it is sensitive only to velocity fluctuation in the direction of the mean flow.

Ježdinsky et al., (1967) mention a combination of Prandtl and yaw tubes, similar to the above devices, which can discern two components of the fluctuating velocity. They claim a natural frequency of 20 Hz for this device.

F. Miscellaneous Techniques

Hot thermistor probes are used like hot film probes, but are constructed from a different type of material. The thermistor is a semi-conductor with a large resistivity and thermal coefficient of resistivity. They are rugged enough for use in water, and give good spatial resolution but as Lumley (1962) points out, their low thermal conductivity limits their usefulness.

Aksoy (1967) used the deflection of a cantilever beam with a sensor mounted at the end as an indication of longitudinal turbulent velocity fluctuations. Hartung and Csallner (1967) used the vibration of a metal strip parallel to the main stream as an indication of the magnitude of the transverse velocity fluctuations.

G. Propeller Flow Meter

There are several factors which must be considered when a propeller flow meter is to be used as a turbulence and/or mean velocity transducer. These are: (1) the

effect of the turbulence on the mean velocity registered by the meter, (2) the frequency response characteristics of the meter, and (3) the spatial averaging effect of the meter. These factors have all been studied to some extent in the currently available literature.

Plate (1967) has derived an equation of motion for a propeller-type flow meter. The equation is first order with mean-velocity and frequency dependent coefficients. Using this equation of motion, he has shown that this type meter will over-register the mean velocity when the mean velocity has a small-amplitude sinusoidal velocity fluctuation superimposed on it. This conclusion is confirmed by the work of Chaix (1962); however, for Chaix's propeller if the relative intensity is less than fifteen percent, the over-registration is less than one percent. Chaix has also done some work on the effect of vertical oscillations on the output of current meter. He found that the effect was variable depending on the meter type, some over-register and some under-register. Here again, the effect is negligible if the intensity is less than fifteen percent.

Jepson (1964) has developed an equation of motion similar to Plate's. When applied to a step function input, this equation predicts that the natural frequency (in the sense of a first order equation) will be directly proportional to the step height (the final velocity). He gives experimental evidence to indicate that this is true. Iwasa (1967) accounts for the frequency response of the propeller by

defining an averaging time which is due to propeller inertia. This averaging time is considered to be the amount of time over which the propeller averages the instantaneous input velocity to yield a "propeller averaged" output velocity. He states that a propeller may be used to measure turbulent velocity intensities as long as the ratio of this averaging time to the Eulerian time scale is less than 0.1.

Schuyf (1966) deduces the spatial averaging effect of a propeller in grid turbulence by comparing the spectra from water with those from a similar grid turbulence in air. He says that the averaging effect will be negligible for this type of turbulence when the ratio of the longitudinal macro-scale to the propeller diameter is greater than 3.5. This figure may be somewhat in error, however, because the natural frequency of the propeller used by Schuyf was probably lower than he thought, and the effect of this is present in the spectrum. Ishihara and Yokosi (1967) recognize that spatial averaging can be a problem by stating that it is meaningless to record fluctuations with frequencies greater than the ratio of the mean velocity to the diameter of the sensor.

Probably one of the earliest attempts to analyze open channel flow turbulence with a flow meter was made by Kalinske (1943) using a Price meter in the Mississippi River. One of the most recent was by Tiffany (1967), again using a Price meter in the Mississippi.

Chapter III

PROPELLER RESPONSE THEORY

The response of a flow meter propeller to longitudinal velocity fluctuations is determined by its inertia and spatial averaging effect. The inertia effect is a function of propeller geometry, mean velocity, and the frequency of the fluctuations. The inertia effect can be compensated for to obtain the input from the measured output if the response of the propeller to small amplitude, sinusoidal velocity fluctuations is known. The spatial averaging effect is a function of the propeller geometry and the structure of the turbulence. In order to obtain the input from the measured output, it can be compensated for by using an experimentally determined efficiency factor for the particular type of turbulence present.

A. Effect of Lateral Velocity Components

As in hot-wire or hot-film anemometry (McQuivey, 1967), the effect of the velocity fluctuations perpendicular to the axis of the propeller can be shown by an order of magnitude analysis. The instantaneous total flow velocity is

$$R = \sqrt{(\bar{U} + u)^2 + v^2 + w^2}$$

where $(\bar{U} + u)$ is the total velocity in the flow direction (\bar{U} the average velocity and u the fluctuating component), v is the fluctuating component in the depthwise direction,

and w is the fluctuating component in the lateral direction. Expanding and dividing by \bar{U} ,

$$\left(\frac{R}{\bar{U}}\right)^2 = 1 + 2 \frac{u}{\bar{U}} + \left(\frac{v}{\bar{U}}\right)^2 + \left(\frac{w}{\bar{U}}\right)^2 .$$

Since the values of u/\bar{U} , v/\bar{U} , and w/\bar{U} are seldom greater than .1, the values of the squared terms are one order of magnitude smaller than the u/\bar{U} term, and the total velocity may be approximated by

$$R = \sqrt{\bar{U}^2 + 2u\bar{U}} .$$

Thus, the sensitivity of the propeller to lateral velocity fluctuations is one order of magnitude less than its sensitivity to longitudinal velocity fluctuations.

B. Propeller Equation of Motion

The two basic methods available for the analysis of a propeller are the momentum theory and the blade element theory. Glauert (1963) points out that the momentum theory is concerned mainly with the motion of the fluid, and that the forces acting on the propeller are those necessary to impart this motion to the fluid. The propeller is treated as an actuator disc, and no information is obtained about the forces on the individual blades.

The blade element theory considers the forces experienced by the individual blades as they move through the fluid. The forces experienced by the blade elements are computed using standard airfoil theory.

The blade element theory is used here to write an equation of motion for a propeller turning in a time-varying flow. Non-stationary airfoil theory as developed by von Karman and Sears (1938) and simplified by Sears (1941) has been used to determine the lift on a blade element. The torque produced by the lift and drag on a blade has been equated to the inertial torque of the propeller to give an equation of motion.

1. Lift and Drag on a Blade

The lift on an airfoil in arbitrary motion can be divided into four parts. The first, L_0 , is due to the average angle of attack as in uniform motion. The other three as given by von Karman and Sears (1938) are:

- a. The apparent mass lift, L_1 ;
- b. The quasi-steady lift, L_2 ;
- c. The lift due to the vorticity in the wake, L_3 .

If the motion of the airfoil is sinusoidal, Sears (1941) has expressed the latter three as

$$L_1 = \frac{\pi}{4} \rho \ell^2 \frac{dp}{dt} \quad (3-1)$$

$$L_2 = \pi \rho \ell R p \quad (3-2)$$

$$L_3 = -[L_2 1 - C(v)] \quad (3-3)$$

where ρ is the mass density of the fluid, ℓ is the chord of the airfoil, p is the velocity of the blade perpendicular to the flow velocity R , $C(v)$ is a complex function of v the reduced frequency of oscillation $\omega \ell / 2R$, which contains a

phase shift between the vertical velocity p and the lift, and ω is the angular frequency of the wing oscillations. The lift due to the average angle of attack may be written

$$L_0 = \pi \rho R^2 \ell \alpha \quad (3-4)$$

where α is the angle of attack (α must be small).

The assumptions made in the derivation of equations 3-1 through 3-3 are: (a) the fluid is incompressible and non-viscous, (b) the flow is two-dimensional, (c) the amplitude of the sinusoidal airfoil oscillations is small enough that the wake can be considered to be flat, and (d) the Kutta condition applies. When the non-stationary lift equations are applied to a propeller blade, these conditions are not met because: (a) the fluid is viscous, (b) the blades are of low aspect ratio, and therefore the flow is not two-dimensional, (c) the wake is not flat, but spiral, and furthermore the wake from one blade can cause interference velocities at the one following, changing the lift on it. Because of these conditions, each of the terms of the lift equation for a propeller blade is modified by multiplying by a coefficient which is assumed to be a function of \bar{U} and ω .

The equation for the lift on a blade at a radial position r is

$$dL = \pi \rho \ell \left\{ C_0(\bar{U}, \omega) R^2 \alpha + C_1(\bar{U}, \omega) \frac{\ell}{4} \frac{dp}{dt} + C_2(\bar{U}, \omega) R p \left[1 - C_3(\bar{U}, \omega) \{ 1 - C(v) \} \right] \right\} dr \quad (3-5)$$

where $C_0(\bar{U}, \omega)$, $C_1(\bar{U}, \omega)$, $C_2(\bar{U}, \omega)$, and $C_3(\bar{U}, \omega)$ are the modifying coefficients for the corresponding lift equations 3-1 through 3-4.

The drag on the blade element at r is

$$dD = \rho R^2 \ell C_D(\bar{U}, \omega) dr, \quad (3-6)$$

where $C_D(\bar{U}, \omega)$ is a mean-velocity and frequency dependent drag coefficient.

2. Propeller Blade Equation of Motion

A radial element of a flow meter propeller blade may be treated as a flat plate subject to mean and fluctuating flow velocity components parallel to the propeller axis, and a mean and a fluctuating motion perpendicular to the axis. Figure 1 shows this situation from outside the flow field while Figure 2 shows the flow situation with a velocity of $(-2\pi n_o r)$ superimposed perpendicular to the axis, where n_o is the rotational speed of the propeller corresponding to a mean velocity \bar{U} .

The effective instantaneous velocity at an angle θ to \bar{U} is

$$R = \bar{U}/\cos\theta + u \cos\theta + 2\pi nr \sin\theta \quad (3-7)$$

where

$$\theta = \tan^{-1} \frac{2\pi n_o r}{\bar{U}} \quad (3-8)$$

The effective instantaneous velocity of the plate perpendicular to R is

$$p = - (2\pi nr \cos\theta - u \sin\theta) \quad (3-9)$$

(p is positive downward).

The torque on the propeller is balanced by its inertial torque, thus the equation of motion of the propeller may be written

$$2\pi\rho_m J \frac{dn}{dt} = s \int_{R_i}^{R_o} r(dL \cos\theta - dD \sin\theta) \quad (3-10)$$

where ρ_m is the mass density of the propeller, J is its polar moment of inertia, s is the number of blades, and R_i and R_o are respectively root and tip blade radii.

Using equations 3-5, 3-6, 3-7, 3-9, and the fact that $\alpha = (\beta - \theta)$, where β is the blade pitch angle, equation 3-10 becomes

$$\frac{dm}{dt} + M_2 m - M_3 m^2 + M u' m = M_5 (u')^2 + M_6 u' + M_7 \frac{du'}{dt} + M_8 \quad (3-11)$$

where

$$m = \frac{n - n_o}{n_o} \quad (3-12)$$

$$u' = u/\bar{U} \quad (3-13)$$

$$\rho' = \frac{\rho_m}{\rho} \quad (3-14)$$

$$M_1 = \frac{1}{n_o \bar{U}^2} \left\{ 2\rho' J + \frac{sC_1\pi}{2} \int_{R_i}^{R_o} (\ell r \cos\theta)^2 dr \right\} \quad (3-15)$$

$$M_2 = \frac{2\pi s}{\bar{U} M_1 n_o} \int_{R_i}^{R_o} \ell r^2 \cos\theta \{ C_2 [1 - C_3(1-C)] + \frac{2C_D}{\pi} \tan^2\theta - 2C_0(\beta - \theta) \tan\theta \} dr \quad (3-16)$$

$$M_3 = \frac{4\pi^2 s}{\bar{U}^2 M_1} \int_{R_i}^{R_o} \ell r^3 \sin\theta \{ C_2 [1 - C_3(1-C)] \cos^2\theta - \frac{C_D}{\pi} \sin^2\theta + C_0(\beta-\theta) \sin\theta \cos\theta \} dr \quad (3-17)$$

$$M_4 = \frac{2\pi s}{\bar{U} n_o M_1} \int_{R_i}^{R_o} \ell r^2 \cos\theta \{ C_2 [1 - C_3(1-C)] \cos^2\theta - 2 \sin\theta [C_0(\beta-\theta) \cos\theta - \frac{C_D}{\pi} \sin\theta] \} dr \quad (3-18)$$

$$M_5 = \frac{s}{n_o^2 M_1} \int_{R_i}^{R_o} \ell r \cos^2\theta \{ C_2(\beta-\theta) \cos\theta \frac{C_D}{\pi} \sin\theta + C_2 [1 - C_3(1-C)] \sin\theta \} dr \quad (3-19)$$

$$M_6 = \frac{s}{n_o^2 M_1} \int_{R_i}^{R_o} \ell r \{ C_0(\beta-\theta) \cos\theta - \frac{C_D}{\pi} \sin\theta + C_2 [1 - C_3(1-C)] \sin\theta \} dr \quad (3-20)$$

$$M_7 = \frac{s}{n_o^2 \bar{U} M_1} \int_{R_i}^{R_o} C_1 \frac{\ell^2 r}{4} \sin\theta \cos\theta dr \quad (3-21)$$

$$M_8 = \frac{s}{n_o^2 M_1 \bar{U}} \int_{R_i}^{R_o} \frac{\ell r}{\cos\theta} \{ C_0(\beta-\theta) - \frac{C_D}{\pi} \tan\theta \} dr. \quad (3-22)$$

In equations 3-15 through 3-22 the coefficients C , C_0 , C_1 , C_2 , C_3 , and C_D are equal to those with the same subscripts in equations 3-5 and 3-6, with the \bar{U} and ω dependency understood. Thus, the coefficients M_1 through M_8 are functions of \bar{U} and ω , as well as being functions of propeller geometry and density.

If the quantities R_0 and $1/n_o$ are of the same order of magnitude, the coefficients M_3 , M_4 , and M_5 will be of the

same order of magnitude as M_2 and M_6 , and if u' and m are small with respect to one, the terms containing m^2 , $(u')^2$, and $u'm$ may be dropped from the equation of motion. If this is done, equation 3-11 becomes

$$\frac{dm}{dt} + M_2 m = M_6 u' + M_7 \frac{du'}{dt} + M_8 \quad (3-23)$$

Equation 3-23 is a linear first order differential equation with the modifying parameters being functions of mean velocity and the frequency of the velocity fluctuations. The propeller and its associated flow pattern may be thought of as a linear system being excited by a sinusoidally varying input quantity. The coefficient M_8 must be identically zero, because when $u'=0$, $n=n_0$ and $m=0$, which in equation 3-23 yields $M_8=0$. The coefficient M_7 in the second term on the right of equation 3-23 represents the acceleration sensitivity of the propeller as discussed by Schuyf (1966). Equations of motion of the same type as 3-23 were found by Plate (1967) and Jepson (1964).

C. Frequency Response of the Propeller

As was pointed out in section B, the propeller and its associated flow system may be thought of as a linear system. The response of a linear system to a time varying signal is determined by its system function or frequency response function $H(\omega)$. As is demonstrated in the following section, the frequency response function can be determined analytically if the differential equation of the system is known. The response function may be determined experimentally by

exciting the system with a sinusoidal input and measuring the output amplitude and phase shift.

The unit impulse function is defined by Bracewell (1965) as:

$$\begin{aligned} \delta(t) &= 0 \quad t \neq 0 \\ \int_{-\infty}^{\infty} \delta(t) dt &= 1 \end{aligned} \quad (3-24)$$

The response of a linear system at time t to a unit impulse occurring at $t = 0$ is the unit impulse response function, $h(t)$.

Following Lee (1960), the sinusoidal input and output of a linear system may be written respectively $\text{Re} \left[E_i e^{i\omega t} \right]$ and $\text{Re} \left[E_o e^{i\omega t} \right]$ where E_i and E_o are the complex input and output amplitudes respectively, $i = \sqrt{-1}$, and Re signifies the real component of the quantity in brackets. The system function is then defined as

$$H(\omega) = \frac{E_o}{E_i} \quad (3-25)$$

so that $\text{Re} \left[E_o e^{i\omega t} \right] = \text{Re} \left[H(\omega) E_i e^{i\omega t} \right]$. Lee shows (p. 329) that $H(\omega)$ is the Fourier transform of $h(t)$,

$$H(\omega) = \int_{-\infty}^{\infty} h(t) e^{-i\omega t} dt. \quad (3-26)$$

The derivative theorem for Fourier transformation (Bracewell, 1965) states that the Fourier transform of the derivative of a function is the product of $i\omega$ and the Fourier transform of the function itself, that is

$$\int_{-\infty}^{\infty} f'(t)e^{-i\omega t} dt = i\omega F(\omega) \quad (3-27)$$

where

$$\int_{-\infty}^{\infty} f(t)e^{-i\omega t} dt = F(\omega) \quad (3-28)$$

Using the above definitions and equations 3-26 and 3-27, the system function for the system described by equation 3-23 can be found quite easily. If the driving function u' in equation 3-23 is the unit impulse $\delta(t)$, then m is the unit impulse response function $h(t)$ and equation 3-23 becomes

$$\frac{dh}{dt} + M_2 h = M_6 \delta + M_7 \frac{d\delta}{dt} \quad (3-29)$$

If both sides of equation 3-29 are Fourier transformed, equation 3-30 results.

$$\int_{-\infty}^{\infty} \frac{dh}{dt} e^{-i\omega t} dt + \int_{-\infty}^{\infty} M_2 h e^{-i\omega t} dt = \int_{-\infty}^{\infty} M_6 \delta e^{-i\omega t} dt + \int_{-\infty}^{\infty} M_7 \frac{d\delta}{dt} e^{-i\omega t} dt \quad (3-30)$$

Since M_2 , M_6 , and M_7 are functions only of \bar{U} and ω , they may be taken outside the integral, and using equation 3-26 and 3-27, equation 3-30 becomes

$$i\omega H(\omega) + M_2 H(\omega) = M_6 + i\omega M_7 \quad (3-31)$$

or

$$H(\omega) = \frac{M_6 + iM_7\omega}{M_2 + i\omega} \quad (3-32)$$

In equations 3-16 and 3-20, the quantities $C_0(\beta-\theta)$ and C_D/π will be small with respect to the quantity $C_2 [1-C_3(1-C)]$. Ignoring the former two quantities and noting from figure 2 that $\tan\theta = 2\pi r n_0 / \bar{U} \doteq \pi r / 15B$, it is seen that $M_2 = M_6$. M_2 is complex because it contains the coefficient $C(v)$; it may be written

$$M_2 = |M_2| (\cos\gamma + i \sin\gamma) \quad (3-33)$$

where γ is the phase shift and $|M_2|$ the magnitude of the coefficient M_2 . Using equation 3-33 and rationalizing the denominator, equation 3-32 becomes

$$H(\omega) = \frac{1 + \frac{\omega}{|M_2|} (1+M_7) \sin\gamma + M_7 \left(\frac{\omega}{|M_2|}\right)^2 + i \frac{\omega}{|M_2|} (M_7-1) \cos\gamma}{\cos^2\gamma + \left(\sin\gamma + \frac{\omega}{|M_2|}\right)^2} \quad (3-34)$$

It is often more convenient to have the system function divided into its magnitude and phase components. In this case, equation 3-34 becomes

$$H(\omega) = |H(\omega)| e^{i\phi} \quad (3-35)$$

where $|H(\omega)|$ is the absolute value of the system function and ϕ is its phase shift. From equation 3-34 it is seen that

$$M = \left\{ \left(\frac{\omega}{|M_2|}\right)^4 M_7^2 + \left(\frac{\omega}{|M_2|}\right)^3 2M_7(1+M_7) \sin\gamma + \left(\frac{\omega}{|M_2|}\right)^2 \left[(1+M_7)^2 + 2(\sin^2\gamma - \cos^2\gamma)M_7 \right] + \left(\frac{\omega}{|M_2|}\right)^2 (1+M_7) \sin\gamma + 1 \right\}^{\frac{1}{2}}$$

$$|H(\omega)| = M / \left\{ \cos^2\gamma + \left(\sin\gamma + \frac{\omega}{|M_2|}\right)^2 \right\}$$

and

$$\phi = \tan^{-1} \frac{\frac{\omega}{|M_2|} (M_7 - 1) \cos \gamma}{1 + \frac{\omega}{|M_2|} (1 + M_7) \sin \gamma + \left(\frac{\omega}{|M_2|}\right)^2 M_7} \quad (3-36)$$

If $M_7 = 0$ and $\gamma = 0$, equations 3-36 reduce to

$$|H(\omega)| = 1/\sqrt{1 + (\omega/\omega_n)^2} \quad \text{and} \quad \phi = \tan^{-1} \omega/\omega_n \quad (3-36a)$$

Equations 3-36a give the system function of an ordinary first order system in which $M_2 = |M_2| = \omega_n$ is real. ω_n is defined as the natural frequency of the first order system; it is the angular frequency at which the amplitude ratio has decreased to 0.707.

If $M_7 = 0$ but $\gamma \neq 0$, equations 3-36 become

$$|H(\omega)| = 1/\sqrt{\cos^2 \gamma + (\sin \gamma + \omega/|M_2|)^2} \quad \text{and} \quad (3-36b)$$

$$\phi = \tan^{-1} \frac{-\frac{\omega}{|M_2|} \cos \gamma}{1 + \frac{\omega}{|M_2|} \sin \gamma}$$

and if $\gamma = 0$ but $M_7 \neq 0$, they become

$$|H(\omega)| = \sqrt{\frac{1 + (M_7 \frac{\omega}{|M_2|})^2}{1 + (\frac{\omega}{|M_2|})^2}} \quad \text{and}$$

and

$$\phi = \tan^{-1} \frac{-\frac{\omega}{|M_2|}}{1 + M_7 (\frac{\omega}{|M_2|})} \quad (3-36c)$$

From equation 3-36c it is seen that if the coefficient M_7 dominates the behavior of the system, the amplitude ratio $|H(\omega)|$ becomes constant for $\omega/|M_2|$ large, while from 3-36b, if the coefficient $|M_2|$ dominates, the amplitude

ratio decreases with the first power of $\omega/|M_2|$, for large values of this parameter.

Although the differential equation of the system was derived for sinusoidally varying input velocities, the system equation can be used to evaluate the response of the propeller to turbulent velocity fluctuations. This is because turbulence can be thought of as consisting of the linear combination of an infinite number of sinusoidal velocity fluctuations of infinitesimal amplitude, each varying in angular frequency from its neighbor by $d\omega$. This is the standard Fourier integral spectral analysis approach to the study of turbulence. The system equation can be used to compute the input spectrum from the output spectrum, since as shown by Lee (1960),

$$S_{oo}(\omega) = |H(\omega)|^2 S_{ii}(\omega) \quad (3-37)$$

where $S_{oo}(\omega)$ is the spectrum of the output of the system and $S_{ii}(\omega)$ is the spectrum of the input. Implicit in equation 3-37 is the assumption that the velocity fluctuations are uniform over the entire width and length of the propeller. The effects of deviations from this assumption are discussed in the next section.

In summary, equation 3-34 is the system equation of a flow meter propeller and its associated flow. The importance of the coefficients M_2 and M_7 in the system function can be determined by examining the high frequency asymptote of the absolute value of the system function $|H(\omega)|$. The

system function must be determined experimentally, due to the deviations of the actual flow conditions from those assumed in the lift equations (3-1 through 3-4). Finally, the output spectrum can be corrected for the frequency response of the propeller if its system equation is known, and if the velocity fluctuations are uniform over the width and length of the propeller.

D. Spatial Averaging

Equation 3-23 was derived under the assumption that u' was uniform over the length and width of the propeller blade. In turbulent flow this is not the case, and the system responds to a "propeller averaged velocity". The velocity weighting function can be derived from equation 3-20.

Using a propeller averaged excitation u'_1 , and assuming acceleration sensitivity negligible, equation 3-23 becomes

$$\frac{dm}{dt} + M_2 m = u'_1 \quad (\omega > 0) \quad (3-38)$$

where from equation 3-20

$$u'_1 = \frac{1}{n_o^2 M_1} \sum_{i=1}^s \int_{R_i}^{R_o} \left[\int_{\ell/2}^{\ell/2} u' dx \right] r G(\bar{U}, \omega, r) dr. \quad (3-39)$$

In equation 3-39,

$$G(\bar{U}, \omega, r) = C_2 [1 - C_3 (1 - C)] \sin \theta \quad (3-40)$$

and the r dependency is indicated because θ may be found for a given r and \bar{U} from the mean velocity calibration curve of the propeller.

Because the output spectrum is quite easily corrected for the frequency response of the propeller (through equation 3-37), and because the spectrum of axial velocity fluctuations is of great interest in the analysis of turbulence, the possibility of correcting the spectrum for the spatial averaging effect of the propeller is investigated in this section.

The time autocorrelation of the propeller averaged velocity is

$$R_{11}(\tau) = \lim_{T \rightarrow \infty} \frac{1}{2T} \int_{-T}^T u_1'(t) u_1'(t+\tau) dt \quad (3-41)$$

where T is the sampling time.

Using equation 3-39, equation 3-41 becomes

$$R_{11}(\tau) = \frac{1}{(n_o^2 M_1)^2} \sum_{k=1}^s \sum_{j=1}^s \int_{r_1=R_i}^{R_o} \int_{r_2=R_i}^{R_o} \int_{x_1=-\frac{\ell}{2}}^{\ell/2} \int_{x_2=-\frac{\ell}{2}}^{\ell/2} R_{kj}(x_1, x_2, r_1, r_2, \tau) r_1 r_2 G(\bar{U}, \omega, r_1) G(\bar{U}, \omega, r_2) dr_1 dr_2 \quad (3-42)$$

where

$$R_{kj}(x_1, x_2, r_1, r_2, \tau) = \lim_{T \rightarrow \infty} \frac{1}{2T} \int_{-T}^T u_k'(x_1, r_1, t) u_j'(x_2, r_2, t+\tau) dt. \quad (3-43)$$

R_{kj} is the autocorrelation between the point velocities at the point (x_1, r_1) on the k th blade and the point (x_2, r_2) on the j th blade. The value of R_{kj} for $x_1=x_2$ and $r_1=r_2=0$ for any two blades is the true autocorrelation of the point velocities at the propeller axis. With the present state of knowledge of turbulence, it is impossible to write a general expression for R_{kj} .

The spectrum of the propeller averaged velocity $S_{11}(\omega)$ is obtained by Fourier transforming $R_{11}(\tau)$,

$$S_{11}(\omega) = \int_{-\infty}^{\infty} R_{11}(\tau) e^{-i\omega\tau} d\tau. \quad (3-44)$$

Using equation 3-42, equation 3-44 becomes

$$S_{11}(\omega) = \frac{1}{n_0^2 M_1} = \sum_{k=1}^S \sum_{j=1}^S \int_{r_1=R_i}^{R_0} \int_{r_2=R_i}^{R_0} \int_{x_1=-\ell/2}^{\ell/2} \int_{x_2=-\ell/2}^{\ell/2} S_{kj}(x_1, x_2, r_1, r_2, \omega) r_1 r_2 G(\bar{U}, \omega, r_1) G(\bar{U}, \omega, r_2) dr_1 dr_2 \quad (3-45)$$

where

$$S_{kj}(x_1, x_2, r_1, r_2, \omega) = \int_{-\infty}^{\infty} R_{kj}(x_1, x_2, r_1, r_2, \tau) e^{-i\omega\tau} d\tau. \quad (3-46)$$

S_{kj} is the spectrum of the point velocities at the points (x_1, r_1) and (x_2, r_2) on the k th and j th blades, respectively. The value of S_{kj} for $x_1=x_2$ and $r_1=r_2=0$ for any two blades is the point spectrum of the axial velocity fluctuations at the propeller axis. Since it is the transform of R_{kj} , it is impossible at the present time to obtain a general expression for S_{kj} .

Expression 3-45 may be written

$$S_{11}(\omega) = \eta_1(\omega) S(\omega) \quad (3-47)$$

where $S(\omega)$ is the point spectrum of the axial velocity fluctuations at the propeller axis and

$$\eta_1(\omega) = \frac{1}{(n_{O_2} M_1)^2} \sum_{k=1}^S \sum_{j=1}^S \int_{r_1=R_i}^{R_O} \int_{r_2=R_i}^{R_O} \int_{x_1=-\ell/2}^{\ell/2} \int_{x_2=-\ell/2}^{\ell/2} \frac{S_{kj}(x_1, x_2, r_1, r_2, \omega)}{S_{kj}(0, 0, 0, 0, \omega)} r_1 r_2 G(\bar{U}, \omega, r) G(\bar{U}, \omega, r_2) dr_1 dr_2. \quad (3-48)$$

A spectral recovery efficiency $\eta(\omega)$ may be defined as

$$\eta(\omega) = \eta_1(\omega) |M_6|^2. \quad (3-49)$$

$\eta(\omega)$ may be obtained experimentally for a particular propeller and turbulent flow field from comparison of the propeller averaged spectrum to the spectrum of a probe which is small enough to have negligible spatial averaging problems, such as a hot film anemometer.

Using equations 3-49 and 3-47, equation 3-37 becomes (because $|H(\omega)|^2$ contains the factor $|M_6|$ in the numerator)

$$S_{OO}(\omega) = |H(\omega)|^2 \eta(\omega) S(\omega) \quad (3-50)$$

or

$$S(\omega) = S_{OO}(\omega) |H(\omega)|^{-2} \eta^{-1}(\omega) \quad (3-51)$$

Equation 3-51 is the means by which the point spectrum can be recovered from the output spectrum of a propeller meter. Both $|H(\omega)|$ and $\eta(\omega)$ will have to be determined experimentally, the former due to imperfect knowledge of the flow field near three-dimensional airfoils with spiral wakes, and the latter because of incomplete knowledge of the space-time correlation of the axial velocity fluctuations.

Chapter IV

EXPERIMENTAL EQUIPMENT AND PROCEDURES

The goals of the experimental portion of this study are: a) to evaluate the system function $H(\omega)$ for three axial flow meter propellers, b) to determine the spectral recovery efficiency $\eta(\omega)$ for several open-channel flow situations, for the same propellers, and c) to use the results of a and b to evaluate the turbulence in open channel flows in the field.

The propellers were mounted on a special meter body which produced thirty pulses per revolution. The pulses were converted to an analog signal which could be recorded either on magnetic tape or on a strip chart. The system function was determined by axially oscillating the propeller, with a known angular frequency and amplitude, while towing it through still water. The output signal was recorded on a strip chart so the amplitude ratio and phase shift could be determined. The spectral recovery efficiency was determined by dividing the system-function-corrected output spectrum by a hot-film anemometer spectrum for the same open channel flow. Evaluation of $\eta(\omega)$ as a function of the ratio of the longitudinal macroscale to propeller diameter and an energy distribution parameter was attempted.

A. The Flow Meter and Associated Electronics

The propellers used were standard Ott Minor propellers, numbers 1, 1-3, and 2-3. The dimensions of the propellers are:

No.	Diameter (in)	Pitch (in)
1	1.97	1.97
1-3	1.18	1.97
2-3	1.18	3.94

Pitch, here, indicates the advance of the propeller per revolution. The 1 propeller is a component propeller which senses only the component of the flow velocity parallel to the axis of the propeller, up to an angle of deviation of 30° of the total velocity vector from the direction of the propeller axis.

The meter body was constructed for the U.S. Geological Survey by the Colorado State University Engineering Research Center machine shop. It consists of a propeller mounting shaft which rides in two stainless steel bearings, a thirty-toothed gear fixed to the shaft, and an electrode mounted in the case directly above the gear, see figure 3. Figure 4 shows the propellers and the meter body disassembled. In operation, the meter case is filled with water, and as the shaft turns changes in resistance are produced between the probe and the gear as the teeth move by the probe. This produces thirty pulses per revolution of the shaft. The resistance changes between electrode and gear amplitude-modulate a twenty kHz carrier signal produced by a Mimosa

apparatus which is manufactured by Waterloopkundig Laboratorium, Delft, Holland (Waterloopkundig Laboratorium, undated). The Mimosa converts the amplitude modulated signal into a square wave with the frequency at which the teeth of the gear pass the electrode. The amplitude frequency response of the Mimosa is determined by the time constant of the differentiating circuit which is 10^{-4} sec. This provides an amplitude-frequency response curve which is flat well beyond the range of concern of the propeller amplitude-frequency response so that no correction is required for the Mimosa amplitude-frequency response.

For all of the work described herein, except the step-velocity experiments, the signal from the Mimosa was fed to a Hewlett-Packard 5212A counter (Hewlett-Packard, 1963). The counter has a frequency response range of 2 Hz to 300 k Hz and the display time is variable down to one millisecond. The counter was operated in the one-period sampled mode. The response of the output of the counter to changes in frequency in this mode of operation is limited by the period length (one to six milliseconds, depending on velocity) and the display time (approximately two milliseconds). For this work, the longest time constant would be about eight milliseconds. This is adequate uncompensated frequency response for use with the propellers of this study. The two parts per million error in the 100 k Hz crystal standard contributes a measurement error of about \pm one percent for the one-period mode, and for the frequencies encountered in this study.

When the counter was used, it was used in combination with a Hewlett-Packard 580A digital-to-analog converter (Hewlett-Packard, 1964), so the counter output could be recorded on a strip chart or magnetic tape recorder. The time constant of the 580A is 1 millisecond, and the accuracy is 0.5% of full scale or better.

The strip chart recorder used was a Brush Mark 280. It has a full scale response flat to thirty-five Hz, chart speeds to 200 mm per sec, and a system accuracy of 0.5% of full scale (Brush Instruments, undated). The strip chart recorder was used in the portion of this study in which the system function was determined, and in the step velocity experiments.

The magnetic tape recorder used in the spatial averaging portion of this study was a Consolidated Electrodynamics Corp. PR-3300. The tape transport speed used was 30 ips. The frequency response at this speed is flat from D.C. to five kHz, the accuracy is ± 0.5 db, and the full scale signal to noise ratio is 46 db (Consolidated Electrodynamics Corp., undated). The analog root mean square voltage meter used in this portion of the study was the Disa 55D35. The frequency response of this meter is flat above 2.5 Hz, and down 3 db at 0.5 Hz.

In the step input experiments, the counter and digital to analog converter could not be used due to erratic behavior at zero frequency (infinite period). In this phase of the study, the analog signal was obtained using a

Hewlett-Packard 500B electronic frequency meter. The 500B has a time constant of five milliseconds, which provides adequate frequency response for the propellers of this study, accuracy is $\pm 2\%$ of full scale (Hewlett-Packard, 1955).

B. Flow Meter Mean Velocity Calibration

The propellers and U.S. Geological Survey meter body were calibrated to determine the relation between output frequency in Hz and mean flow velocity by towing them through still water. The curves obtained in this fashion for the three propellers are shown in figure 5. The stability of the instrument is shown by the points obtained from towing tests performed after the experiments described here.

C. Determination of the System Function

In the case where the coefficient M_2 of the first order differential equation 3-23 is frequency dependent, it is necessary to investigate both the amplitude ratio $|H(\omega)|$ and the phase shift ϕ to completely describe the system function. This can be done by comparing the system output to its input when the excitation function is sinusoidal. The sinusoidal excitation used in this study was produced by oscillating the flow meter sinusoidally as it was towed through still water. Prior to the towing experiments, an attempt was made to perform similar experiments in which the sine motion generator was clamped to the walls of a flume and the flow meter was oscillated in an oncoming flow. This type of experimentation proved unsuccessful due

to the impossibility of distinguishing the low frequency velocity fluctuations produced by the sine motion generator from the turbulent velocity fluctuations of the flume flow.

When M_2 of equation 3-23 is frequency independent, the system function can be completely determined by evaluating the response of the propeller to a step input in velocity. Experiments of this nature have been performed to compare natural frequencies determined in this way to those obtained from the sinusoidal excitation experiments.

A problem related to the determination of the system function is the problem of determining mean velocity in the presence of turbulence. The possibility that a propeller flow meter over-registers the mean flow velocity in flows of high turbulent intensity was checked by comparing the output velocity of a propeller meter to the velocity of a towing cart while the meter was being towed and oscillated at a known frequency and radius.

1. Sinusoidal Excitation Experiments

To investigate the system function of a propeller, a flow field must be produced which varies sinusoidally yet is instantaneously the same over the entire length and width of the propeller. This type of flow field is difficult to produce in water, so the sinusoidal excitation of the propeller was produced by oscillating the flow meter as it was towed through still water. This is an extension of the usual flow meter calibration technique of towing the flow meter at a known constant velocity through still

water. That this procedure is justified can be shown from an examination of the basic ideal fluid equations from which the differential equation of the system was derived.

The equations for the lift on a propeller blade were derived assuming frictionless, irrotational, incompressible flow. The equations which must be satisfied for this type of flow are (Sears, 1960):

$$\nabla^2 \theta = 0 \quad (4-1)$$

$$\frac{\partial \theta}{\partial t} + \frac{1}{2} q^2 + \frac{p}{\rho} + v = p_{\infty} \quad (4-2)$$

where θ is the velocity potential, q is the magnitude of the velocity vector, p the pressure, ρ the fluid density, and v the body force potential.

The flow situations which must be considered are: a) the velocity of the flow past a propeller which rotates but does not translate varies sinusoidally about some mean value, and b) the propeller moves through the stationary fluid with some mean velocity about which it oscillates sinusoidally.

For these two cases the boundary conditions on θ at the body surface are identical, therefore, from equation 4-1 the flow patterns are identical. The instantaneous lift on the propeller is the integral over its surface of the pressure term on the left of equation 4-2. Since the flow patterns are the same, the only difference in the p/ρ terms of the two cases must come from p_{∞} . Since p_{∞} is a constant with respect to integration over the propeller

surface, it drops out of the solution for the lift on the propeller, and the lift on a propeller blade is the same in both cases. Thus the towing procedure is justified.

The sine motion generator consists of a circular disc tapped to receive a pin at radii variable from 0.109 to 2.000 inches. The pin drives a slotted yoke which is attached to the flow meter support rod. The disc is rotated by a shaft driven by a variable speed DC motor. As the disc rotates, the pin drives the yoke and meter support rod longitudinally in pure sinusoidal motion. The lateral motion of the pin is lost in the slot in the yoke. The sine motion generator is illustrated schematically in figure 6, figure 7 shows the bottom of the disc and yoke, and figure 8 shows a side view of the entire generator.

The displacement x of the sine motion generator pin in the direction along the meter support rod may be expressed as

$$x = r_1 \sin \omega t \quad (4-3)$$

where r_1 is the radius of the center of the pin as measured from the center of the disc, ω is the angular velocity of the disc, and t is time. The velocity v of the meter support rod relative to axes tied to the sine motion generator is then

$$v = \omega r_1 \cos \omega t, \quad (4-4)$$

and the amplitude of the velocity fluctuation produced by the generator is $2\omega r_1$.

From an examination of equations 3-15 and 3-16, it is seen that the coefficient M_2 can be expected to be highly mean velocity dependent. If the ratio

$$\frac{2\pi s \int_{R_i}^{R_o} r^2 \{ \cos\theta C_2 (1-C_3 (1-C)) + \frac{2C_D}{\pi} \tan^2\theta - 2C_o (\beta-\theta) \tan\theta \} dr}{\{ 2p' J + \frac{sC_1\pi}{2} \int_{R_i}^{R_o} (lr \cos\theta)^2 dr \}} \quad (4-5)$$

is insensitive to mean velocity, M_2 will be directly proportional to mean velocity.

If the coefficient M_2 is real, it is called the natural frequency of the propeller. Jepson (1964) predicts from an equation of motion similar to 3-23 that the natural frequency of a propeller will be directly proportional to the mean velocity. He uses the results of Higson (1964) to show that this is indeed the case. Higson used step-velocity experiments similar to those described later in this chapter. Because of the expected mean velocity dependency of the natural frequency of a propeller, system functions were evaluated at four different mean velocities for each of the three propellers used in this study.

Corresponding to the usual definition of the turbulent intensity \bar{u}' as the root mean square of the turbulent velocity deviations from the mean velocity, a velocity fluctuation intensity \bar{v}' , due to the sine motion generator, may be defined as the root mean square of v in equation 4-4, or

$$\bar{v}' = \omega r_1 / \sqrt{2} \quad . \quad (4-6)$$

At large \bar{v}' to mean velocity ratios, the propeller blades can be expected to approach a condition of zero lift, or stall. In this case, the lift equations used in the derivation of chapter three are no longer applicable. When this happens, it might be expected that the measured system function would become, at least in part, a function of the intensity. To evaluate the effect of velocity fluctuation intensity on the measured system function, system functions were measured for three or four sine motion generator radii for each propeller and mean velocity investigated.

The system function was determined for a particular mean velocity and sine motion generator radius by towing the flow meter through still water at that mean velocity while at the same time oscillating it with the sine motion generator at several known angular frequencies ω . As shown in figure 9, the towing tank was Colorado State University's 200 foot long by eight foot wide by four foot deep flume. The towing vehicle was the electrically powered instrument carriage of this flume.

As the flow meter was towed, the signal from it was demodulated by the Mimosa apparatus. The demodulated signal was fed to the Hewlett-Packard digital-to-analog converter, and then to the Brush strip chart recorder. An analog velocity trace was, thus, recorded on one channel of the Brush recorder. The position of the flow meter was recorded on the other channel by recording a voltage pulse produced by a photocell and pulse generator. The photocell was activated when the drive shaft of the sine motion generator

was at one particular point in each revolution. Due to space limitations, the tapped pin holes at the various radii were located in different angular positions on the sine motion generator disc. Since the disc was fixed to the shaft, the position trace generation point was different for each sine motion generator radius used. For this reason, the pulse generation point was referenced to full forward position of the generator for each radius used in this study. The location of the position trace with respect to the full forward position was determined by calibration. The calibration procedure involved simultaneously recording (on the Brush recorder) the position trace and a voltage which was controlled by a microswitch which was on only when the generator was at the full forward position. From this recording, the phase angle between the position trace and the full forward position of the generator was easily found. Figure 10 is a typical velocity-position record. The asymmetry of the velocity trace is due to the fact that the quantity recorded is inversely proportional to the flow meter frequency of revolution, while the velocity is directly proportional to this frequency.

When the system function is written as in equation 3-35, the absolute value of the system function $|H(\omega)|$ is the amplitude ratio, the ratio of the magnitude of the amplitude of the output of the system to the magnitude of the input amplitude. In this case, the amplitude ratio is the ratio of the difference between the maximum and minimum recorded

velocities to $2\omega r_1$, the input velocity amplitude. The maximum and minimum recorded velocities are determined from the recorded trace by means of the mean-velocity calibration curve of the propeller being used.

The phase shift ϕ of equation 3-35 is determined from the relative time positions (lengthwise dimension on the strip chart) of the maximum and minimum output velocity traces and the flow meter position trace. The time positions of the actual occurrence of the maximum and minimum velocities can be related to the position of the pulse trace (meter position trace) if the location of the sine motion generator pin at pulse generation and the direction of rotation of the generator are known. The phase shift ϕ in radian is 2π times the ratio of the time deviation of the occurrence of the maximum (or minimum) velocity trace in the output from the actual time of occurrence of the maximum (or minimum) velocity in the input, to the amount of time required for one revolution of the generator.

The system function $H(\omega)$ is completely determined when the values of the amplitude ratio and phase shift are known for all ω 's in the range of interest.

2. Step-Input Experiments

Equation 3-23 describes a first order system in which M_2 can be complex. If M_2 is complex in a linear equation such as 3-23, knowledge of both amplitude response and phase shift is required to describe the system response function, however, if M_2 is real and constant, knowledge of only one parameter is required.

If M_2 is a constant at a given mean velocity, equation 3-23 may be written

$$\frac{dn}{dt} + \omega_n n = u', \quad (4-7)$$

if the acceleration sensitivity is assumed to be negligible, where

$$M_2(\omega) = \text{constant} = \omega_n. \quad (4-8)$$

If u' in equation 4-7 is a step function such that

$$\frac{dn}{dt} + \omega_n n = \begin{cases} 0 & \text{for } t < 0 \\ a & \text{for } t \geq 0 \end{cases} \quad (4-9)$$

the solution to 4-7 is

$$n = (1 - e^{-\omega_n t}) n_f \quad (4-10)$$

where n_f is the equilibrium value of n corresponding to a step input of height a . Equation 4-10 may also be written

$$\frac{n_f - n}{n_f} = e^{-\omega_n t}. \quad (4-11)$$

From 4-11 it is clear that ω_n is simply the reciprocal of the time elapsed between the application of the step function and the arrival of the meter output frequency n at a value such that $(n_f - n)/n_f = e^{-1} = 0.368$.

It was expected that M_2 would be experimentally discovered to be complex, however, since it is much easier to perform step input experiments than sine function excitation experiments, it was hoped that it would be found that the complex component of M_2 would be small so that the behavior would be essentially that of a first order constant parameter system. In such a case, $M_2 \doteq |M_2| \doteq \omega_n$ and the behavior of

the system for a sinusoidal input could be described by equations 3-35 and 3-36a with ω_n determined from step input experiments. For this reason, step-velocity-input experiments were also performed on the propellers for which complete system functions were available from sinusoidal excitation experiments.

The step velocity experiments were performed with the flow meter mounted on the towing cart as described in the previous section. The step inputs were produced by holding the propeller immobile with a slender rod until the towing cart had reached a uniform speed, then instantaneously releasing the propeller. This procedure effectively produced a step input with a height equal to the velocity of the towing cart. Due to the erratic behavior of the digital to analog converter at very large periods (very low frequencies), a Hewlett-Packard 500B frequency meter was used to produce an analog voltage output proportional to the frequency of revolution of the flow meter. This output frequency trace was recorded on the Brush strip chart recorder. The natural frequency was determined as described above by measuring the amount of time required for $(n_f - n)/n_f$ to reach a value of 0.368. A typical step velocity output record is shown in figure 11.

3. Effect of Velocity Fluctuations on Output Mean Velocity

A problem closely related to the one of recovering information about the structure of turbulence from the flow meter output is the one of recovering the true mean velocity

from this output in the presence of a turbulent flow field. It is well known that a pitot tube registers a higher velocity than the true mean in an intensely turbulent flow field (Goldstein, 1965, p. 253). It is reasonable to believe that a similar phenomenon occurs when a propeller flow meter is used to measure the velocity of such a flow.

There has been considerable discussion in Civil Engineering literature of the incorrect registration of the mean velocity by flow meters in turbulent flows. As early as 1913, Groat reported on the relationship between flow velocity measurements made with cup and screw (propeller) type flow meters and pitot tube velocity measurements in a power-house tail race. He reported an average of 6% over-registration by a cup meter and 1% under-registration by a screw meter; the maximum over-registration of the cup meter was 25% and the maximum under-registration of the screw meter was 4%. Carter and Anderson (1963) report considerably smaller differences between discharge measurements made with the same two types of meters on the Mississippi River at Vicksburg. They conclude that the Price (cup) current meter is not noticeably affected by naturally occurring stream turbulence.

Two recent French publications show that there is an over-registration of the mean velocity by propeller type flow meters in high intensity turbulent flows. In the first, Castex and Carvounas (1962) report discharges measured at various distances behind a grid with 0.13 ft square bars

spaced 0.33 ft on centers. The grid was located in an open channel flow about 13 ft wide and 13 ft deep. An over-registration as high as 13.6% was reported. In the second publication, Chaix (1962) reports that he generated his fluctuating velocities by oscillating a meter in an oncoming flow. In this fashion he generated effective turbulent intensities as high as 40%. According to his results, the over-registration is less than 1% for intensities as high as 20%. At intensities of 35 to 40%, the over-registration is 5 to 6% depending on the flow meter being tested.

An analytical evaluation of the effect that the fluctuating axial velocity components have on the reported mean velocity of a propeller flow meter has been presented by Plate (1967). He developed an equation of motion similar to the one developed in chapter three of this paper and solved it for a small amplitude sinusoidal velocity fluctuation. His results indicate that a propeller flow meter should over-register by an amount proportional to the square of the ratio of the amplitude of the velocity fluctuation to the mean velocity.

Tests of the type reported by Chaix (1962) were made on two of the propellers used in this study. The equipment was the same as in section one, except that the counter was set to manual count mode. To determine the deviation of the reported mean velocity from the true mean velocity, at a particular intensity of velocity fluctuations, the total number of revolutions of the propeller was obtained

in two situations. In the first, the number of revolutions in 100 ft was obtained as the meter was towed at a given mean velocity but without oscillation. In the second, the number of revolutions in the same distance and at the same mean velocity was obtained with the meter oscillating axially at a known frequency and radius. The difference between the number of propeller revolutions in the two cases was taken as an indication of the deviation of the indicated mean velocity from the true mean velocity for the intensity corresponding to the known frequency and radius. Two mean velocities were checked at three different radii and for ω 's running to sixteen Hz for each of the two propellers.

D. Spectral Recovery Efficiency

Recalling the discussion in section D of chapter three, it is impossible to obtain an analytical expression for the spectral recovery efficiency $\eta(\omega)$. There are two reasons for this. First, the present state of knowledge of the turbulent flow field is not sufficient to predict the values of the autocorrelation of the longitudinal velocity fluctuations at the various points on the propeller blades. (Indeed, one component of this function is what it is desired to measure.) Second, even if this autocorrelation were available, the flow field in the vicinity of the propeller blades is not well enough understood so that one could obtain the lift and drag coefficients necessary to compute the spatially averaged autocorrelation. $\eta(\omega)$ can be obtained, however, for a particular flow field and

propeller by dividing the system function-corrected ordinates of a power spectrum of the propeller angular velocity fluctuations by the ordinates of a power spectrum of the same flow field obtained from a point velocity sensor.

That is, from equation 3-50

$$\eta(\omega) = \frac{S_{oo}(\omega)}{|H(\omega)|^2 S(\omega)} \quad (4-12)$$

Such an approach was used in this study, wherein the point velocity sensor was a hot film anemometer. The hot-film anemometer may be treated as a point when its dimensions are considered relative to those of the significant scale parameters of the turbulence and relative to the dimensions of a propeller. If the low frequency portion of the spectrum of the propeller fluctuations is unaffected by spatial averaging, then it is possible to fit an empirical spectrum function to this low frequency portion and extend it to the higher frequency portion thus avoiding the use of $\eta(\omega)$ curves. This approach was also used, but again, its validity must be judged on the basis of a comparison of the power spectra so obtained with corresponding ones from the hot film anemometer. In a particular type of turbulent flow, the spectral recovery efficiency would be expected to be a function of the ratio of propeller diameter and/or length to one or more of the standard length scales of the turbulence, as well as a function of the angular frequency of fluctuations ω . The flow in which the spectral recovery efficiency was investigated was a large scale rough boundary

open channel flow. The propellers used were the three for which system function information was obtained. They are described in section A.

1. The Hot-Film Anemometer

The standard which was used to produce the spectra of turbulence for the computation of the spectral recovery efficiency was the hot-film anemometer. There has been considerable use of the hot-film anemometer recently as a tool for the evaluation of turbulence in water flows, see for example, Richardson and McQuivey (1968), McQuivey (1967), Raichlen (1967), and Dell'Osso (1966). The general advantages and disadvantages of the use of the hot-film anemometer in turbulent water flows are discussed in section A of chapter two.

The hot-film probe used was a Thermo-Systems parabolic wedge with an equivalent diameter of .004" and a length of .04". The self balancing bridge was the Thermo Systems model 1050 Anemometer Module. It was used in conjunction with a Thermo Systems 1051-6 Monitor and Power Supply Module and a 1057 Signal Conditioner Module. The frequency response range of the anemometer module is DC to 80 k Hz and the output noise level corresponds to a 0.05% equivalent turbulent intensity. The output of the anemometer was recorded on the CEC PR-3300.

Because the diameter of a hot-wire sensor is small in comparison with its length, the only dimension of the wire which must be considered when evaluating the spatial

averaging effect of the sensor is its length. Frenkiel (1954) showed that a hot-wire behaves as a point velocity sensor for measuring turbulent intensities if the quantity $(l_w/\lambda_y)^2$ is small, where l_w is the wire length and λ_y is the lateral microscale of the longitudinal velocity fluctuations. This argument can be extended to the hot-film probes used in this study. If local isotropy is assumed, λ_y can be inferred from the measured power spectrum from

$$\frac{1}{\lambda_x^2} = \frac{4\pi^2}{\bar{U}^2} \int_0^{\infty} f^2 S(f) df \quad (4-13)$$

and

$$\lambda_x = \sqrt{2} \lambda_y, \quad (4-14)$$

where λ_x is the longitudinal microscale of the longitudinal velocity fluctuations, $S(f)$ is the normalized power spectrum, and f is frequency in Hz. It will be shown in chapter five that $(l_w/\lambda_y)^2 \ll 1$ for all cases considered, therefore, the assumption that the hot-film probe is a point velocity sensor is justified in the cases cited here.

The quartz-coated hot-film probes have adequate frequency response for use in measuring turbulence in water. The manufacturer claims a frequency response to 70 k Hz for the probes described above. Richardson et al. (1967) showed that the turbulent intensities measured in air by a 0.002 inch diameter hot-film were the same as those measured with a 0.0002 in hot-wire; while the intensities measured with a 0.006 in film were only five to ten percent low. The equivalent diameter of the probes used here was 0.004 inches,

and the frequencies encountered in water are lower than those in air, therefore, the frequency response of the probes used is considered adequate.

The drift problem mentioned in chapter two, section A, was solved here using the techniques of Richardson and McQuivey (1968).

2. Power Spectral Density Computation

Digital techniques were used in this study for computation of the power spectral densities of the velocity fluctuations of both the propellers and the hot-film anemometer. This was done for two reasons; first, digital techniques make it possible to obtain reliable power spectral densities at much lower frequencies than with the available analog techniques. Second, digital techniques permit the transformation of the recorded voltage fluctuations into velocity fluctuations before the computation of the power spectral density whereas analog techniques do not.

When using the propeller output data, intermediate computations were necessary before the power spectral densities could be computed, due to the form in which the raw data was received from the digital-to-analog converter. Because the counter was operated in single-period-sampled mode (section C-1 of this chapter), the output voltage from the digital-to-analog converter was inversely proportional to velocity. Before the power spectral density of the velocity fluctuations could be computed, this voltage had to be converted to a velocity using the mean velocity calibration curve of

the propeller. That is, the preliminary computation required was

$$U = A + \frac{B}{KE}, \quad (4-15)$$

where A and B are the calibration constants of the propeller, E is the output voltage of the digital-to-analog converter, and K is the proportionality constant between E and the period of the flow meter pulses.

The analysis of the autocorrelation and power spectral density (power spectrum) of the Eulerian velocity time series provides much of the background of the turbulence literature of today. The autocorrelation of the time series of output velocities from a flow meter may be written

$$R_{OO}(\tau) = \lim_{T \rightarrow \infty} \frac{1}{2T} \int_{-T}^T u'_O(t) u'_O(t+\tau) dt, \quad (4-16)$$

where $u'_O(t) = (u_O(t) - \bar{U}) / \sqrt{u'^2}$ and τ is the lag time. The power spectrum of this series $S_{OO}(\omega)$ is the Fourier transform of $R_{OO}(\tau)$, that is

$$S_{OO}(\omega) = \int_{-\infty}^{\infty} e^{-i\omega\tau} R_{OO}(\tau) d\tau. \quad (4-17)$$

The one sided physically realizable power spectrum function written in terms of frequency in Hz, f , is written

$$S_{OO}(f) = 4 \int_0^{\infty} R_{OO}(\tau) \cos 2\pi f\tau d\tau, 0 < f < \infty. \quad (4-18)$$

The discrete data equivalent of R_{OO} in equation 4-16 is \hat{R}_{OO} where

$$\hat{R}_{OO}(rh) = \frac{1}{N-r} \sum_{n=1}^{N-r} u'_O(nh) u'_O((n+r)h), r=0,1,2,\dots,m, \quad (4-19)$$

where N is the total number of points in the time series, r is the lag number, m is the maximum number of lags, and h is the time increment between the points in the series. The discrete equivalent of equation 4-18 then becomes

$$\begin{aligned} \hat{S}_{OO} \left(\frac{kf_c}{m} \right) = 2h \left[\hat{R}_{OO}(0) + 2 \sum_{r=1}^{m-1} \hat{R}_{OO}(rh) \cos \left(\frac{\pi rk}{m} \right) + \right. \\ \left. (-1)^k \hat{R}_{OO}(mh) \right], \end{aligned} \quad (4-20)$$

where f_c is the cutoff frequency and $k = 0, 1, 2, \dots, m$.

(Bendat and Piersol (1966), p. 292). \hat{S}_{OO} is a raw spectral estimate, it should be smoothed by a procedure called Hanning (Bendat and Piersol, p. 293)

$$\begin{aligned} \hat{S}_{OO}(0) &= 0.5 \hat{S}_{OO}(0) + 0.5 \hat{S}_{OO} \left(\frac{f_c}{m} \right) \\ \hat{S}_{OO} \left(\frac{kf_c}{m} \right) &= 0.25 \hat{S}_{OO} \left(\frac{k-1}{m} f_c \right) + 0.5 \hat{S}_{OO} \left(\frac{kf_c}{m} \right) + \\ &0.25 \hat{S}_{OO} \left(\frac{k+1}{m} f_c \right) \quad k=0, 1, 2, \dots, m \\ \hat{S}_{OO}(f_c) &= 0.5 \hat{S}_{OO} \left(\frac{m-1}{m} f_c \right) + 0.5 \hat{S}_{OO}(f_c) \end{aligned} \quad (4-21)$$

where \hat{S}_{OO} is called the smoothed spectral estimate, or the spectrum. Once $\hat{S}_{OO}(f)$, $|H(f)|$ and $S(f)$ are known, $\eta(f)$ may be computed using equation 4-12. In this study, $S(f)$ has been taken to be the power spectrum of the velocity fluctuations as obtained from the hot-film anemometer.

The values selected for the parameters, N , m , and H of equations 4-19 through 4-21 are based on a compromise

between the desired degrees of resolution and accuracy of the estimate of the spectral density function and the length of record which can be processed economically on the available computer, and on a cutoff frequency f_c selected through trial and error, or previous knowledge of the highest frequency in the process. Once f_c has been selected, the time increment between sample points is determined by the requirement that to analyze a periodic function one must have at least two samples per cycle of the highest frequency component, that is

$$h = \frac{1}{2f_c} . \quad (4-22)$$

The resolution of the estimate is determined by the equivalent band width B_e of the digital filter, where

$$B_e = \frac{1}{\tau_{\max}} = \frac{1}{mh} . \quad (4-23)$$

The accuracy of the estimate is determined by the number of degrees of freedom d_f of the chi-square of the power spectral density, at a chosen confidence level. It is customary to assume that in the interval $\Delta f = B_e$ the power spectrum is the same as that for a band width limited with noise. In this case,

$$d_f = 2B_e T , \quad (4-24)$$

where T is the length of record, and

$$T = Nh . \quad (4-25)$$

Now d_f controls the accuracy of the estimate, B_e the resolution, and T is controlled by economic factors or computer

storage limitations, and since they are related through equation 4-24, it is seen that a compromise must be reached in their selection. References which give a guide to the selection of these factors are Roesner and Yevdjovich (1966), or Bendat and Piersol (1966). As an example, for a confidence level of 90 percent and $d_f = 20$, the true value of the power spectral density can be between 0.54 and 1.57 times the computed value.

The equipment used for conversion of the angular velocity of the propeller into an analog voltage signal is described in section A of this chapter. In addition, an AC amplifier with a gain of 100 and a low frequency cutoff of one Hz was necessary to bring the output voltage of the digital-to-analog converter up to a level which could be recorded by the magnetic tape recorder. The output signal from the hot film anemometer was recorded directly on the CEC PR-3300.

For the digital data processing, the recorded analog signals were converted to digital magnetic tape recordings using the Analog to Digital Data Conversion System ZA-31340 produced for the National Bureau of Standards of Boulder, Colorado by Electronic Engineering Company of California. The primary components of this system are the EECO 8-1024 SI Magnetic Core Memory and the EECO 760-10 BS Analog to Digital converter. The data were stored on the digital magnetic tape at six bits per digit, in blocks of 540 digits, using a format compatible with the Control Data

Corporation 6400 computer belonging to Colorado State University. The voltages were read from the analog data tapes to three significant figures, thus the CDC 6400 was programmed to extract 180 data words from each block of digital data information on the digital data tape.

The data were analyzed on the CDC 6400 computer. In processing the flow meter data, the program consisted mainly of four parts: 1) reading and unpacking the digital data tape, 2) conversion of voltages to velocities, 3) standardizing, and 4) computation of the autocorrelation and power spectral density functions. The hot-film anemometer data processing procedure omitted step number two. The subroutine for the computation of the power spectral density was built around equations 4-19 through 4-21. Figure 12 shows a simplified flow chart of the program used.

3. Computation of Spectral Recovery Efficiency

Once $\hat{S}_{oo}(f)$, $\hat{S}(f)$, and $|H(f)|$ have been obtained, $\eta(f)$ can be obtained through equation 4-12. The approach which most clearly illustrates the distortion of the spectrum due to the spatial averaging is the one in which the ordinates of $\hat{S}_{oo}(f)$ are multiplied by $|H(f)|^{-2}$ and then divided by $\hat{S}(f)$. On logarithmically scaled paper, this is a simple addition-subtraction procedure, see figure 13 for an example.

Another approach to obtaining a close approximation to the point velocity spectrum from the spatially averaged spectrum which has been corrected for the system function is one in which an empirical spectrum function is fit to a

portion of the spatially averaged spectrum which is relatively unaffected by this spatial averaging. This procedure must, of course, be justified by comparison of the spectra so obtained with point velocity spectra. An inspection of the hot-film anemometer spectra obtained in this study shows the $-5/3$ slope fairly well established over the range of interest here. This indicates that one should fit a spectrum function of the type suggested by von Karman (1948)

$$S(f) = \frac{4L_x/U_{loc}}{(1 + (2.546\pi \frac{L_x}{\bar{U}_{loc}})^2)^{5/6}} \quad (4-26)$$

where \bar{U}_{loc} is the local mean stream velocity and L_x is the macro length scale in the flow direction. The macroscale, formally defined using Taylor's analogy, is

$$L_x = \bar{U}_{loc} \int_0^{\infty} R(\tau) d\tau \quad (4-27)$$

however it is more easily obtained from the $f = 0$ ordinate of equations of the type of 4-26 (Raichlen, 1967). This approach eliminates the necessity of computing separate spectral recovery efficiencies.

4. Flow Parameter Dependency of Spectral Recovery Efficiency

It is expected that the spectral recovery efficiency for a particular propeller is a function of the size and shape of the eddies of the flow exciting the propeller. For a particular shape of eddy, it should be a function of the ratio of some characteristic size of the eddies to a

characteristic dimension of the propeller. Because the longitudinal velocity fluctuations are of concern, it would seem that the characteristic eddy scale should have some relation to the longitudinal velocity fluctuations. Characteristic scales of the longitudinal velocity fluctuations are L_x , L_y , and L_z , where L_x has been defined in equation 4-27. L_y and L_z are defined as

$$L_y = \int_0^{\infty} R_u(y) dy \text{ and } L_z = \int_0^{\infty} R_u(z) dz \quad (4-28)$$

where

$$R_u(y) = \lim_{T \rightarrow \infty} \frac{1}{2T} \int_{-T}^T \frac{u'(x_0, y_0, z_0, t) u'(x_0, y_0 + y, z_0, t)}{\bar{u}'^2} dt \quad (4-29)$$

and

$$R_u(z) = \lim_{T \rightarrow \infty} \frac{1}{2T} \int_{-T}^T \frac{u'(x_0, y_0, z_0, t) u'(x_0, y_0, z_0 + z, t)}{\bar{u}'^2}$$

where x is the coordinate in the direction of flow, y is in the flow depth direction and z is perpendicular to the first two. Either the propeller diameter or length is a convenient length parameter describing the scale of the propeller. Their dimensions are generally of the same order of magnitude.

Assuming two-dimensional flow, a convenient eddy shape parameter might be the ratio L_y/L_x . In an isotropic turbulent flow, this ratio has a value of 0.5. The work of Laufer (1951) indicates that this ratio is even smaller than 0.5 in shear flows of the type in which it is desirable to use the propeller flow meter. From this discussion, it appears that an important parameter defining the flow

dependency of $\eta(f)$ might be d/L_y , where d is the propeller diameter.

Unfortunately, while a good estimate of L_x is easily obtained from the system function corrected power spectral density of the propeller, L_y must be obtained from a more difficult and time consuming measurement involving two sensors for which propellers are not suitable unless L_y is very large.

Hinze (1959) p. 105 shows that

$$R_u(y) = \frac{\overline{(e_o + e_y)^2} - \overline{(e_o - e_y)^2}}{4\bar{e}'_o \bar{e}'_y} \quad (4-30)$$

where e_o is the fluctuating component of the voltage of the sensor located at $y = 0$, e_y the fluctuating component at $y = y$, the overbars indicate a time averaging procedure, and the primes indicate root mean square values. This type of measurement has been made in flows similar to the ones of interest here by Dell'Osso (1966) and Laufer (1951). Their results are presented in the next chapter of this study.

Since L_y is difficult to measure, it will not often be available as a basis for the functional behavior of $\eta(f)$, so some more readily available scaling parameter should be selected. One such measure is the scale L_x which is easily obtained from the power spectrum. Fortunately, there is already a small amount of information available about the relation between L_x and L_y for the flow of interest here. The use of L_x as a basis for the functional behavior of $\eta(f)$

is discussed in the next chapter. Another parameter which might give a basis for the functional behavior of $n(f)$ is some physical scale of the flow which is known, at least approximately, to determine the scale of turbulence. Such measures are bar size or spacing in grid generated turbulence, pipe diameter in pipe flow, or channel depth or width in open channel flow. Finally, if one is certain that the scaling of the flow is such that the low frequency portion of the propeller spectrum is undistorted by spatial averaging, one can simply fit an empirical curve to this portion of the spectrum and avoid entirely the need to use a spectral recovery efficiency.

E. Conversion of Voltage Fluctuations to Velocity Fluctuations

As explained previously, the angular velocity of the propeller rotating in a velocity field is converted by the instrument system into an analog voltage inversely proportional to the instantaneous flow velocity. Similarly, the hot-film anemometer instrumentation system produces a voltage which is directly proportional to the instantaneous flow velocity. Once this voltage has been recorded, or analyzed, say by a root-mean-square (rms) voltmeter, there remains the problem of converting the voltage fluctuations back to velocity fluctuations. One method of converting voltage fluctuations to velocity fluctuations is to assume that the mean velocity calibration curve applies also to the instantaneous voltage-velocity relation for small

fluctuations. This method will not work, however, when the voltage fluctuations are analyzed using a rms volt meter. In this study, when rms meter analyses or hot-film anemometer power spectral density computations were made, the method presented by Richardson and McQuivey (1968) has been used to convert voltage fluctuations into velocity fluctuations.

The use of the method of Richardson and McQuivey (1968) for either the hot-film or the flow meter involves five assumptions. These are:

1. The velocity vector U can be expressed by a mean value U and the fluctuating components u , v , and w .

2. The propeller (hot-film) is sensitive only to the mean value and the fluctuating component of the velocity in the mean flow direction.

3. The relation between mean voltage and mean velocity can be used to convert voltage fluctuations to velocity fluctuations.

4. The change in the slope $d\bar{E}/d\bar{U}$ of the calibration curve is small over the range of the velocity fluctuations encountered during a measurement.

5. The root-mean-squares of the small voltage fluctuations \bar{e}' and the small velocity fluctuations \bar{u}' are interchangeable with the differentials dE and dU .

Richardson and McQuivey (1968) show that all these assumptions are justified in hot-film anemometry. The only arguments which must be modified for the propeller flow

meter are those for assumptions two and three. That assumption two is valid for a propeller flow meter has been proved in section A of chapter three. Assumption three implies that small velocity fluctuations are followed ideally by the propeller. Due to inertial and spatial averaging, this is not the case. Thus this procedure is incorrect when applied to propeller flow meters to the degree that inertial and spatial averaging effects prevent the achievement of assumption three. This means that the intensities measured using this method will be too small by the fraction of the area between the propeller output velocity power spectral density and the true power spectral density of the turbulent flow phenomenon. As long as this is realized, it is permissible to use this method to convert propeller measuring system output voltage fluctuations to velocity fluctuations. As will be shown later, the loss of turbulent energy due to spatial and inertial averaging is relatively constant over a wide range in power spectral density energy distribution parameters so that correction for the loss of energy in open channel turbulence is relatively simple.

Richardson and McQuivey (1968) show that under the above assumptions the relation between voltage and turbulent velocity root-mean-squares may be written

$$\bar{u}' = \frac{d\bar{U}}{d\bar{E}} \bar{e}', \quad (4-31)$$

where \bar{U} and \bar{E} refer to the mean velocity-mean voltage calibration curve and $d\bar{U}/d\bar{E}$ is evaluated at the mean velocity

of the measurement. The calibration equation of a propeller in terms of the digital-to-analog converter output voltage may be written

$$\bar{U} = A + \frac{B}{\bar{t}_p} = A + \frac{B}{K\bar{E}}, \quad (4-32)$$

where $\bar{t}_p = 1/f$, f is frequency of propeller revolution, and K is a proportionality constant between propeller period \bar{t}_p and voltage \bar{E} . Differentiating equation 4-32 with respect to \bar{E} , one obtains

$$\frac{d\bar{U}}{d\bar{E}} = \frac{-B}{K\bar{E}^2}. \quad (4-33)$$

This is the relation used in equation 4-31 for conversion of voltage fluctuations to velocity fluctuations for propeller flow meters. The value of $d\bar{U}/d\bar{E}$ used for the hot-film anemometer is obtained by graphical differentiation of its mean velocity versus voltage calibration curve.

The root-mean-square voltage meter used in this study was the Disa 55D35. It has a low frequency cut off point of 0.5 Hz, and a high frequency response flat well beyond the range of frequencies of interest in this study.

Chapter V

In this chapter is a discussion of the results of experimental measurements made on and with Ott minor propellers 1, 1-3, and 2-3. One group of experiments was designed to: 1) evaluate the dynamic behavior of the system which consisted of the propeller rotating in a spatially uniform velocity field, and 2) evaluate the spatial averaging effect of a propeller being used to measure a particular natural flow field which was, in this case, a rough boundary open channel flow. In the second group of experiments, the results of the first group were used to interpret the power spectra and relative intensities of the longitudinal velocity fluctuations in several field situations.

A. Dynamic Behavior of the Propeller-Flow System

This subgroup of the first group of experiments was designed to evaluate the dynamic behavior of a propeller in a spatially-uniform but time-varying flow field. Sinusoidal excitation experiments were used to determine the entire system function $H(\omega)$. Step-input experiments were used to see if the results of the sinusoidal excitation tests could be reproduced in a simpler fashion. High velocity fluctuation intensity experiments were made to check the range of validity of the linearization assumptions made in the derivation of the equation of motion. The results of the entire subgroup of experiments are discussed

with respect to the applicability of the model described by equation 3-11, and to the design of propellers with a high frequency response.

1. Sinusoidal Excitation Experiments

As explained in chapter IV, section C-1, the output signal from the flow meter via the instrumentation system was recorded along with a position trace on a strip chart as shown in figure 10. These two traces along with calibration information relating the position trace to the full forward position of the sine motion generator contain all the information necessary to obtain the system function of a propeller if the recorder chart speed and generator radius are known. The instantaneous output velocity is determined from the flow chart ordinate using the mean velocity calibration curve, that is

$$U = A + \frac{B}{KE} , \quad (5-1)$$

where A and B are calibration constants, E is the recorded voltage, and K is a proportionality constant between E and the flow meter period. The absolute value of the system function $|H(\omega)|$ is determined from

$$|H(\omega)| = \frac{U_{\max} - U_{\min}}{2 \omega r_1} \quad (5-2)$$

where r_1 is the sine motion generator radius, and

$$\omega = 2\pi \frac{S}{L} \quad (5-3)$$

in which S is the chart speed and L is the distance between position pulses. The phase shifts of the occurrences of

the output maximum and minimum velocities ϕ_{\max} and ϕ_{\min} are determined from

$$\phi_{\max} = \frac{L_{\max}}{L} 2\pi - \phi_p + \frac{\pi}{2}$$

$$\phi_{\min} = \frac{L_{\min}}{L} 2\pi - \phi_p - \frac{\pi}{2} ,$$
(5-4)

where L_{\max} and L_{\min} are the distances from the position pulse to the occurrence of the maximum velocity in the output, positive from right to left (in the direction of increasing time, figure 10) and where ϕ_p is the phase lag between occurrence of the position pulse and full forward of the sine motion generator. The true input maximum velocity occurred when the generator pin was one-fourth of a revolution ahead of full forward. This is the reason for the plus sign on the $\pi/2$ in the first of equations 5-4 and the minus sign in the second. The phase shift used in this study was the average of ϕ_{\max} and ϕ_{\min} . The actual solution of equations 5-2 and 5-4 was computerized so that the data analysis simply required transferring from the chart to IBM cards the ordinates of the maximum and minimum velocities and the abscissas of these points and the position trace. $|H(\omega)|$ and ϕ were taken to be their averages over six or more cycles of the generator. Their standard deviations were generally of the order of 0.05 for $|H(\omega)|$ and 0.10 for ϕ .

To determine the mean velocity dependency of the system function, it was evaluated for four mean velocities for each of the propellers. To evaluate the intensity effect, three or four sine motion generator radii were used for each mean

velocity and propeller. The results of the $|H(\omega)|$ measurements on the 1, 1-3, and 2-3 propellers are presented in figures 14, 15, and 16. These same results are given in figure 17 as $|H(\omega/\omega_n)|$ in comparison with the first order model given by equation 3-36a. In this case, ω_n has been defined to be the ω for which the experimental amplitude ratio of the propeller-flow system is $|H(\omega)| = |H(\omega_n)| = 0.707$. This is in agreement with the first order system definition of ω_n from equation 3-36a. Similarly, figures 18, 19, and 20 present the individual ϕ curves for these propellers and figure 21 shows the same information in comparison with a ϕ defined by equation 3-36a with the ω_n as indicated on the graphs.

The natural frequency defined here as the angular frequency at which the experimental amplitude ratio has decreased to 0.707 is shown in figure 22 as a function of mean velocity. This figure will be discussed at length later in this section.

Examination of figures 17 and 21 shows that the actual system equations of the propellers tested here deviate considerably from the first order constant coefficient model described by equations 3-36a.

One factor which is quite noticeable is the systematic increase with decreasing mean velocity of the ordinates of the $|H(\omega/\omega_n)|$ curves of figure 17, at a constant value of ω/ω_n . This is an over registration of the amplitude ratio curve with respect to the first-order, constant-coefficient

model. As shown for selected points on figure 15a and d, the sine motion generator relative intensity \bar{v}'/\bar{U} at the larger generator radii exceeds 0.1 over a large portion of the amplitude ratio curves. At a constant radius and ω , the intensity increases as the mean velocity decreases. Referring to the work of Plate (1967) (discussed in chapter IV) it is tempting to speculate that the apparent over registration is due to the fact that \bar{v}'/\bar{U} is outside the range of validity of the small amplitude assumption made in simplifying equation 3-11. If there is to be an effect of \bar{v}'/\bar{U} on the amplitude response, it must enter through the term $M_5(u')^2$ of equation 3-11. From equations 3-13, 3-15, and 3-19 it is seen that $M_5(u')^2 \propto \frac{1}{\bar{U}} (r_1 \omega)^2$. For ω constant, it is evident that a change in \bar{U} from 2.0 to 5.0^f/s should change $M_5(u')^2$ to 0.4 times its previous value, while a change of r_1 from 0.109 in to 0.969 in should change this quantity to 79 times its previous value. Since the effect of varying r_1 at a given ω should be much more pronounced than the effect of varying \bar{U} , it is clear that if there is no discernible difference between experimental points obtained for different sine motion generator radii r_1 at high \bar{v}'/\bar{U} the effect of the term $M_5(u')^2$ on $|H|$ is negligible, and the speculation of a significant \bar{v}'/\bar{U} dependency of $|H|$ is not justified. An examination of figures 14 through 16 shows that there is no persistent trend in variation of $|H|$ which can be attributed to the different radii, thus \bar{v}'/\bar{U} is not an important factor in determining the behavior of

$|H|$ for the ranges of r_1 and ω used. Furthermore, the work of Plate (1967) predicts a \bar{v}'/\bar{U} effect on the mean output velocity. As will be discussed later, this effect is actually present. The presence of a \bar{v}'/\bar{U} effect on mean velocity does not, however, necessarily imply that such an effect should influence the amplitude response.

The above described systematic deviations from a first order constant parameter model for $|H|$ could also be produced if the differential equation contained a non-negligible acceleration sensitivity inversely proportional to mean velocity. Assuming for simplicity that $\gamma = 0$, the variation of $|H(\omega)|$ with $\omega/|M_2|$ when the acceleration sensitivity M_7 is significant is given by

$$|H(\omega)| = \sqrt{\frac{1 + M_7^2 (\omega/|M_2|)^2}{1 + (\omega/|M_2|)^2}} \quad (5-5)$$

(equation 3-36c). From figure 2, and from the calibration equation of a propeller, and because the calibration constant A is generally small,

$$\tan \theta = \frac{2\pi n_o r}{\bar{U}} \doteq \frac{\pi r}{15B} \quad (5-6)$$

Using equation 5-6, equation 3-21 becomes

$$M_{77} = \left(\frac{15B}{\pi}\right)^2 \frac{s\pi \ell^2 C_1}{2} \int_{R_i}^{R_o} \frac{r^2 dr}{\left[\left(\frac{15B}{\pi}\right)^2 + r^2\right]} \quad (5-8)$$

and it is assumed that the virtual mass coefficient C_1 and the blade chord ℓ are not functions of radial position on the propeller blade. Note that equation 5-7 does not

predict an inverse mean velocity dependency for the acceleration sensitivity, whereas such a relationship is required to produce the variation of the system function with mean velocity that is indicated by the experimental results of figure 17.

Using the propeller dimensions given in table I, the calibration constants of figure 5, and assuming the virtual mass coefficient $C_1=1$, acceleration sensitivities as calculated by equation 5-7 are:

Propeller		
1		$M_7=0.704$
1-3		$M_7=0.786$
2-3		$M_7=0.820.$
		(5-9)

If equation 5-5 governs the behavior of the amplitude ratio the M_7 values of equation 5-9 are the minimum values to which $H(\omega)$ should asymptote for $\omega/|M_2|$ large. As seen from figure 17, the experimentally obtained values of $|H|$ at high angular frequencies are considerably lower than the values given in equation 5-9. In addition, there is no indication in the experimental $|H|$ curves of the reverse curvature required for these curves to asymptote to some finite constant value. This indicates that the virtual mass coefficient C_1 is considerably smaller than the value of one assumed in calculation of the coefficients M_7 in equations 5-9 and that insofar as the propellers of this study are concerned the acceleration sensitivity is negligible.

From the above discussion, it is clear that the deviation of the measured system function from the first order-

constant coefficient model must arise from the complex nature of M_2 . The system function behavior is therefore described by equations 3-36b and not equations 3-36a. The system function is, for a given mean velocity, then a function of ω through the phase angle γ and the magnitude $|M_2|$. The behavior of these parameters with ω and \bar{U} is not amenable to analytical prediction, so they must be determined by experimental methods. Once the equations 3-36 have been solved for γ and $|M_2|$, these quantities can be calculated from the experimentally determined values of $|H|$ and ϕ . This was done and these quantities are plotted for the 1-3 propeller in figures 23 and 24. The mean velocity dependency of $|M_2|$ is seen from figure 23 to follow the same general trend as the ω_n defined by the 0.707 value of the $|H|$ curves. The mean velocity dependency of γ seems to be restricted to the lower angular excitation frequencies.

The determination of $|M_2|$ and γ from the measured $|H|$ and ϕ curves is purely academic. The real interest here lies with the $|H|$ curves because these are the ones needed to correct the turbulent velocity spectrum for the inertia effect of the propeller. Before moving on, however, it is interesting to discuss the general behavior of the functions $|H|$ and ϕ . First, the $|H|$ curves do not deviate significantly from the first-order model shape until $|H|$ is less than 0.707. Second, the ϕ curves do not deviate significantly from the shape predicted by this model until $\phi > 0.95$ rad. There is, however, considerable difference between

natural frequencies as defined by the $|H(\omega_n)| = .707$ criterion and as defined by a $\phi(\omega_n) = .785$ criterion (For a first order-constant parameter system, the natural frequencies so defined should be identical.). The ω_n defined by the first criterion increases systematically and considerably with mean velocity (see figure 22) while that defined by the second increases only slightly with mean velocity, and the variation is not as systematic. There is, apparently, then a much greater mean velocity dependency in $|H|$ than in ϕ .

The failure of the experimental $|H|$ and ϕ curves to fit the classical first order model makes the possibility of prediction of system behavior from the step input behavior characteristics appear bleak. The behavior of the $|M_2|$ curves indicates that it will probably not even be possible to obtain an indication of the mean velocity behavior of a parameter corresponding to the ω_n defined by $|H(\omega_n)| = 0.707$ from the step velocity experiments.

2. Step-Input Experiments

Step input experiments were performed to determine the possibility of obtaining a parameter to describe the behavior of the system when subjected to periodic excitations, but without the necessity of resorting to sinusoidal excitation experiments. As explained in chapter IV, section C-2, a constant parameter first order linear system such as the one described by equation 4-7 should give the exponential response function of equation 4-11 when excited with a step input.

In this work, the parameter ω_n of equation 4-11 was determined as a function of step height (mean velocity) by replotting the experimental results from the strip chart (figure 11) on semilog paper with $(n_f - n)/n_f$ on the logarithmic axis. This should result in a straight line plot with the parameter ω_n being the reciprocal of the time intercept at which $(n_f - n)/n_f = e^{-1}$. Figure 25 displays typical experimental records so plotted for the range of mean velocities used in this study. It is noticed that the linearity of the results is good and without any systematic deviation.

The natural frequencies determined in this fashion have been plotted in figure 22 along with those determined from the $|H| = 0.707$ criterion of the preceding section. The natural frequencies so defined are seen to be directly proportional to mean velocity, and considerably different from those determined in the previous section. This discrepancy is due to the complex nature of the coefficient M_2 . Unfortunately, step input experiments do not provide sufficient output information to evaluate the behavior of such a coefficient when the phase shift is as significant as shown in figure 24.

It is unfortunate that the frequency dependency of the propeller and its associated flow system is so complex, because this makes it impossible to predict the behavior of the amplitude ratio from one relatively simple step input experiment and the standard first-order system amplitude

response function 3-36a. Instead, use must be made of sine input experiments which are more lengthy both to perform and in data reduction. In part four of this section is a discussion of a method of presentation of data from sine input experiments which allows prediction of the amplitude response function with a minimum amount of experimental work.

3. Effect of Velocity Fluctuations on Output Mean Velocity

The determination of the true point mean flow velocity from a current meter output velocity record is a problem of considerable importance. Among the factors causing mis-registration of the mean velocity by a current meter are the presence of an appreciable velocity gradient and the presence of high intensity turbulent velocity fluctuations. The latter effect is evaluated here by producing an artificial turbulence of known intensity using the sine motion generator. The experimental setup was as described in chapter IV, section C-3. The quantities measured were: the time elapsed in covering a known distance, sine motion generator radius and angular velocity, and the total number of pulses generated by the flow meter. The propellers used were the Ott minor numbers 1 and 1-3.

Because it was impossible to set the towing cart velocity at exactly the desired value, the output velocity deviation from the true mean was referenced to the calibration curve of the propeller using the true mean velocity as computed from the distance covered and the elapsed time. That is, the percent deviation D was computed from

$$D = 100 \frac{n_o - n_c}{n_c} \quad (5-10)$$

where

$$n_c = \frac{U_{cart} - A}{B} \quad (5-11)$$

and n_o is the average flow meter frequency. To correct for the small deviation from the calibration curve, the average value of the D obtained from the $\omega = 0$ runs at a particular mean velocity and generator radius was subtracted from the results of the rest of the runs at that mean velocity and generator radius. In figure 26, percent deviation D has been given as a function of the velocity fluctuation intensity to mean velocity ratio \bar{v}'/\bar{U} , where the velocity fluctuation intensity has been computed using equation 4-6.

The results have been presented in this form because it is in this form that they are most conveniently used for correcting the mean output velocity once the turbulent velocity intensity is known.

There is considerable scatter in the results of figure 26, especially for small \bar{v}'/\bar{U} , however, this does not appear to be a function of either generator radius or mean flow velocity. The significance of this result will be discussed later with reference to the work of Plate (1967).

Considering specific propellers, it is interesting to note that both over register the mean velocity when subjected to high relative velocity fluctuation intensities, and that the larger-heavier number 1 propeller is considerably less influenced than the number 1-3. The over

registration of the 1-3 propeller does not exceed one percent until the relative intensity \bar{v}'/\bar{U} exceeds 0.1, that of the 1 propeller does not exceed one percent until \bar{v}'/\bar{U} exceeds 0.2. Relative intensities as high as 0.2 should seldom be encountered, even in turbine outlets or in supercritical open channel flow.

Chaix (1962) who worked with heavier propellers than the ones used here reports equivalent results. As would be expected, however, the relative intensities producing an over registration of one percent are slightly higher.

Plate's (1967) analysis using an equation of motion similar to equation 3-23, except that the squares of infinitesimals were not neglected, indicated that

$$D\left(\frac{\bar{U}}{\bar{v}'},\right)^2 = g(\omega) \quad (5-12)$$

where $g(\omega)$ is a function characteristic of a particular propeller. The analysis involves a double integration of the propeller equation of motion, once to obtain the instantaneous value of m the nondimensionalized angular frequency of the propeller, and once more to obtain the average value of this quantity. A nonzero average value of the nondimensionalized angular frequency indicates a misregistration of the mean velocity due to the turbulence. If one performs the same analysis on the equation of motion derived here, one finds that no misregistration is predicted, no matter how large the relative intensity \bar{v}'/\bar{U} becomes. Thus, the relative intensity at which the output mean

velocity deviates appreciably from the true mean indicates the end of the range of validity of the small amplitude assumption made in simplifying equation 3-11, at least insofar as the determination of the mean velocity is concerned. Arbitrarily setting a mean velocity misregistration of one percent as the limit on the range of validity of the small amplitude assumption, it is seen from figure 26 that this range extends to $\bar{v}'/\bar{U} = 0.2$ for the number 1 propeller and to $\bar{v}'/\bar{U} = 0.1$ for the number 1-3.

Analysis of equation 5-12 indicates that plots of the form of figure 26 might be an inappropriate means of presentation of meter misregistration data. This is due to the fact that at the same angular velocity two different sine motion generator radii produce different \bar{v}' values, while $g(\omega)$ is supposedly independent of sine motion generator radius. This should lead to a multiple valued plot in the form of figure 26, unless $g(\omega)$ is a constant. An examination of figure 27 shows that $g(\omega)$ is indeed constant. In figure 27, the experimental data used in figure 26 have been presented as prescribed by equation 5-12. These plots show that for ω above about six and ten rad./sec for the 1 and 1-3 propellers respectively, $g(\omega)$ is a constant. Below these values the behavior of $g(\omega)$ is uncertain. Thus at least for $\omega > 6$ and $\omega > 10$ rad./sec. for the 1 and 1-3 propellers respectively, the presentation used in figure 26 is correct.

It is seen, then, that the output mean flow velocity of a propeller flow meter of the type used in this study is probably within one percent of the true value if the turbulent intensity is less than ten percent of the true velocity. If the relative intensity is greater than ten percent, it may be desirable to correct the mean velocity for the distortion due to the turbulence. This can easily be done using figures of the same type as figure 26, if $g(\omega)$ is a constant, for in this case the correction is independent of the amplitude of the velocity fluctuations. If $g(\omega)$ is not a constant, a correction procedure could be worked out using the power spectrum to determine the amount of correction required for the turbulence in a particular band width.

4. Generalized System Description and Propeller Design

It has been demonstrated in the previous discussion that the parameters of the differential equation describing the behavior of a propeller and its associated flow are functions both of mean velocity and of the frequency of the exciting function. The complex nature of the coefficient, M_2 makes it impossible to define system behavior from a relatively few, simple to perform, step input experiments. A generalized description of system behavior which would reduce the amount of the more complex and time consuming sine function input experiments which have to be performed would be quite welcome. Such a generalized function could

become a part of the program for computation of the power spectrum to eliminate the necessity for a separate correction for system frequency response.

A comparison of the experimentally evaluated system behavior with the values of M_2 calculated from equation 3-16 shows which factors need to be stressed in the design of propellers with high frequency response. The ideal would, of course, be a propeller with a flat frequency response through the frequency range of interest in water, so the frequency response of the system would not even have to be evaluated.

Plate and Bennett (1968) found that the magnitude of the coefficient M_2 can be presented in generalized form if the term $|M_2|/\bar{U}^{1/2}$ is plotted as a function of ω/\bar{U} . The ratio ω/\bar{U} may be thought of as a Strouhal number or reduced frequency from which the length dimension, which is a constant for a particular propeller, has been omitted. The observed generalized relation can, for a particular propeller, be written $|M_2|/\bar{U}^{1/2} = n(\nu)$ whereas the relation predicted by equation 3-16 is roughly $|M_2|/\bar{U} = K|C(\nu)|$, or $|M_2|/\bar{U}^{1/2} = \bar{U}^{1/2} K|C(\nu)|$. This means that 1) the lift coefficient is inversely proportional to the square root of the mean velocity, or b) the virtual mass of the system is directly proportional to this quantity. The second alternative is unlikely, because the virtual mass is simply a volume of fluid which must be accelerated when the system oscillates; it is not likely to change with mean velocity. It

is possible, however, that at the low blade Reynolds number of the flows about the propellers used here that the lift coefficient might vary approximately with the inverse of the square root of mean velocity (Jacobs, 1963). The relationship $|M_2|/\bar{U}^{1/2} = m(v)$ is given for the three propellers in figure 28.

To completely describe the behavior of the system, a general relationship for the phase shift γ must also be found. If instead of γ , as in figure 24, the function $\cos\gamma$ is plotted as a function of ω , as in figure 29, the dependency of γ on mean velocity disappears. This indicates that the slight variation of γ with mean velocity in figure 24 is probably more apparent than real.

The use of the generalized functions $|M_2|/\bar{U}^{1/2} = m(v)$ and $\cos\gamma = n(\omega)$ makes possible the description of propeller system behavior after sine input testing at only one mean velocity. If the propeller to be tested differs markedly in geometry or size from the ones used here, it might be wise to check two mean velocities bracketing the velocity range of interest to verify the generality of the functions $m(v)$ and $n(\omega)$. Once $m(v)$ and $n(\omega)$ are available, the amplitude ratio $|H(\omega)|$ can be computed using equation 3-36. The dotted curve of figure 15b was computed using equation 3-36 and figures 28b and 29b. It fits well within the scatter of the experimentally measured amplitude ratios. It would be a simple matter to correct digitally computed power spectral densities for output amplitude attenuation by including the

experimentally determined $m(\nu)$ and $n(\omega)$ curves in the program for computing power spectral density.

In the design of a propeller with the most desirable frequency response characteristics, one must maximize the complex natural frequency M_2 . This coefficient is given analytically by equation 3-16 and is presented graphically from experimental results in figures 28 and 29 for the Ott minor propellers 1, 1-3, and 2-3.

The solution of equation 3-16 requires an expression describing the functional behavior of $\cos\theta$ with radius r ; this can be seen from figure 2 to be

$$\cos\theta = \frac{\bar{U}}{[\bar{U}^2 + (2\pi n_o r)^2]^{\frac{1}{2}}} \quad (5-13)$$

Upon insertion of the calibration equation of a particular propeller this becomes

$$\cos\theta = \frac{A + Bf}{\left[\{A+Bf\}^2 + \left(\frac{2\pi r f}{30}\right)^2 \right]^{\frac{1}{2}}} \doteq \frac{(15B/\pi)}{\left[\left(\frac{15B}{\pi}\right)^2 + r^2 \right]^{\frac{1}{2}}} \quad (5-14)$$

Using equation 5-14, equations 3-15 and 3-16 become

$$M_1 = \frac{1}{n_o \bar{U}^2} \left\{ 2\rho U + \frac{sC_1 \pi \ell^2}{2} \int_{R_i}^{R_o} \frac{r^2 (15B/\pi)^2 dr}{\left[\left(\frac{15B}{\pi}\right)^2 + r^2 \right]} \right\} \quad (5-15)$$

$$M_2 = \frac{2\pi s C(\nu) \ell}{M_1 \bar{U} n_o} \int_{R_i}^{R_o} \frac{r^2 (15B/\pi) dr}{\left[\left(\frac{15B}{\pi}\right)^2 + r^2 \right]^{\frac{1}{2}}} \quad (5-16)$$

where in 5-16, the effects of all terms in the brackets of 3-16 are assumed to be averaged over r and included in $C(\nu)$. The solution of 5-15 and 5-16 gives

$$M_2 = \frac{15\bar{U}s\ell B \left\{ r \sqrt{r^2 + \left(\frac{15B}{\pi}\right)^2} - \left(\frac{15B}{\pi}\right)^2 \ln \left[r + r^2 + \left(\frac{15B}{\pi}\right)^2 \right] \right\} \Big|_{R_i}^{R_o}}{\left\{ 2\rho \left[\frac{\pi \ell n r}{2} \Big|_{R_i}^{R_o} + \frac{s \ell t_b}{3} r^3 \Big|_{R_i}^{R_o} + \frac{225B^2 \ell^2 s C_1}{2\pi} \left(r - \frac{15B}{\pi} \tan^{-1} \frac{\pi r}{15B} \right) \Big|_{R_i}^{R_o} \right] \right\}} \quad (5-17)$$

where ℓ_h is the hub length and t_b is the blade thickness. The magnitudes of the terms appearing in equation 5-17 are given for the 1, 1-3, and 2-3 propellers in table 1.

For a propeller of a given radius and pitch, and at a constant mean velocity, equation 5-17 shows that if the inertia term dominates in the denominator, the complex natural frequency is directly proportional to B; if the virtual mass term dominates, the complex natural frequency is inversely proportional to ℓB . It is recalled that ℓ is the blade chord and B is a calibration constant of the propeller, determined by the pitch such that B is directly proportional to the pitch. If overall propeller length is a constant, ℓ and B are related such that the product ℓB is approximately constant. This is because dividing the pitch (advance per revolution) of a propeller of a certain length by a particular factor increases the blade chord of the blades on that propeller by approximately the same factor, if the propeller length is constant. Because B appears inside the integrals of equations 5-15 and 5-16, it is difficult to predict the behavior of the calculated M_2 if both ℓ and B are changed while the radius remains approximately constant. This is illustrated in table 1 where it is seen that for the 1-3 and 2-3 propellers the calculated virtual mass term

dominates. In this case, one might expect the calculated M_2 's to vary from the 1-3 to the 2-3 propeller as $(\ell B)_{1-3} / (\ell B)_{2-3}$, however, due to the presence of the calibration constant B inside the integral, the variation is opposite this.

The above two criteria provide design guides which can be used in special cases. For example, if the virtual mass dominates, an increase in M_2 should be obtained at constant pitch and radius by decreasing ℓ and if the inertia term dominates, an increase in M_2 should result if the pitch is increased. When designing a propeller, two other factors which must be considered are: 1) the greater the pitch, the slower the propeller turns at a given mean velocity; the slower a propeller turns, the less information can be obtained about the flow in a given amount of time. 2) The less the blade area and the greater the pitch, the less torque is developed, so that a point might be reached where bearing torque is important.

Taking from figure 28 mean values of $|M_2|/\bar{U}^2$ to be about 11 for the 1 propeller, 11.5 for the 1-3, and 14 for the 2-3, the ratio of the measured average $|M_2|$ to the calculated $|M_2|$ assuming $|C(v)| = 1$ is, as the mean velocity varies from 2.0 to 5.0^f/s, 0.731 to 1.160 for the 1 propeller, 0.69 to 1.09 for the 1-3, and 0.68 to 1.08 for the 2.3. These results are very good, considering the uncertainties involved in the fluid mechanics of the finite blade rotating system.

The natural frequency of a propeller can also be defined as a cutoff frequency, analogous to the cutoff frequency of a first order electronic filter. That is, the propeller cut off frequency is the frequency at which the amplitude ratio has decreased to 0.707 (The power passed by the propeller at the cutoff frequency is then fifty percent of the power in the spectrum at this frequency.). In this case, the variation of the cutoff frequency with mean velocity is given by figure 22. Thus for the propellers of this study, at mean velocities varying from 2.0 to 5.0 ft/sec, the cutoff frequency varies from 2.55 Hz to 5.58 Hz for the 1 and 1-3 propellers and from 5.90 Hz to 8.36 Hz for the 2-3 propeller.

From equation 5-7 and the fact that the acceleration sensitivity of the propellers used in this study was negligible, it can be concluded that the inertia term determines the behavior of the coefficient M_1 , for propellers with the same general geometry and size as those used in this study. In this case, the natural frequency or cutoff frequency can be greatly increased by simply constructing propellers of a less dense material than the aluminum alloy used in the construction of the propellers used here. For example, if a plastic such as Lucite or Plexiglass which has a density 1.2 times that of water were used to construct propellers identical in geometry to those of this study, the cutoff frequencies at velocities ranging from 2.0 to 5.0 ft/sec should range from 5.73 Hz to 12.58 Hz for the 1 and 1-3

propellers and from 13.29 Hz to 18.82 Hz for the 2-3 propeller.

B. Correction for Spatial Averaging

At the present state of understanding of the mechanics of turbulent flow, the spectral recovery efficiency as defined in section D of chapter III cannot be determined analytically. It can be determined experimentally for a particular flow and propeller by comparing the propeller output power spectral density to that from a point velocity sensor. If enough of the power spectral density is unaffected by spatial averaging, it is possible to avoid entirely the use of a spectral recovery efficiency by fitting an empirical power spectral density curve to the unaffected portion of the propeller output power spectral density.

The power spectral densities used in this section were computed using the CDC 6400 computer belonging to Colorado State University. The program was built around equations 4-19 through 4-21. The raw power spectral densities for the various propellers and the hot film anemometer are shown in figures 30 through 33. The flow conditions for which the power spectral densities were computed were established in Colorado State University's 200 foot long by eight foot wide by four foot deep tilting-recirculating flume. The bed roughness consisted of 1 1/16" high by 1 1/4" wide by 6" long wooden blocks glued to the flume floor with their long dimension perpendicular to the flow.

The blocks were placed at the nodes of two 12" square grids, one displaced with respect to the other by six inches along the flume and six inches perpendicular to it, so there were staggered rows of blocks every six inches along the flume. Flow parameters pertinent to the various runs are listed in table 2. Correction of propeller output power spectral densities for propeller frequency response was accomplished using equation 3-36 and the generalized plots of figures 28 and 29. The curves so obtained are given by the dashed lines of figures 30 through 33.

1. Spectral Recovery Efficiency

The spectral recovery efficiency $\eta(f)$ for a particular flow and propeller is calculated by means of equation 4-12 from the output power spectral density of the propeller, the magnitude of the system function of the propeller, and the power spectral density of an ideally-responding point-velocity sensor. As has been shown by Richardson et al. (1967), the hot film-anemometer has a flat frequency response over a wide enough range to be treated as ideally responding in water turbulence. The work of Frenkiel (1954) shows that if $(l_w/\lambda_y)^2 \ll 1$ then a hot-wire (-film) anemometer may be treated as a point sensor, at least insofar as the measurement of the turbulent intensity (or power spectrum) is concerned. Calculating λ_x from $1/\lambda_x^2 = 4\pi^2/\bar{U}_{loc} \int_0^\infty f^2 S(f)df$, assuming local isotropy of the energy dissipating eddies, and hence calculating λ_y from $\lambda_x = \sqrt{2}\lambda_y$, it is found that $(l_w/\lambda_y)^2$ varies from about 0.01 for run 12 to

0.001 for run 16. This should be sufficiently small to insure that the hot-film anemometer behaves as a point sensor.

The power spectral densities of figures 30 through 33 were computed for a sampling time T of 50 seconds and a maximum lag time τ_{\max} of 5 seconds. Using equations 4-23 and 4-24, these quantities yield an equivalent band width B_e of 0.2 Hz and 20 degrees of freedom d_f . The 90 percent confidence limits of a power spectral density are defined such that 90 percent of the calculated power spectral densities can be expected to fall within these limits which are established with respect to the true power spectral density of the phenomenon. Bendat and Piersol (1966), page 139, point out that for $d_f = 20$ these limits are defined by curves such that the upper one is 1.57 times the true power spectral density, and the lower one is 0.54 times this quantity. Taking the hot-film anemometer power spectral density as the true power spectral density, the 90 percent confidence limits for the runs of figures 30 through 33 have been shown on figure 34 along with the hot-film anemometer and frequency-response-corrected propeller output power spectral densities. For this comparison the power spectral densities must be presented in non-normalized form, or in the form of

$$S_t(f) = \overline{u^2} S_{oo}(f), \quad (5-18)$$

where $\overline{u^2}$ is the root mean square of the output velocity fluctuations.

It is noted in figure 34 that in all cases except two the low frequency portions of the frequency-response-corrected propeller output power spectral densities fall within the 90 percent confidence limits on the corresponding hot-film anemometer power spectral densities. This indicates that the deviations of the low frequency portions of these curves from the corresponding hot-film anemometer power spectral densities are probably due only to sampling error. For this reason, and because it is difficult to imagine the spectral recovery efficiency being greater than one, the frequency-response-corrected propeller output power spectral densities, before the computation of the spectral recovery efficiencies, have been shifted to coincide with the low frequency portions of the corresponding hot-film anemometer power spectral densities.

As mentioned in chapter IV, section D-4, the most useful scaling parameter for describing the behavior of the spectral recovery efficiency $\eta(f)$ would probably be L_y , the depthwise length scale of the longitudinal velocity fluctuations. Unfortunately, in most cases where propeller turbulence measurements are necessary, it is impossible or at least impractical to obtain this parameter. It has, however, been measured by at least two investigators for wall shear generated turbulence of the type that is of interest here. Laufer (1951) made extensive measurements of various turbulence parameters in air flowing in a rectangular duct; Dell'Osso (1966) made measurements of the lateral scale in

water flowing in a small rectangular open channel. Some of the results of these investigations are presented in figure 35. From this figure, it is seen that the measured L_y values occur in a range from 0.1 to 0.43 times Y the mean depth (the half-width of the duct in Laufer's case). If these results can be extended to larger scale flows, it might be expected that an output velocity power spectral density from a propeller which has a diameter d of the order 0.05 to 0.1 times Y would be free of spatial averaging effects.

Also given in figure 35 are Laufer's results in terms of the eddy shape parameter L_y/L_x , where L_x is the longitudinal scale of the longitudinal velocity fluctuations. The value of this ratio in homogeneous isotropic turbulent flow is 0.5. Laufer's observed values in the wall shear generated turbulence of the duct flow varied from 0.24 to 0.52. Taking the lower limit of this ratio to be 0.25, the output velocity power spectral density of a propeller should be relatively free of spatial averaging effects if the ratio d/L_x is on the order of 0.125 to 0.25. From the measurements listed in table 2, it is seen that the quantities $0.1Y$ and $0.25L_x$ are of the same order for the flows of this study.

Another parameter which might be useful in describing the behavior of the spectral recovery efficiency would be an energy distribution parameter. The quantity L_x/\bar{U}_{loc} is such a parameter. As can be seen from equation 4-26, the smaller this parameter, the broader and flatter is the

power spectral density curve of the flow. The broader and flatter the power spectral density, the more energy is contained in the high-frequency, small-scale velocity fluctuations. Relatively speaking, the more energy contained in the small scale velocity fluctuations, the less efficient would one expect a propeller to be, due to a mutual cancellation of torque by different small eddies acting on different propeller blades at the same time.

In figure 36, the spectral recovery efficiencies have been plotted for the Ott minor 1, 1-3, and 2-3 propellers in the flows of table 2. The parameters d/L_x and L_x/\bar{U}_{loc} discussed above have been listed on the figure along with the curves to which they apply. Attempts to reduce these curves to a more general form using the parameters d/L_x and L_x/\bar{U}_{loc} were not successful.

Figure 36 shows that, in general, the spectral recovery efficiency decreases with increasing d/L_x and with decreasing L_x/\bar{U}_{loc} . The behavior of $\eta(f)$ with d/L_x is qualitatively as expected, except for run 18 using the 2-3 propeller. For this run, $\eta(f)$ was considerably larger than that for the 1-3 propeller, which had very nearly the same d/L_x . This could be due to any number of reasons that would cause the high frequency portion of the raw propeller output power spectral density to register high. For example there might have been a loose ground on the digital-to-analog-converter which would have caused increased 60 Hz interference. Another source of high frequency interference was the occasional operation

of a fork lift tractor in the vicinity of the flume. The dependency of $\eta(f)$ on the energy distribution coefficient L_x/\bar{U}_{loc} is seen to be quite pronounced. This is illustrated by comparison of the $\eta(f)$ curves obtained for the 1 propeller from runs 16 and 18. At 25 Hz, there is a four-fold increase in $\eta(f)$ with a 35 percent increase in L_x/\bar{U}_{loc} , while d/L_x is essentially constant at 0.34. The magnitudes obtained here for $\eta(f)$ show that even for d/Y on the order of 0.1 or less, the spatial averaging effect of a propeller on open channel flow turbulence can be considerable. In fact, at ten Hz, the attenuation factor on the power spectral density varies from 0.32 times that due to inertia for run 12 using the 1-3 propeller ($d/L_x = 0.48$ and $L_x/\bar{U}_{loc} = 0.163$) to 3.11 for run 17 using the 1 propeller ($d/L_x = 0.43$ and $L_x/\bar{U}_{loc} = 0.110$).

In summary, the spectral recovery efficiency $\eta(f)$ can be calculated for a particular flow and propeller by using the power spectral densities of the propeller and an ideal point-velocity sensor. Probably the best parameter describing the behavior of $\eta(f)$ would be a lateral scale factor d/L_y , but this parameter is generally unavailable. In the absence of the parameter d/L_y , the parameter d/L_x , along with an energy distribution parameter L_x/\bar{U}_{loc} , can be used to describe the behavior of the spectral recovery efficiency.

2. Empirical Power Spectral Density Curves

A second approach which can be used for obtaining power spectral densities which are undistorted by spatial

averaging is the fitting of an empirical power spectral density curve to that portion of the propeller output power spectral density which is not affected by spatial averaging. Inspection of figures 30 through 33 indicates that in the frequency range of this study the hot-film anemometer power spectral densities of the open channel flows evaluated here fit quite well the $-5/3$ power law postulated by von Karman (1948). An empirical power spectral density equation which becomes asymptotic to a $-5/3$ power law is equation 4-26.

The easiest method for fitting such a curve to a calculated power spectral density is to use the zero frequency ordinate of the normalized power spectral density. This is because at zero frequency, equation 4-26 becomes

$$S(0) = 4L_x/\bar{U}_{loc} \quad (5-19)$$

Equation 5-19 gives directly, without the need for a trial and error solution, the parameter L_x/\bar{U}_{loc} of the family of curves described by equation 4-26.

In the case of this study, however, it is impossible to obtain normalized power spectral density curves for the propeller output power spectral densities, because the spectral recovery efficiency is unknown. This difficulty can be overcome by using equation 4-26 in a modified form. Let a nondimensional frequency P be defined, such that

$$P = 4L_x f/\bar{U}_{loc} \quad (5-20)$$

and equation 4-26 becomes

$$\frac{S(f)}{4L_x/\bar{U}_{loc}} = \frac{1}{1 + (2P)^2} \frac{5}{6} \quad (5-21)$$

This generalized curve represents all members of the family of equations given by equation 4-26; it is shown graphically in figure 37. All members of this family of curves have the same shape on a full logarithmic plot. Because of this, it is possible to obtain the parameter L_x/\bar{U}_{loc} by matching the curvature of the curve in figure 37 with that of the low frequency portion of an experimental, frequency-response-corrected, propeller output velocity power spectral density. The parameter L_x/\bar{U}_{loc} is obtained using equation 5-19 and the P and f values from a section of the curves where their curvatures match. In the use of this procedure on frequency-response-corrected propeller output velocity power spectral densities, it is assumed that the portion of the propeller output power spectral density used for curvature matching is free from spatial averaging effects.

In table 3 have been listed the values of P, f, and L_x that were obtained by matching the curvature of the curve of figure 37 to that of the one to two Hz range of the frequency-response-corrected propeller output and the hot-film anemometer power spectral densities of figures 30 through 33. Also listed is an L_x as obtained from the $S(0) = 4L_x/\bar{U}_{loc}$ criterion for the hot film anemometer power spectral densities of these figures. The discrepancies between the L_x 's obtained by the curve matching and S(0) techniques as indicated

in table 3 for the hot-film anemometer indicate a need to extend power spectral densities to frequencies below one Hz for open channel turbulence. The fact that the curve matching L_x 's obtained from the propeller output power spectral densities are greater than those obtained by the same method from the hot-film anemometer curves indicates that spatial averaging has increased the slopes of the propeller curves relative to those of the hot-film anemometer even in the one to two Hz range.

In figure 38, the following normalized power spectral densities have been plotted for runs 16 through 18: 1) The experimental hot-film anemometer, taken from figures 30 through 33, 2) The empirical hot-film anemometer, determined from $S(0) = 4L_x/\bar{U}_{loc}$, and 3) The empirical hot-film anemometer and the three propeller output velocity, determined from the L_x/\bar{U}_{loc} obtained by the curve fitting procedure.

The empirical curves of figure 38 do not differ markedly in shape or slope from the experimentally observed hot-film anemometer power spectral densities in the one to 25 Hz range. However, as can be seen from the figure, in the range below one Hz, the empirical curves differ considerably from each other. This is due to the difficulty of matching the curvature of the empirical power spectral density to that of the experimental curve when the change in slope is small, and it points out the desirability of working with the strongly curved portion of an experimental propeller output velocity power spectral density when using the curve fitting

technique to determine the parameter L_x/\bar{U}_{loc} . In water flows of the type investigated here, this requires computation of power spectral densities in the range below one Hz. Unfortunately, power spectral densities in this range are not available for the flows used here; obtaining them would require slightly different instrumentation than that used in this study.

No really firm conclusions can be drawn about the usefulness of the curve fitting technique in determining the parameter L_x/\bar{U}_{loc} (and hence the empirical power spectral density) from an experimentally-measured, frequency-response-corrected propeller-output-velocity, power spectral density. Although this technique provided empirical propeller-output-velocity power spectral densities with the same general slope and shape as those of the hot-film anemometer standard, the lower frequency (highly curved) portions of these curves are considerably different from each other. Thus, conclusions as to the validity of this approach must await further investigation where the lower frequency portions of the propeller output velocity power spectral densities are available. The technique is worth developing further, because its use avoids the necessity for extensive simultaneous power spectral density measurement using a flow meter and some point velocity sensor such as a hot film anemometer. Its use might require trial and error least squares curve fitting by a computer as the only practical way to obtain reliable values of the parameter L_x/\bar{U}_{loc} .

C. Turbulent Intensity Recovery

In many cases in which turbulent flow measurements are made, it is only the turbulent intensity \bar{u}' which is necessary, and not the entire power spectral density. It is inconvenient and costly in these cases to have to compute the power spectral density and make inertia and spatial averaging corrections to determine only the intensity, but this must be done if accurate values of this quantity are necessary. Because the inertia and spatial averaging have their greatest effect at the high frequency end of the spectrum (where the energy is low anyway) it might be accurate enough in certain cases to take without correction the turbulent intensity as measured by a propeller flow meter to be the true intensity of the flow.

To determine under what conditions it is permissible not to correct the propeller flow meter measured turbulent intensity for inertia and spatial averaging effects equation 3-50 can be integrated numerically over all f for several values of the parameter L_x/\bar{U}_{loc} at several different mean velocities. In this integration, experimental values of the system function and spectral averaging efficiency can be used along with equation 4-26 for the power spectral density. The square root of the numerical value of the integral will be a fraction less than one; this is the fraction e' of the true intensity which is output by the flow meter. In the case that e' is near unity, it will usually be permissible

to treat the output intensity as the true intensity of the turbulent velocity fluctuations.

In table 4 have been listed the fractions of turbulent intensity output by the flow meter as computed by numerical integration of equation 3-50 for several different values of L_x/\bar{U}_{loc} at several mean velocities. For the L_x/\bar{U}_{loc} and mean velocity range of this study, the recovery ratios range from 0.77 to 0.89. These values are too low to be ignored, but it is seen that for the large range in L_x/\bar{U}_{loc} and mean velocity, the range of the recovery ratios is small. This should allow one to make a reliable estimate of true intensity from the propeller output intensity. The importance of the energy distribution parameter is again seen from table 4, where it is noticed that for the 2-3 propeller at $L_x/\bar{U}_{loc} = 0.17$ the recovery ratio is smaller than for $L_x/\bar{U}_{loc} = 0.11$, even though the spectral recovery efficiency is much higher for the former value of this parameter.

D. Field Measurements of Turbulence

1. Power Spectral Densities

The primary use for propeller meter measurements of turbulence is in field situations where conditions are so severe as to damage a hot-film anemometer probe, or where water conditions are too dirty for its drift free operation. Some preliminary field measurements were made using the propeller flow meter of this study, both for comparison with hot-film anemometer measurements, and to evaluate the performance of the flow meter measuring system in the field.

The only change in instrumentation from that described for the spatial averaging studies was the substitution of a portable Lockheed Model 417 magnetic tape recorder for the CEC magnetic tape recorder.

The measurements were made on the Atrisco feeder canal on the Rio Grande fifteen miles north of Albuquerque, New Mexico. The average flow conditions were:

Depth	= 1.70 ft
Width	= 56 ft
Mean Velocity	= $Q/A = 2.13$ ft/sec
Discharge	= 203 ft ³ /sec
Slope	= 0.00057
Shear Velocity	= .177 ft/sec
Darcy Weisbach f	= 0.055
Mannings n	= 0.024
Bed form	= Ripples and Small Dunes

The vertical at which measurements were taken was twelve feet from the channel center line. The mean velocity in this vertical was 1.59 ft/sec, mean depth was 1.83 ft.

The field measurements were all made with the Ott minor 1-3 propeller. The propeller output velocity power spectral densities for the flow situation described above are given in figure 39. The frequency-response-corrected propeller output velocity power spectral densities are shown by the dashed lines of this figure. Table 5 lists the computations for obtaining the frequency response correction of figure 39a from figures 28 and 29. Hot film anemometer velocity

power spectral densities over a relative depth range corresponding to that of figure 39 are given in figure 40. Table 6 lists the energy distribution coefficients L_x/\bar{U}_{loc} as determined by the curve fitting technique for the runs of figures 39 and 40. Also given in this table are the local mean velocities and the scale parameter d/L_x where applicable.

In table 5 it is noted that for the field measurements the energy distribution parameter L_x/\bar{U}_{loc} of the propeller runs varies from 0.172 to 0.248, while d/L_x varies from 0.26 to 0.35. Except for run 43, which has $L_x/\bar{U}_{loc} = 0.17$ and $d/L_x = 0.35$, all the field measurements have energy distribution parameters considerably greater than those for any of the curves of figure 36, and even for run 43, d/L_x is smaller than the values for the curves of figure 36 which have the same L_x/\bar{U}_{loc} . This makes it impossible to estimate the spatial averaging correction required, however, observing the trend of the variation of the spectral recovery efficiency with L_x/\bar{U}_{loc} in figure 36, it is expected that, with the exception of run 43, little or no correction for spatial averaging should be required for the frequency-response-corrected propeller output velocity power spectral densities. That this is indeed the case can be seen from figure 41 where the frequency-response-corrected power spectral densities of figure 39 have been plotted along with hot film anemometer velocity power spectral densities from the nearest available relative depth. The difference in

the vertical positions of these normalized power spectra is due to the exclusion of frequencies below one Hz from the propeller power spectral density, and not to propeller characteristics. For comparison with the spectral recovery efficiency curves of figure 36, a reference $\eta(f)$ can be computed from the power spectral densities of figure 41. If the one Hz ordinates of the curves of figure 41 are made to coincide, and choosing ten Hz as the reference frequency, the reference spectral recovery efficiencies are:

H.F.A. Run	1-3 Run	$\eta(10)$
12	36	.97
12	37	.60
13	37	.72
15	38	.48
15	43	.58
15	42	.32
16	42	.46

In all but one case, the reference η 's are larger than the $\eta(10) = .41$ of the $L_x/\bar{U}_{loc} = 0.17$, $d/L_x = 0.45$ curve of figure 36, but it is seen that spatial averaging correction is still required even at these large values of L_x/\bar{U}_{loc} .

Using the values of the energy distribution parameter for the propeller runs, as listed in table 6, empirical power spectral densities can be plotted as was done in the preceding section of this chapter. These curves are given in figure 41. The low frequency portions of the empirical curves in most cases agree quite well with the measured hot-film anemometer power spectral densities, however, the

empirical model seems to have a greater slope at the high frequency portions than was measured in the field. It should be determined whether this phenomenon is real, or whether the field set up of the hot-film anemometer measuring system contained noise sources not present in the laboratory set up which would cause the high frequency portions of the hot-film anemometer power spectral densities to register high. If the phenomenon is real, an empirical model can easily be designed to fit this slope, however, from the mechanics of turbulence, it would be expected that $-5/3$ or higher power on the high frequency portion of the power spectral density should be correct.

The results of the field measurements are encouraging in that they indicate that in large scale open channel flows it is possible to accurately measure turbulence using propeller flow meters. The large values of the spectral recovery efficiency obtained indicate that spatial averaging is not a problem in turbulence measurement, using Ott minor propellers, over a large part of the flow depth in channels on the order of three feet deep. The major problem encountered in making these field measurements was propeller stoppage caused by wedging of suspended sediment between the propeller and the meter body or between the body and the propeller shaft. This problem is solvable by making slight meter design changes.

2. Turbulent Intensities

In addition to the power spectral density measurements of this study, several measurements were made in which only longitudinal turbulent intensities were obtained. The measurements were made using the propellers of this study and a Disa 55D35 root-mean-square voltmeter. In several cases, there are available simultaneous hot-film anemometer intensity measurements made using the rms meter and also digitally computed hot-film anemometer intensity measurements.

The use of a propeller flow meter and an analog rms voltmeter to measure turbulent intensities involves two factors which cause measured intensities to be lower than those which actually occur. The first factor is the reduction in turbulent energy output by the propeller meter due to inertial and spatial averaging. The second is the energy loss due to the analog rms meter which has a low frequency cutoff of 0.5 Hz. Neither of these factors can be corrected for, because the exact shape of the power spectral density of the turbulence being measured is unknown. Despite this, it is felt that a brief presentation of this data is in order, especially in light of the scarcity of turbulence data on large scale rough boundary open channel flows.

The first case in which turbulent intensities were measured was in the eight foot flume in the flows for which the spectral recovery efficiencies were measured. The flow conditions are described in table 2 and in section B of

this chapter. The intensity information on these flows has been included in table 7. The voltage root-mean-squares were measured with the Disa rms voltage meter and were converted to turbulent intensities using the method of section E of chapter IV.

Another set of turbulent intensity measurements were made, using the 1-3 propeller, in conjunction with the Atrisco power spectral density measurements of the first part of this section. The average cross-section flow conditions are described there. In addition to the intensities obtained from the rms meter, digitally computed intensities (which obtain the energy of the fluctuations down to zero frequency) have been obtained for the hot-film anemometer runs of this set. The mean velocity and longitudinal relative intensity profiles are presented in figure 42. The mean velocity used as a nondimensionalizing parameter for the relative intensities was the local mean.

A second set of natural open channel turbulent intensity measurements was made on the Rio Grande in the Bernardo Conveyance Channel near Bernardo, New Mexico. The mean cross-section flow conditions were as follows:

Mean depth	2.80 ft
Mean width	68.0 ft
Mean velocity	2.46 ft/sec
Discharge	468 ft ³ /sec
Slope	0.00055
Shear velocity	0.222 ft/sec

Darcy Weisbach f	0.066
Mannings n	0.028
Bed form	Dunes and plane with sediment motion

The measurements were made using the 1-3 propeller and the hot-film anemometer. Both rms meter and digital intensities are reported. The mean velocity and relative intensity profiles are given in figure 43. At the measurement cross-section, the right one-third of the channel was running in dunes of a height of approximately eight to twelve inches. The rest of the channel was in plane bed with sediment motion.

The last set of experimental field turbulent intensity measurements were taken behind a trashrack on the inlet to the number one turbine of the Gavins Point Dam on the Missouri River near Yankton, South Dakota. The inlet is completely submerged, 37 ft high, and 17 ft wide. The bars of the trashrack are 3/4 in. thick and eight in. long in the direction of flow. They are placed parallel to the sidewalls of the inlet and slope back toward the top at seven horizontal to 48 vertical. The measurement section was 28 ft behind the center of the rack. The measurements were taken in a vertical section on the center line of the rack and ranging in elevation from the center to the top of the inlet. Mean velocity and relative intensity information taken with the 1-3 propeller are presented in table 8.

The information of figures 42b and 43b gives an indication of how much of the turbulent energy is lost in the

propeller and rms meter, by comparison of the digitally computed hot-film anemometer and the rms meter measured intensities. The ratio of the rms meter measured to the digitally computed hot-film anemometer intensities can be defined as an efficiency e'' of the propeller-rms meter measuring system. From figures 42b and 43b, values of e'' range from 0.05 at $y/Y = 0.7$ of the center-line Atrisco run to 0.95 at $y/Y = 0.2$ of the center-line Bernardo run. A comparison of the rms meter measured intensities of the hot-film anemometer and the propeller meter for the runs of table 7 and figures 42 and 43 gives an indication of an efficiency e''' of the propeller in recovering the turbulent energy above one-half Hz (the low frequency cutoff of the rms meter). Values of e''' range from 0.1 at $y/Y = 0.7$ of figure 42b to 1.8 for $y/Y = 0.40$ of figure 43c. (This discussion excludes figure 43a where the propeller meter measured intensities are as large as 3.5 times those measured by the hot-film anemometer. This is because at large intensities, the peculiarities of the digital-to-analog converter cause the rms meter to give voltage readings which are too high.) It should be pointed out that part of the difference between propeller and hot-film rms meter measured intensities in any of the runs of figures 42 and 43 could be due to bed form movement in the period between taking the propeller measurements and taking the hot-film measurements. This could be the reason for the e''' values over the lower part of the flow of figure 43c being greater

than one. It is seen that the values of e''' are generally smaller than the e' calculated in table 4. This is because as much as 40 to 50 percent of the turbulent energy of this type of flow is below one-half Hz where the propeller meter is most efficient in energy recovery but below the rms meter low frequency cutoff. It is seen from figures 42 and 43 that the propeller flow meter is considerably more efficient in the lower 0.4 of the flow depth than in the upper 0.6. This indicates that open channel turbulence structure is much coarser in the zero to 0.4 relative depth range. Furthermore, the propeller was much more efficient in the deeper flow of the Bernardo measurements, indicating an increase in open channel turbulence coarseness with flow depth.

A matter open to considerable discussion in Hydraulic Engineering is the extent of the hydraulic equivalency of geometrically similar open channel flows in flumes and in the field. A comparison of the flow conditions for run twelve in the flume to the Atrisco reach on the Rio Grande and for run 18 in the flume to the Bernardo reach on the Rio Grande indicates a rough equivalency in flow depths, velocities, and slopes. Comparison of table 7 with figures 42 and 43 shows that these flow situations also have roughly comparable turbulent relative intensities (8 to 10 percent) at the same relative depth. In this case, at least, flume and field information are equivalent.

As phenomena of interest, with respect to the mechanism of flow in movable boundary open channels, the measured relative intensities of the Atrisco and Bernardo channels on the Rio Grande bear some comment. The bed forms on the Atrisco reach were ripples or small dunes (with a height on the order of 0.1 times the flow depth). The Bernardo channel was running in plane bed over the left two-thirds of the channel; the right one-third was in large dunes (with a height on the order of one-third the flow depth). It is seen from figures 42 and 43 that the relative intensities over the ripples and over the plane bed are about the same order of magnitude (8 to 10 percent) with those over the ripples being slightly larger, while the intensities over the dunes are about twice as large as either of the other two (as high as 16 percent). This reflects the influence of size of bed form in the generation of open channel turbulence.

The intensities measured behind the trashrack and reported in table 8 are probably too low. However, without information on the power spectral density energy distribution of this type of turbulence, it is impossible to say how much too low. The measurements were made in conjunction with a study to determine the effect of trashrack turbulence on the reported mean velocity of large Ott flow meters. Even if these intensities are 50 to 75 percent low, the work of section A-3 of this chapter indicates that the mean velocity misregistration should only be on the order of one percent.

In summary, the dynamic behavior of the propeller-flow system in a spatially-uniform but time-varying velocity field is described by a system function $H(\omega)$ which is determined from sinusoidal input velocity experiments. By solving equations 3-36b for $|M_2|$ and $\cos\gamma$, a generalized system description is developed. The functions $|M_2|/\bar{U}^k = m(\nu)$ and $\cos\gamma = n(\omega)$ are general for a particular propeller in that $|H|$ and ϕ need only be measured for one mean velocity in order that they can be computed for all mean velocities. The solution of equation 3-16 for M_2 describes, at least qualitatively, the variation of the natural frequency of a propeller with \bar{U} , ρ' , l , and R_i and R_o . The natural frequencies or cutoff frequencies of the propellers of this study range from 2.55 Hz to 8.36 Hz, depending on propeller and mean velocity. The natural frequencies of propellers of similar geometry to those of this study could be increased by decreasing the density ratio ρ' . The spectral recovery efficiency of a particular flow is determined from equation 4-12, where the point-velocity spectrum is measured by a hot-film anemometer. The value of the spectral recovery efficiency is found to depend on a propeller diameter scale factor, d/L_x and an energy distribution parameter L_x/\bar{U}_{loc} . The need for computation of the spectral recovery efficiency is removed if an empirical power spectral density can be fit to the low frequency portions of the frequency-response-corrected propeller output velocity power spectral density. Using the empirical power spectral

density, the experimental system function, and the experimental spectral recovery efficiency, the recovery of the turbulent intensity \bar{u}' is shown to be on the order of 85 percent for the propellers of this study. For the field runs, the frequency-response-corrected propeller output velocity power spectral densities compare quite well to those measured with the hot-film-anemometer. The energy distribution parameters L_x/\bar{U}_{loc} are larger in the field runs than for the geometrically comparable flume runs (0.20 sec as compared to 0.12 sec), but the length scales L_x are about the same (0.35 ft). The field relative intensities over ripple beds and plane beds with movement are about equal to those in the flume runs (eight to ten percent), but those over large dunes are larger (as high as sixteen percent).

Chapter VI

SUMMARY AND CONCLUSIONS

As is well known to Hydraulic Engineers, there is currently a great need for reliable turbulence measurements in large scale open channel flows. An instrument which has the required ruggedness and portability for making field measurements is the propeller flow meter. The limitations of the propeller flow meter for making turbulence measurements are its low frequency response and its spatial averaging characteristics. The objectives of this study were to evaluate these two characteristics of propeller flow meters and to use this knowledge to obtain reliable field turbulence measurements.

A differential equation of motion for propellers was developed which gives a qualitative indication of the system behavior when subjected to a uniform fluctuating velocity field superimposed on a mean flow velocity. A correlation function was developed from the equation of motion which gives the spatial averaging characteristics of a propeller in a particular flow field if the statistical properties of the turbulence are known. Experimental evaluations of both the system functions and spatial averaging characteristics of particular propellers were made, and the results were applied to field turbulence measurements with encouraging results.

Conclusions which can be drawn from this study are:

1. If a propeller system function $H(\omega)$, which describes the response of the propeller-flow system to a spatially-uniform fluctuating velocity field, and its spectral recovery efficiency $\eta(\omega)$ for a particular type of turbulent flow field, are known, the input power spectral density of the turbulent flow field can be found from the propeller output power spectral density using

$$S_{00}(\omega) = |H(\omega)|^2 \eta(\omega) S_{11}(\omega). \quad (6-1)$$

2. The derived equation of motion

$$\frac{dm}{dt} + M_2 m = M_2 u' + M_7 \frac{du'}{dt} \quad (6-2)$$

describes the behavior of the propeller-flow system when the propeller is subjected to a spatially-uniform, time-varying flow field. The coefficient M_2 is the complex natural frequency of the propeller-flow system. Its magnitude is directly proportional to the mean velocity, and it is frequency dependent. For the propellers of this study, its behavior is given in figures 28 and 29. The coefficient M_7 is the acceleration sensitivity of the propeller.

3. Sinusoidal excitation experiments indicate that the acceleration sensitivity M_7 in equation 6-2 is negligible; thus the behavior of the propeller flow system is governed by the complex natural frequency M_2 .

4. The sinusoidal excitation experiments yield generalized functions $M_2/\bar{U}^{\frac{1}{2}} = m(v)$ and $\cos\gamma = \eta(\omega)$ which can be

used through equations 3-36b to give the behavior of the system function $H(\omega)$ with mean velocity \bar{U} and angular excitation frequency ω .

5. Equation 3-16 gives an estimate of the variation of the quantity $|M_2|$, which is the magnitude of the complex natural frequency of the propeller, with propeller pitch, radius, blade length, density, and number of blades.

6. Propeller design for high frequency response involves increasing the magnitude of the complex natural frequency $|M_2|$. This quantity can be increased by decreasing ρ' the propeller to fluid mass density ratio, and by decreasing the product ℓB where ℓ is the blade chord and B is a propeller calibration constant which is directly proportional to propeller pitch.

7. Propeller cutoff frequencies for the propellers of this study range from 2.55 Hz for the 1 and 1-3 propellers at 2.0 ft/sec to 8.36 Hz for the 2-3 propeller at 5.0 ft/sec. By constructing these propellers of a plastic such as Lucite or Plexiglass, with a density ratio $\rho' = 1.2$, these values could be raised to 5.73 Hz for the 1 and 1-3 propellers at 2.0 ft/sec and to 18.28 Hz for the 2-3 propeller at 5.0 ft/sec.

8. Step input experiments, while not capable of giving the entire system function, do yield a parameter which appears to be related to mean velocity in the same way as the natural frequency defined by the $|H(\omega_n)| = 0.707$ criterion of the sinusoidal input experiments.

9. The propellers tested here and those tested by Chaix (1962) over register the mean flow velocity when subjected to turbulent velocity fluctuations. The over registration is proportional to the square of the relative intensity of the turbulence, as predicted by Plate (1967). For the propellers tested here, the over registration does not exceed one percent until \bar{v}'/\bar{U} exceeds 0.2 for the number 1 and 0.1 for the number 1-3 propeller.

10. The spectral recovery efficiencies of Ott minor propellers 1, 1-3, and 2-3 have been found, for a rough boundary open channel flow, to be highly dependent on L_x/\bar{U}_{loc} an energy distribution parameter of the power spectral density, and to a lesser extent on the ratio of the propeller diameter to the turbulent length scale L_x .

11. The fitting of empirical power spectral density curves to the low frequency portions (the portions assumed to be undistorted by spatial averaging) of the frequency-response-corrected propeller output velocity power spectral densities is a promising method for obtaining turbulent velocity power spectral densities without having to correct directly for spatial averaging.

12. The recovery of the longitudinal intensities using propeller flow meters generally exceeds 75 percent in the open channel flows encountered in this study, even without correcting for the spatial and inertial averaging effects in the spectrum. This is due to the tendency of open channel flow turbulence to concentrate large amounts of energy at low frequencies.

13. Field measurements of turbulence are relatively easily and accurately obtainable from propeller flow meter measurements if corrections for inertia and spatial averaging, as developed in this study, are employed.

The power spectral density runs on the Atrisco Feeder Canal above Albuquerque, New Mexico, on the Rio Grande, gave relatively larger energy distribution parameters L_x/\bar{U}_{loc} (0.20 sec) than those obtained in a geometrically comparable flume run (0.12 sec), however these macro scales L_x were about the same (0.35 ft). The field longitudinal relative intensities (Atrisco and in the Bernardo Conveyance Channel near Bernardo, New Mexico on the Rio Grande) over ripple beds and plane beds with motion were roughly equal to those measured in the flume runs (\bar{u}'/\bar{U} equal to eight to ten percent), however those over the large dunes (Bernardo) were larger (\bar{u}'/\bar{U} as high as sixteen percent).

Chapter VII

SUGGESTIONS FOR FURTHER RESEARCH

1. One fruitful field for further research would be in the design of propellers for high frequency response. It is suspected that reducing both propeller size and density and increasing pitch should increase sensitivity.

2. It is necessary that the range of the energy distribution parameter for which spectral recovery efficiencies are available be extended. It would be interesting to see if the spectral recovery efficiency ever becomes unity for the entire range of frequencies.

3. A further development of the curve fitting technique involving extension of the power spectral densities to lower frequencies would probably be profitable. Using this approach, it might be possible to avoid using not only the spatial averaging correction but also the inertia correction for certain propellers at high mean velocities.

4. Further work could also be done in measuring the Reynolds stresses using two propeller flow meters or using a rotation technique similar to that used by McQuivey (1967) for hot film anemometers.

5. In really large scale flows, such as the Mississippi river, two propeller flow meters could be used to obtain lateral scales, or space time correlations as was done by Baldwin and Mickelsen (1963), in a turbulent pipe flow using hot wire anemometers.

6. The extreme dependency of the spectral recovery efficiency on the power spectral density energy distribution parameter L_x/\bar{U}_{10c} suggests that it might be interesting to determine the variation of other turbulent flow quantities with this parameter. For example, it is surmised that L_x/\bar{U}_{10c} might vary considerably with the bed form of open channel flow, and that turbulent diffusion and sediment transport might be highly dependent on this parameter.

LITERATURE CITED

LITERATURE CITED

- Aksoy, Sahap; "Measurement Methods of Macroturbulence"; Proceedings 12th Congress IAHR, Vol. II; Colorado State University, Fort Collins, Colo.; September, 1967.
- Baldwin, L.V. and W.R. Mickelsen; "Turbulent Diffusion and Anemometer Measurements"; Transactions ASCE, Vol. 128, Part I; 1963.
- Bendat, Julius S. and Allan G. Piersol; Measurement and Analysis of Random Data; John Wiley and Sons; New York; 1966.
- Bracewell, Ron; The Fourier Transform and its Applications; McGraw-Hill Book Company; New York; 1965.
- Brush Instruments; "Operation Instructions Brush Recorder Mark 280"; Brush Instruments; 37th and Perkins, Cleveland 14, Ohio; Undated.
- Carter, R.W. and I.E. Anderson; "Accuracy of Current Meter Measurements"; Journal of the Hydraulics Division ASCE, Vol. 4, No. 4; July, 1963.
- Castex, L. and E. Carvounas; "Influence of Turbulence on Current Meter Flow Measurements in a Free-Flowing Channel"; ICMG Report No. 13; International Current Meter Group; Glasgow, Scotland; 1962.
- Cermak, J.E. and L.V. Baldwin; "Measurement of Turbulence in Water by Electrokinetic Transducers"; Fluid Mechanics Papers No. 2; Colorado State University, Fort Collins, Colo.; April, 1964.
- Chaix, B.; "Field and Laboratory Tests Concerning the Effect of Turbulence on Various Current Meters"; Translation No. 66-15; U.S. Army Corp of Engineers; Originally ICMG Report No. 9; February, 1962.
- Chuang, Hsing and J.E. Cermak; "Electrokinetic-Potential Fluctuations Produced by Pipe-Flow Turbulence"; Civil Engineering Department, Colorado State University; Fort Collins, Colo.; 1964.
- Chuang, Hsing and Jack E. Cermak; "Turbulence Measured by Electrokinetic Transducers"; Journal of the Hydraulics Division ASCE, Vol. 91, HY6; November, 1965.
- Consolidated Electrodynamics Corp.; "PR-3300 Magnetic Tape Recorder-Reproducer"; Consolidated Electrodynamics Corp.; 360 Siera Madre Villa, Pasadena, Calif.; Undated.

- Dell'Osso, Luino, Jr.; Turbulence Measurements in Water in an Open Channel with the Hot Film Anemometer; Ph.D. Dissertation, Rice University; Houston, Texas; May, 1966.
- Eagleson, P.S. and F.E. Perkins; "A Total Head Tube for the Broad-Band Measurement of Turbulent Velocity Fluctuations in Water"; Proceedings IAHR 9th Convention; Dubrovnik, Yugoslavia; 1961.
- Frenkiel, F.N.; "Effects of Wire Length in Turbulence Investigations with a Hot-Wire Anemometer"; The Aeronautical Quarterly, Vol. 5; May, 1954.
- Glauert, H.; "Airplane Propellers"; Aerodynamic Theory, Ed. by W.F. Durand, Vol. 4; Dover Publications Inc.; New York; 1963.
- Goldstein, S.; Modern Developments in Fluid Dynamics, Vol. 1; Dover Publications Inc.; New York, 1965.
- Groat, B.F.; "Characteristics of Cup and Screw Current Meters"; Transactions ASCE, Vol. 76, 1913.
- Grossman, L.M., H. Li, and H.A. Einstein; "Turbulence in Civil Engineering: Investigations in Liquid Shear Flow by Electromagnetic Induction"; Journal of the Hydraulics Division ASCE, Vol. 83, HY5, October, 1957.
- Hartung, Fritz and Klausotto Csallner; "Experience with Turbulence Meters and Their Improvement"; Proceedings 12th Congress IAHR, Vol. 2; Colorado State University; Fort Collins, Colo., September, 1967.
- Hewlett-Packard; "Operating and Service Manual 580A/581A Digital-Analog Converter"; Hewlett Packard Co.; Palo Alto, Calif.; 1964.
- Hewlett Packard; "Operating and Service Manual 5212A/5512A Electronic Counter"; Hewlett Packard Co.; Palo Alto, Calif.; 1963.
- Hewlett Packard; "Operating and Service Manual Model 500B Electronic Frequency Meter"; Hewlett Packard Co.; Palo Alto, Calif.; 1955.
- Higson, D.J.; "The Transient Performance of a Turbine Flow Meter in Water"; Journal of Scientific Instruments, Vol. 41, No. 5; May, 1964.
- Hinze, J.O.; Turbulence; McGraw-Hill Book Co. Inc.; New York; 1959.

- Ishihara, Yasuo and Shoitiro Yokosi; "The Spectra of Turbulence in a River Flow"; Proceedings 12th Congress of IAHR, Vol. 2; Colorado State University; Fort Collins, Colo.; September, 1967.
- Iwasa, Yoshiaki and Hirotake Imamoto; "Turbulence Measurement by Means of Small Current Meter in Free Surface Flow"; Proceedings 12th Congress of IAHR Vol. 2; Colorado State University; Fort Collins, Colo.; September, 1967.
- Ippen, A.T. and F. Raichlen; "Turbulence in Civil Engineering: Measurement in Free Surface Streams"; Journal of the Hydraulics Division ASCE Vol. 83, HY5, October, 1957.
- Jacobs, Eastman; "Experimental Methods-Wind Tunnels"; Aerodynamic Theory, Ed. by W. F. Durand, Vol. 3; Dover Publications Inc., New York, 1963.
- Jepson, P.; "Transient Response of a Helical Flow Meter"; Journal of Mechanical Engineering Science, Vol. 6, No. 4; 1964.
- Jezdinsky, Valdimir, Jan Cakrt, Miroslav Rudis, and Rados Smutek; "Macro-Turbulence Measurements in Natural Streams"; Proceedings 12th Congress of IAHR, Vol. 2, Colorado State University, Fort Collins, Colo., September, 1967.
- Kalinske, A.A.; "The Role of Turbulence in River Hydraulics"; Proceedings of the Second Hydraulics Conference, Bulletin 27; University of Iowa Studies in Engineering; Iowa City, Iowa; 1943.
- Kalinske, A.A. and C.L. Pien; "Eddy Diffusion"; Industrial and Engineering Chemistry, Vol. 36; American Chemical Society, 1155 Sixteenth Street N.W., Washington, D.C., 1944.
- Kemp, P.H. and A.J. Grass; "The Measurement of Turbulent Velocity Fluctuations Close to a Boundary in Open Channel Flow"; Proceedings 12th Congress of IAHR, Vol. 2; Colorado State University, Fort Collins, Colo., September, 1967.
- Lee, Y.W.; Statistical Theory of Communication; John Wiley and Sons Inc., New York, 1960.
- Ling, S.C. and P.G. Hubbard; "The Hot-Film Anemometer: A New Device for Fluid Mechanics Research"; Journal of Aeronautical Science, Vol. 23, 1956.

- Lumley, J.L.; "The Constant Temperature Hot-Thermistor Anemometer"; Symposium on Measurement in Unsteady Flows ASME; New York; 1962.
- McQuivey, Raul S.; Turbulence in a Hydrodynamically Rough and Smooth Open Channel Flow; Ph.D. Dissertation, Colorado State University, Fort Collins, Colo., August, 1967.
- Plate, Erich J.; "The Effect of Axial Velocity Fluctuations on the Response of a Helical Flow Meter"; Proceedings 12th Congress IAHR, Vol. 2; Colorado State University; Fort Collins, Colorado, September, 1967.
- Plate, E.J. and J.P. Bennett; "The Propeller Flow Meter as a Turbulence Sensor"; Submitted to the Journal of the Hydraulics Division ASCE; July, 1968.
- Raichlen, Fredric; "Some Turbulence Measurements in Water"; Journal of the Engineering Mechanics Division, Vol. 93, No. EM2; April, 1967.
- Richardson, E.V. and R.S. McQuivey; "Measurement of Turbulence in Water"; Journal of the Hydraulics Division ASCE, Vol. 94, No. HY2, March, 1968.
- Richardson, E.V., R.S. McQuivey, V.A. Sandborn, and P.M. Jog; "Comparison between Hot-Film and Hot-Wire Measurements of Turbulence"; Proceedings 10th Midwestern Mechanics Conference; Colorado State University, Fort Collins, Colo.; August, 1967.
- Roesner, L.A. and V.M. Yevdjevich; "Mathematical Models for Time Series of Precipitation and Monthly Runoff"; Hydrology Papers, No. 15; Colorado State University, Fort Collins, Colo.; October, 1966.
- Schraub, F.A., S.J. Kline, J. Henry, P.N. Runstadler, and A. Littell; "Use of Hydrogen Bubbles for Quantitative Determination of Time Dependent Velocity Fields in Low Speed Water Flows"; Stanford University, Department of Mechanical Engineering, Thermosciences Division, Report MD-10; Stanford, California, 1964.
- Schuyf, J.P.; "The Measurement of Turbulent Velocity Fluctuations with a Propeller-Type Current Meter"; The Journal of Hydraulic Research, Vol. 5, No. 2; 1966.
- Sears, W.R.; Theoretical Aerodynamics, Part I: "Introduction to Theoretical Hydrodynamics"; Cornell University; Ithaca, New York, 1960.
- Sears, W.R.; "Some Aspects of Non-Stationary Airfoil Theory and its Practical Application"; Journal of the Aeronautical Sciences, Vol. 8, No. 3; January, 1941.

Sears, W.R.; "Some Aspects of Non-Stationary Airfoil Theory and its Practical Application"; Journal of the Aeronautical Sciences, Vol. 8, No. 3, January, 1941.

Tiffany, Joseph B.; "Turbulence in the Mississippi River"; Proceedings 12th Congress of IAHR, Vol. 2; Colorado State University, Fort Collins, Colo., September, 1967.

von Karman, Th.; "Progress in the Statistical Theory of Turbulence"; Journal of Marine Research, Vol. 7, 1948.

von Karman, Th. and W.R. Sears; "Airfoil Theory for Non-Uniform Motion"; Journal of the Aeronautical Sciences, Vol. 5, No. 10, August, 1938.

Waterloopkundig Laboratorium; "Propeller Current Meter and Mimosa Apparatus"; Waterloopkundig Laboratorium; Delft, Holland; Undated.

APPENDIX I

TABLES

Table 1. Important terms in the calculation of the complex natural frequency M_2 .

	1	1-3	2-3
R_i	.0152 ft	.0152 ft	.0152 ft.
R_o	.0815 ft	.0498 ft	.0482 ft
l_h	.133 ft	.133 ft	.132 ft
l	.294 ft	.207 ft	.134 ft
t_b	.007 ft	.0062 ft	.005 ft
B	.00608 ft/ cycle	.00628 ft/ cycle	.012 ft/ cycle
s	2	3	3
$2\rho'J$	$4.08 \times 10^{-6} \text{ ft}^5$	$8.94 \times 10^{-7} \text{ ft}^5$	$4.55 \times 10^{-7} \text{ ft}^5$
$C_1 = 1.0$			
$\frac{SC_1\pi}{2} \int_{R_i}^{R_o} (lr \cos\theta)^2 dr$	$9.75 \times 10^{-6} \text{ ft}^5$	$3.26 \times 10^{-6} \text{ ft}^5$	$2.09 \times 10^{-6} \text{ ft}^5$
$\frac{2\pi SB}{\bar{U}^2} \int_{R_i}^{R_o} lr^2 \cos\theta dr$	$\frac{1.79 \times 10^{-6} \text{ ft}^5}{\bar{U}^2}$	$\frac{6.14 \times 10^{-7} \text{ ft}^5}{\bar{U}^2}$	$\frac{8.82 \times 10^{-7} \text{ ft}^5}{\bar{U}^2}$
M_2	$21.30 \bar{U}C(v)$	$23.55 \bar{U}C(v)$	$28.90 \bar{U}C(v)$

Table 2. Flow parameters of spectral recovery runs.

Run	Depth D (ft)	$\frac{y}{D}$	Slope S	Q/A (ft/sec)	\bar{U}_{local} (ft/sec)	$U_* = \sqrt{gDS}$ (ft/Sec)	L_x (ft)
12	1.33	.7	.00048	.98	1.26	.144	.22
16	1.33	.7	.00457	2.91	3.92	.443	.49
17	1.33	.4	.00457	2.91	3.47	.443	.38
18	2.50	.7	.00116	2.34	2.62	.304	.46

Table 3. Length scales from the power spectral densities of runs 12, 16, 17, and 18.

Run Number	Probe	P at f=1.50	$L_x = \frac{\bar{U}_{loc}^p}{4f}$ (ft)	$L_x = \frac{S(0)\bar{U}_{loc}}{4}$ (ft)
12	Hot film	1.04	.22	.89
	1	--	--	
	1-3	--	--	
16	Hot film	.76	.49	1.10
	1	1.65	1.08	
	1-3	1.40	.92	
	2-3	1.12	.73	
17	Hot film	.66	.38	.48
	1	.98	.57	
	1-3	.67	.39	
	2-3	1.03	.60	
18	Hot film	1.01	.44	1.26
	1	1.40	.61	
	1-3	1.32	.58	
	2-3	1.55	.68	

Table 4. Calculated turbulent intensity recovery ratios.

Propeller	\bar{U}_{loc} (ft/sec)	L_x/\bar{U}_{loc} (sec)	e'
1	2.0	.11	.77
1	2.0	.17	.79
1	3.2	.11	.79
1	3.2	.17	.80
1	5.0	.11	.82
1	5.0	.17	.82
2-3	2.0	.11	.87
2-3	2.0	.17	.84
2-3	5.0	.11	.89
2-3	5.0	.17	.85

Table 5. Computation of frequency response correction for $\bar{U} = 1.68$ ft/sec,
1-3 propeller.

f (Hz)	ω ($\frac{\text{rad}}{\text{sec}}$)	ω/\bar{U} (1/ft)•	$ M_2 /\bar{U}^{\frac{1}{2}}$ ($\frac{1}{\text{ft}/\text{sec}}$) $^{\frac{1}{2}}$	$\cos^2 \gamma$	$-\sin \gamma$	$ M_2 $ ($\frac{\text{rad}}{\text{sec}}$)	$\frac{\omega}{ M_2 }$	$\sin \gamma + \frac{\omega}{ M_2 }$	$\frac{1}{ H ^2}$
1	6.28	3.74	7.87	.979	.145	10.21	.615	.470	1.20
1.5	9.43	5.61	8.85	.965	.187	11.48	.821	.634	1.37
2	12.56	7.49	9.45	.946	.232	12.26	1.023	.791	1.58
3	18.87	11.22	10.28	.890	.332	13.32	1.416	1.084	2.08
5	31.40	18.70	11.62	.786	.462	15.08	2.080	1.618	3.42
7	44.00	26.20	12.85	.655	.587	16.65	2.642	2.055	4.92
10	62.80	37.40	14.40	.400	.774	18.67	3.362	2.588	7.16
12	75.40	44.90	15.60	.208	.884	20.22	3.728	2.844	8.34

Table 6. Energy distribution coefficients and propeller diameter-length scale ratios for figures 39 and 40.

Run No.	Probe	y/D	P at f=1.5	L_x/\bar{U}_{loc} (sec)	\bar{U}_{loc} (ft/sec)	L_x (ft)	d/ L_x
36	1-3	.94	1.06	.18	1.68	.30	.34
12	H.f.a.	.87	1.22	.20	1.66	.34	
37	1-3	.80	1.26	.21	1.63	.34	.29
13	H.f.a.	.77	1.00	.17	1.64	.27	
38	1-3	.67	1.33	.22	1.47	.33	.31
43	1-3	.66	1.03	.17	1.68	.29	.35
15	H.f.a.	.65	.62	.10	1.64	.17	
42	1-3	.58	1.49	.25	1.54	.38	.26
16	H.f.a.	.45	1.02	.17	1.56	.27	

Table 7. Turbulent relative intensities from a rms voltmeter, flume runs.

Run No.	Slope	Depth (ft)	y/D	\bar{U} (ft/sec)	Probe	\bar{u}'/\bar{U} Percent
12	.00048	1.33	.7	1.26	H.f.a.	8.1
					1	3.1
					1-3	3.3
16	.00457	1.33	.7	3.92	H.f.a.	7.8
					1	5.0
					1-3	5.0
					2-3	4.9
17	.00457	1.33	.4	3.47	H.f.a.	12.8
					1	5.9
					1-3	6.9
					2-3	9.2
18	.00116	2.50	.7	2.62	H.f.a.	7.2
					1	3.3
					1-3	4.1
					2-3	4.7

Table 8. Propeller-rms meter turbulent intensities behind a trashrack, Gavins Point Dam.

$y/\frac{1}{2}H$	\bar{U} (ft/sec)	\bar{u}'/\bar{U}
0.9	4.89	6.3
	4.89	3.3
0.86	4.89	1.2
	4.89	3.1
0.04	5.29	3.2
	5.29	5.1
	4.89	6.7
0.0	5.08	2.6
	5.08	4.5
	5.53	3.0
	5.29	3.1

APPENDIX II

FIGURES

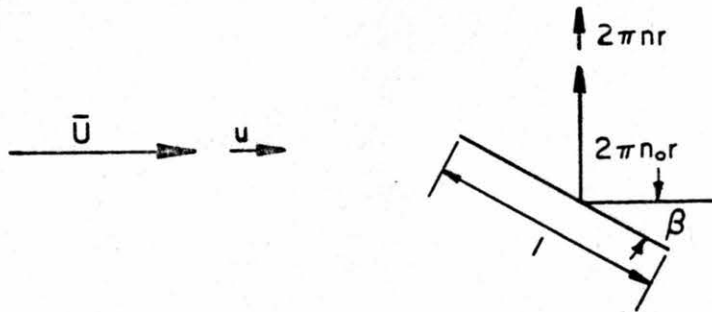


Fig. 1. Flow situation at a propeller blade element.

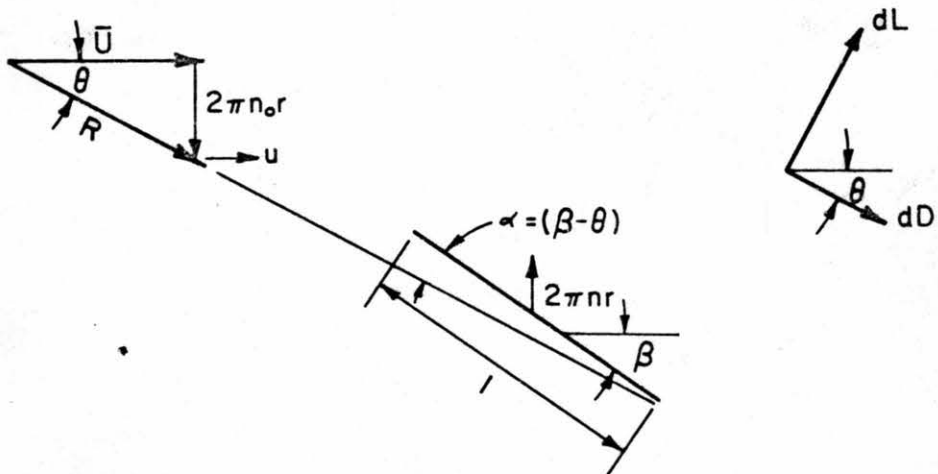


Fig. 2. Flow situation at a propeller blade element with a transverse velocity of $-2\pi n_0 r$ superimposed.

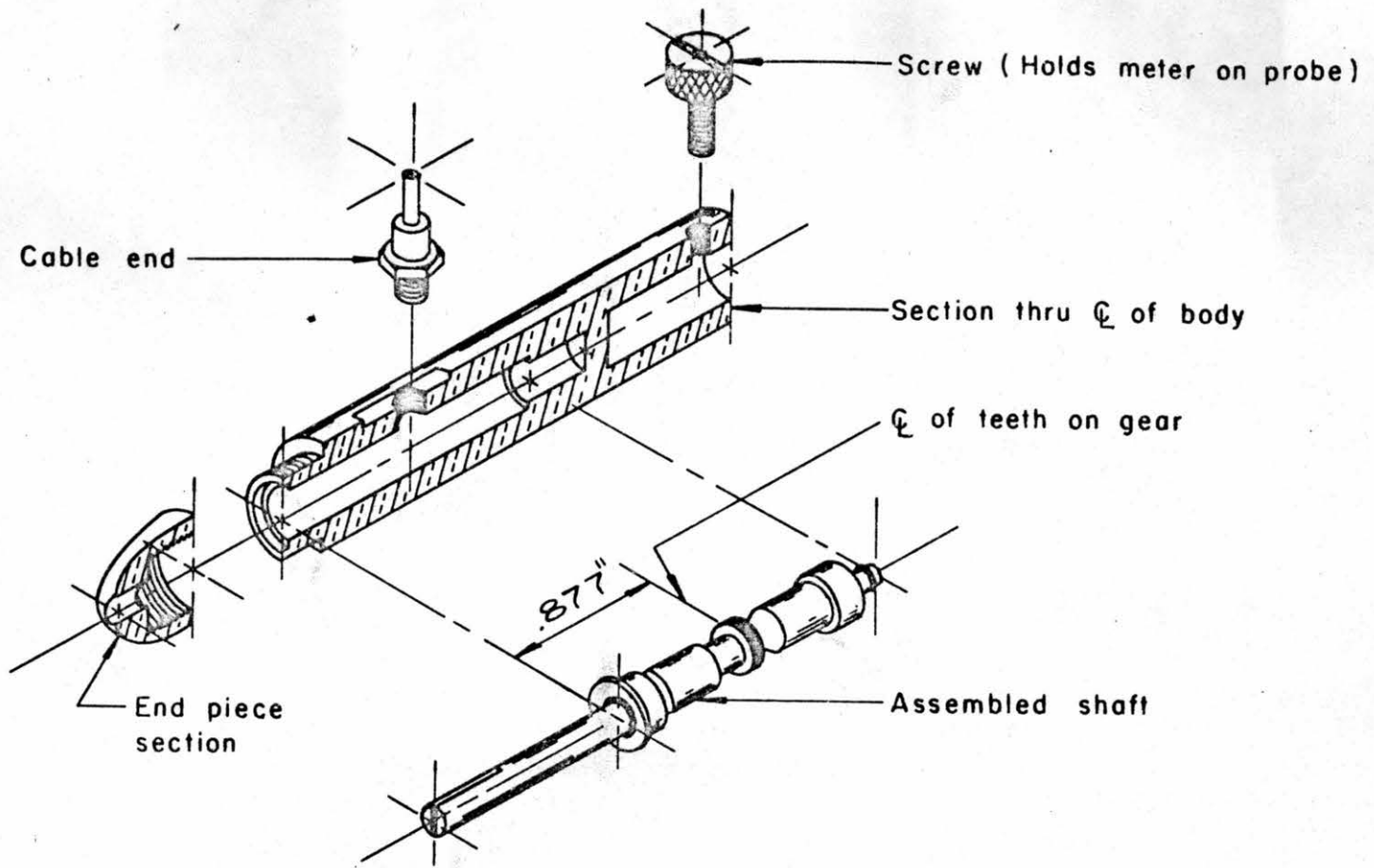


Fig. 3. Meter body.

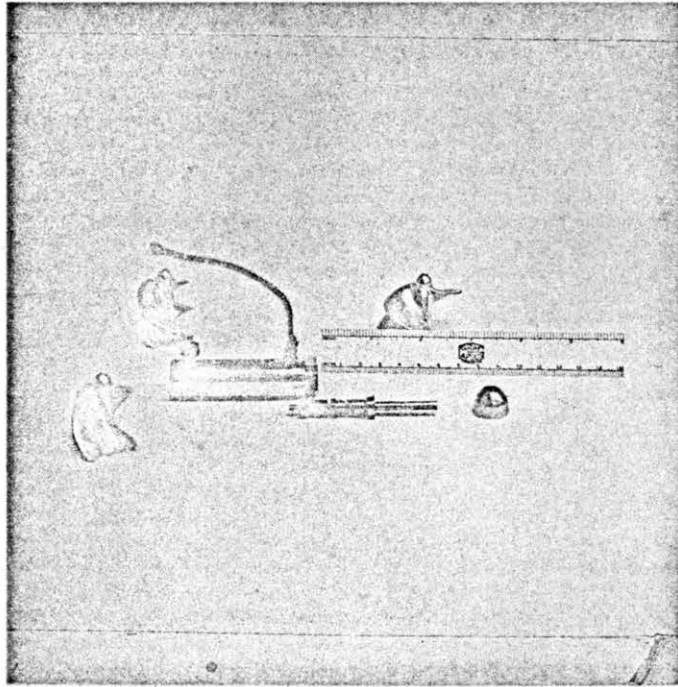


Figure 4.--Propellers and meter body.

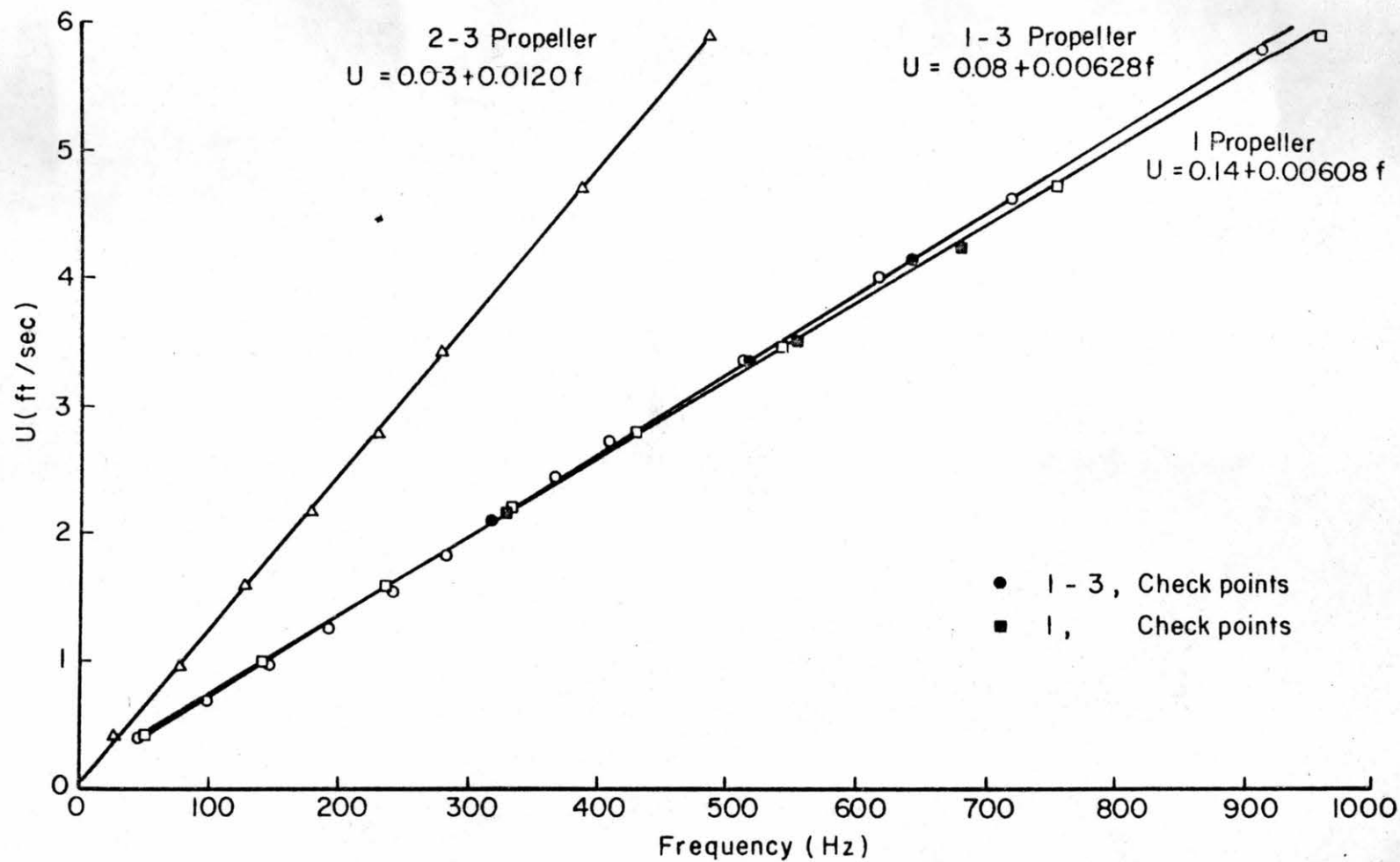


Fig. 5. Propeller mean velocity calibration curves.

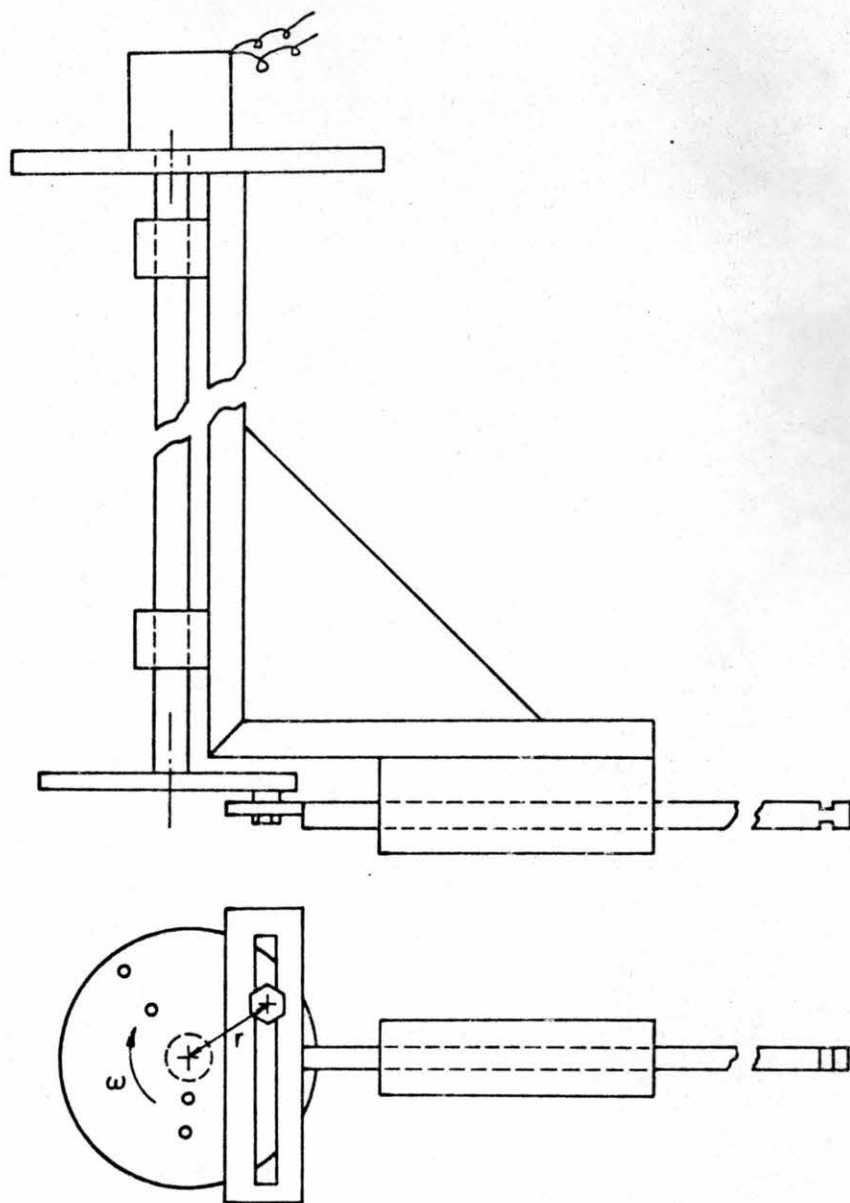


Fig. 6. Schematic of the sine motion generator.

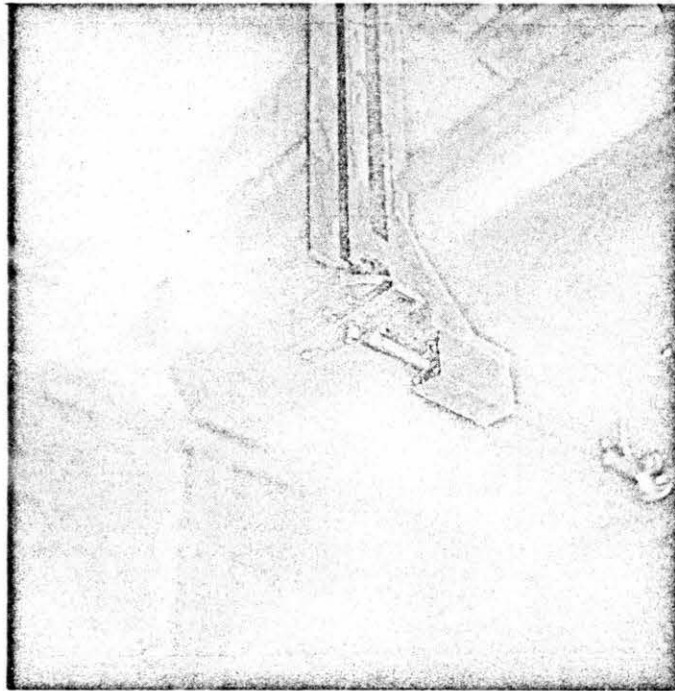


Figure 7.--Bottom view of sine motion generator.

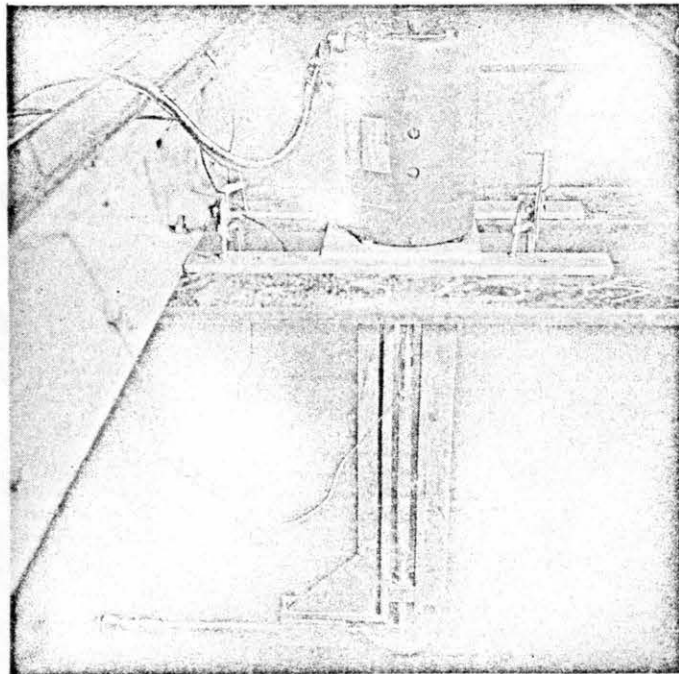


Figure 8.--Side view of sine motion generator.

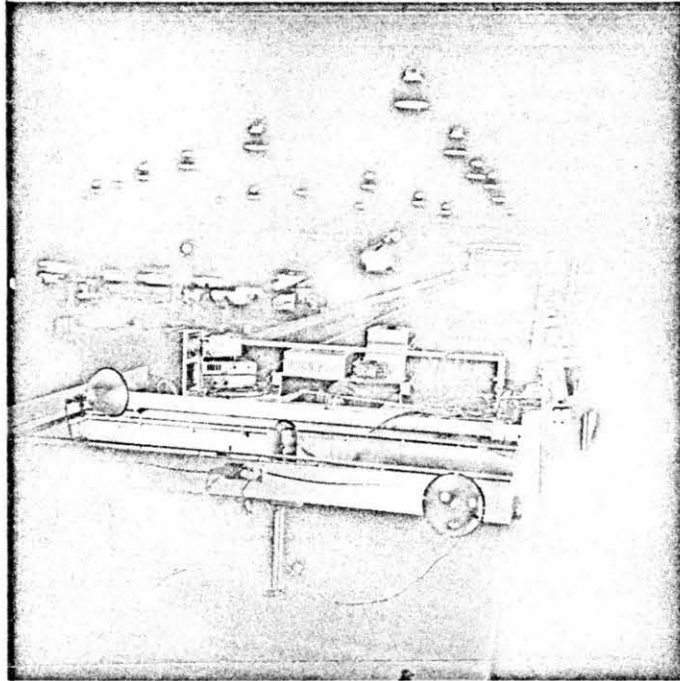


Figure 9.--Towing tank and instrument cart.

Chart Speed $S = 50 \text{ mm/sec}$

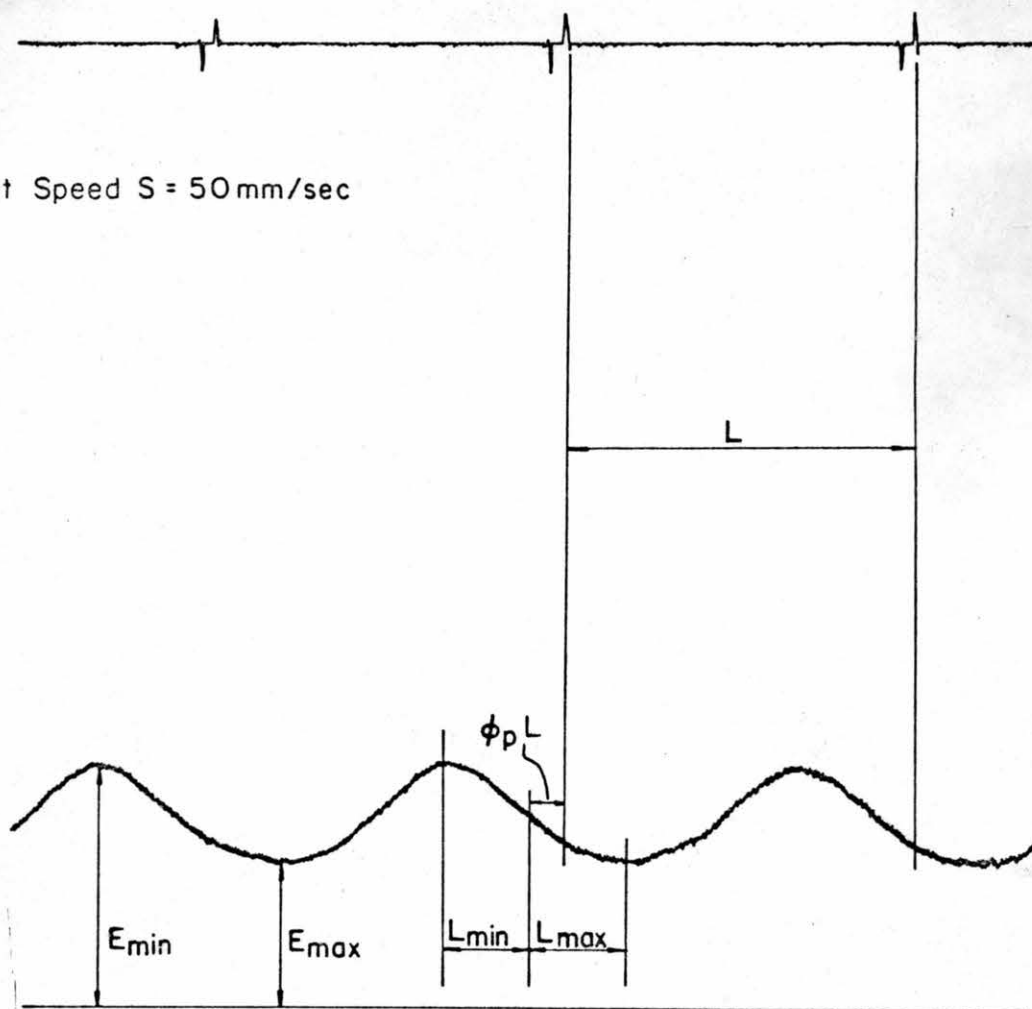


Fig. 10. Typical sine excitation output velocity-position record.

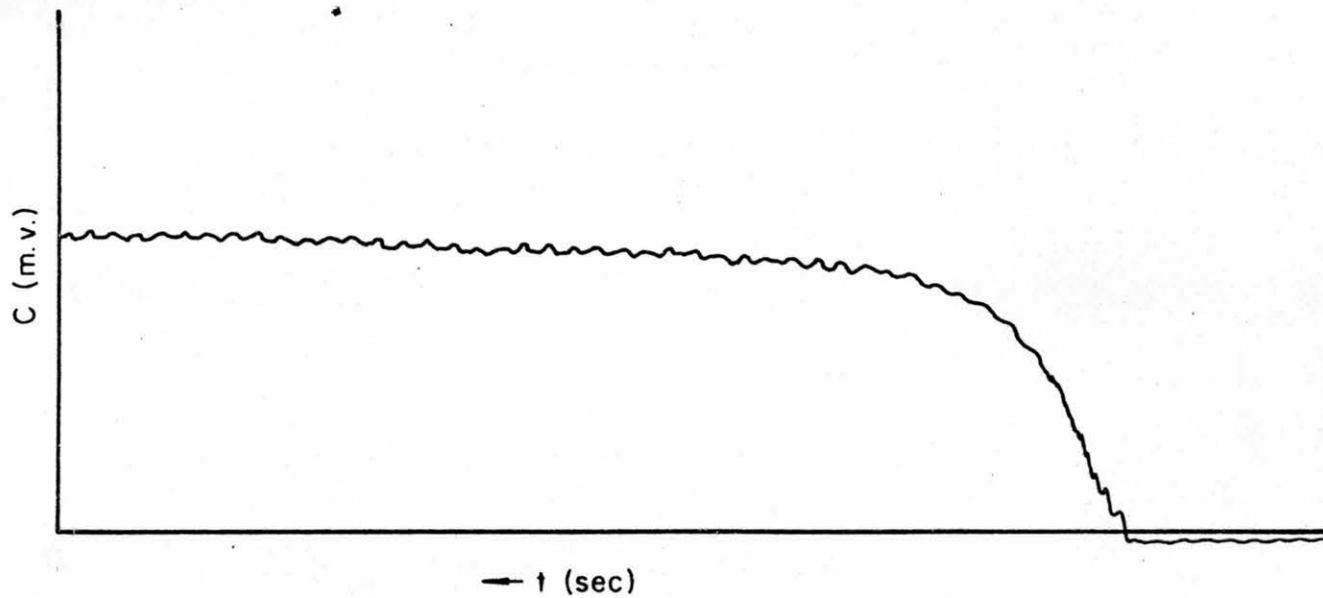


Fig. 11. Typical step-input excitation output record.

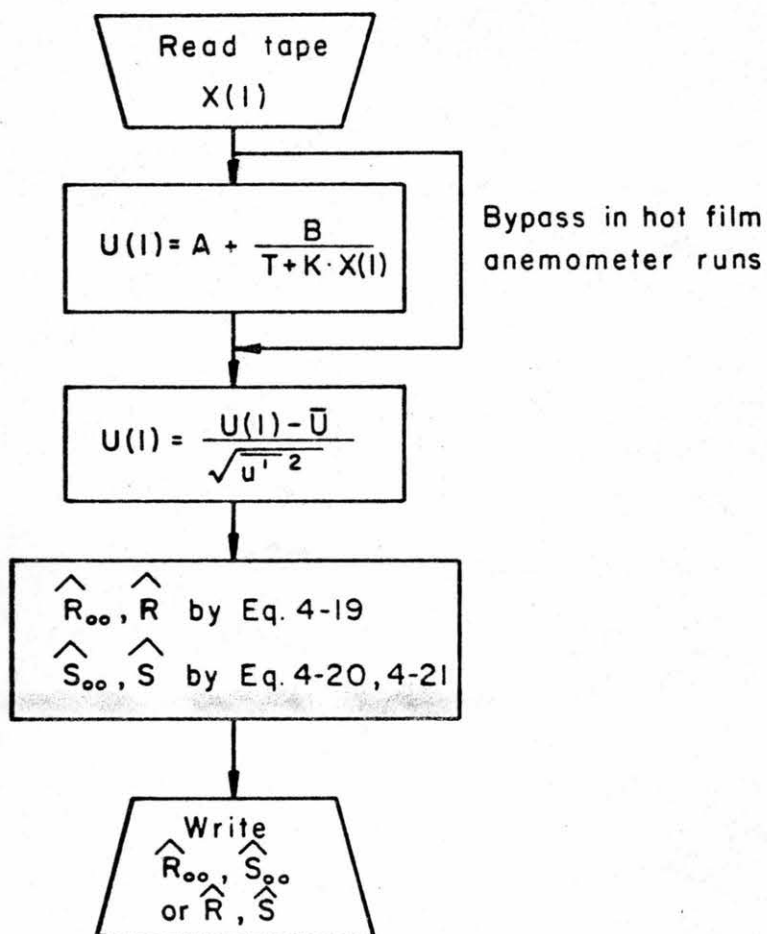


Fig. 12. Simplified flow chart of computer program for spectral recovery efficiency data analysis.

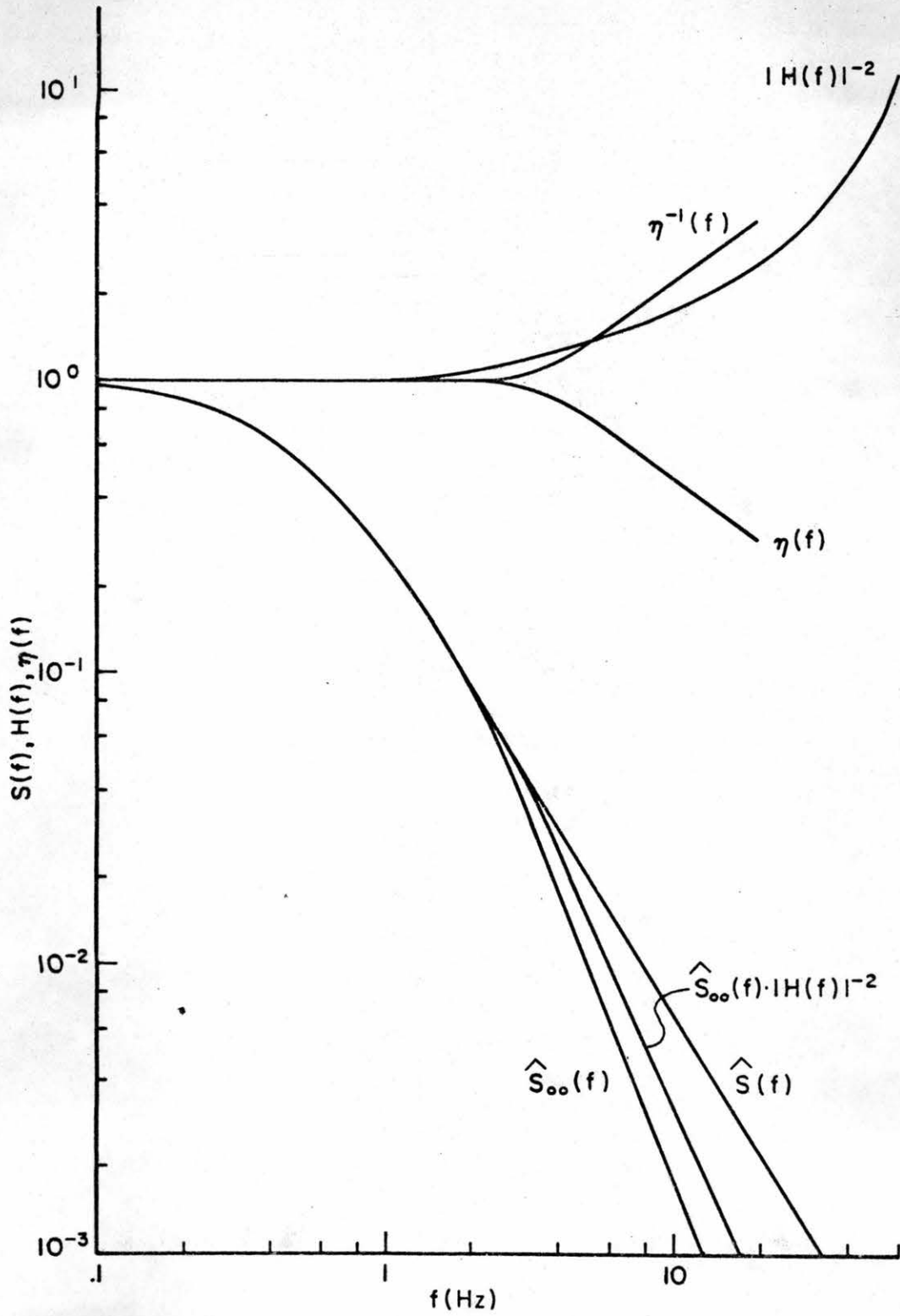


Fig. 13. Example of graphical construction of $\eta(f)$.

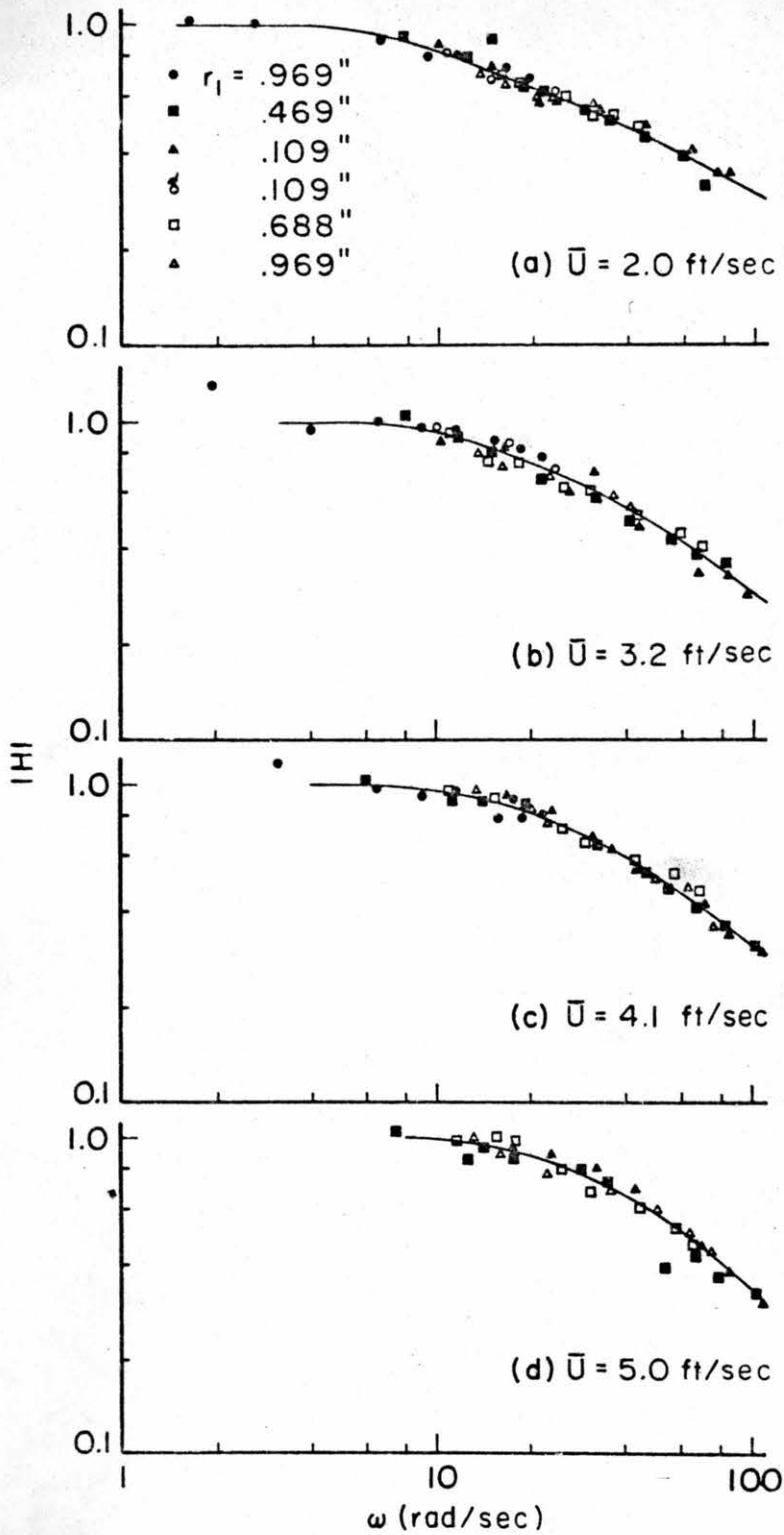


Fig. 14. Absolute value of the system function $|H(\omega)|$ as a function of angular frequency ω , 1 propeller.

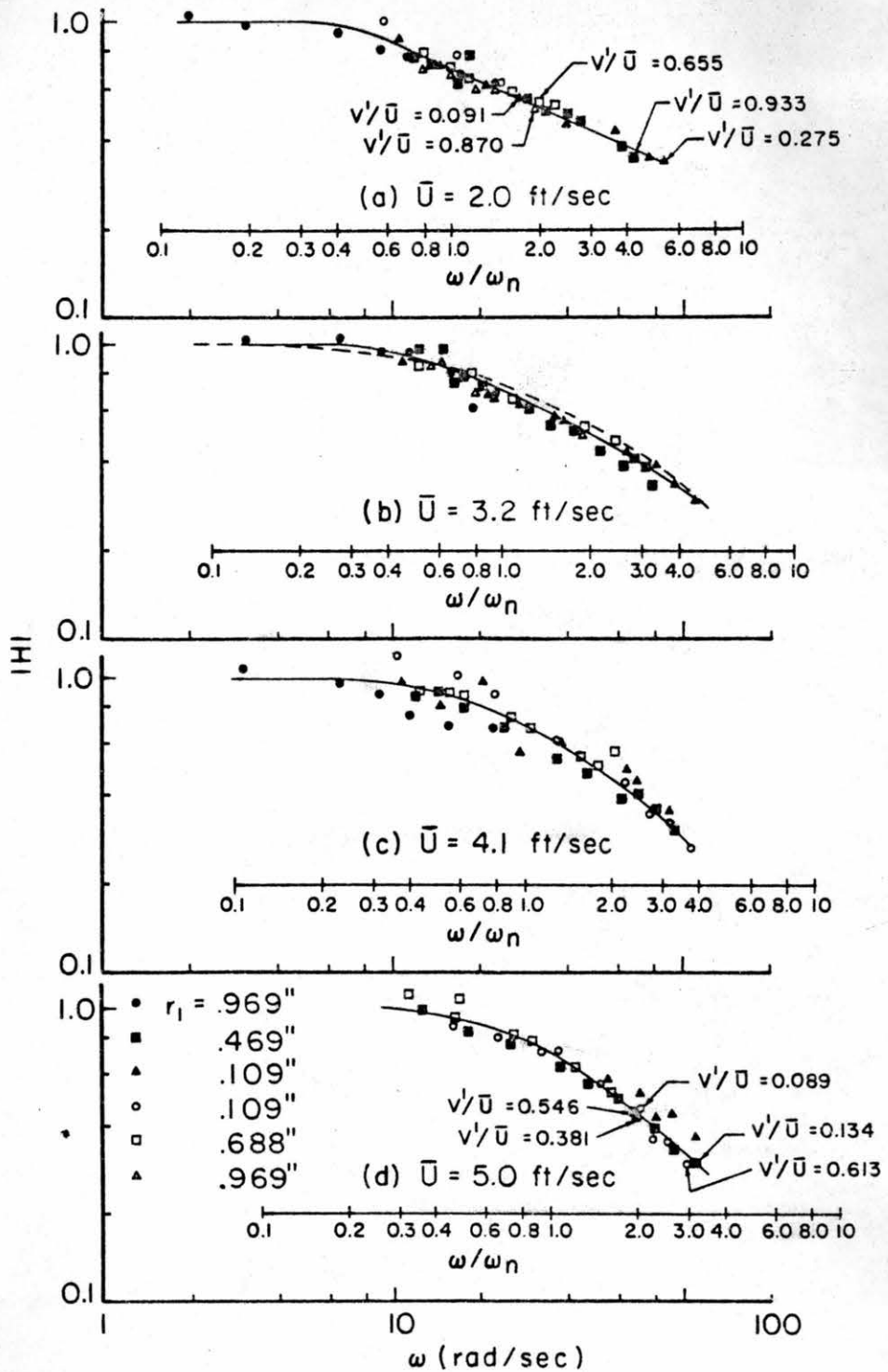


Fig. 15. Absolute value of the system function $|H(\omega)|$ as a function of angular frequency ω , 1-3 propeller.

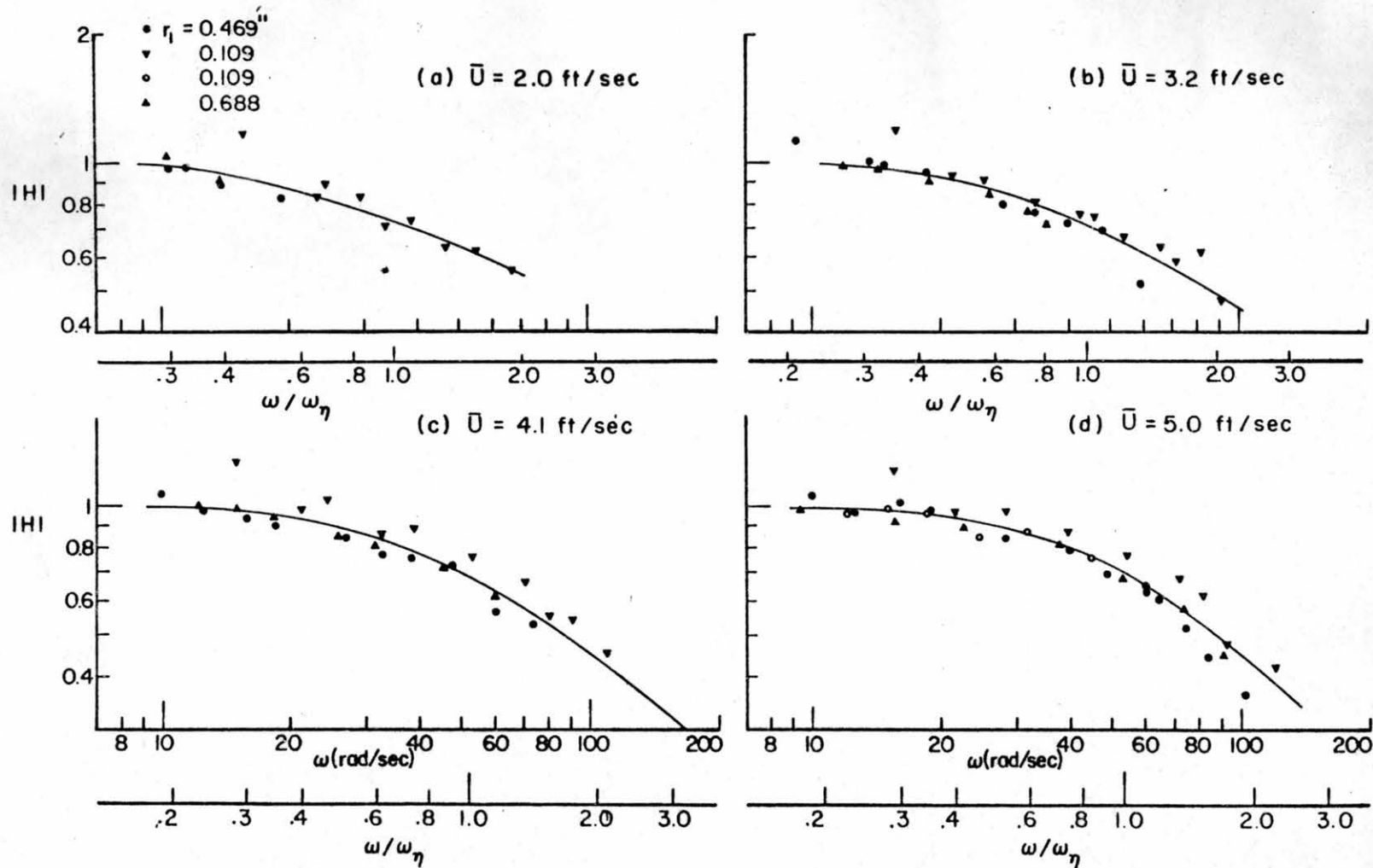


Fig. 16. Absolute value of the system function $|H(\omega)|$ as a function of angular frequency ω , 2-3 propeller.

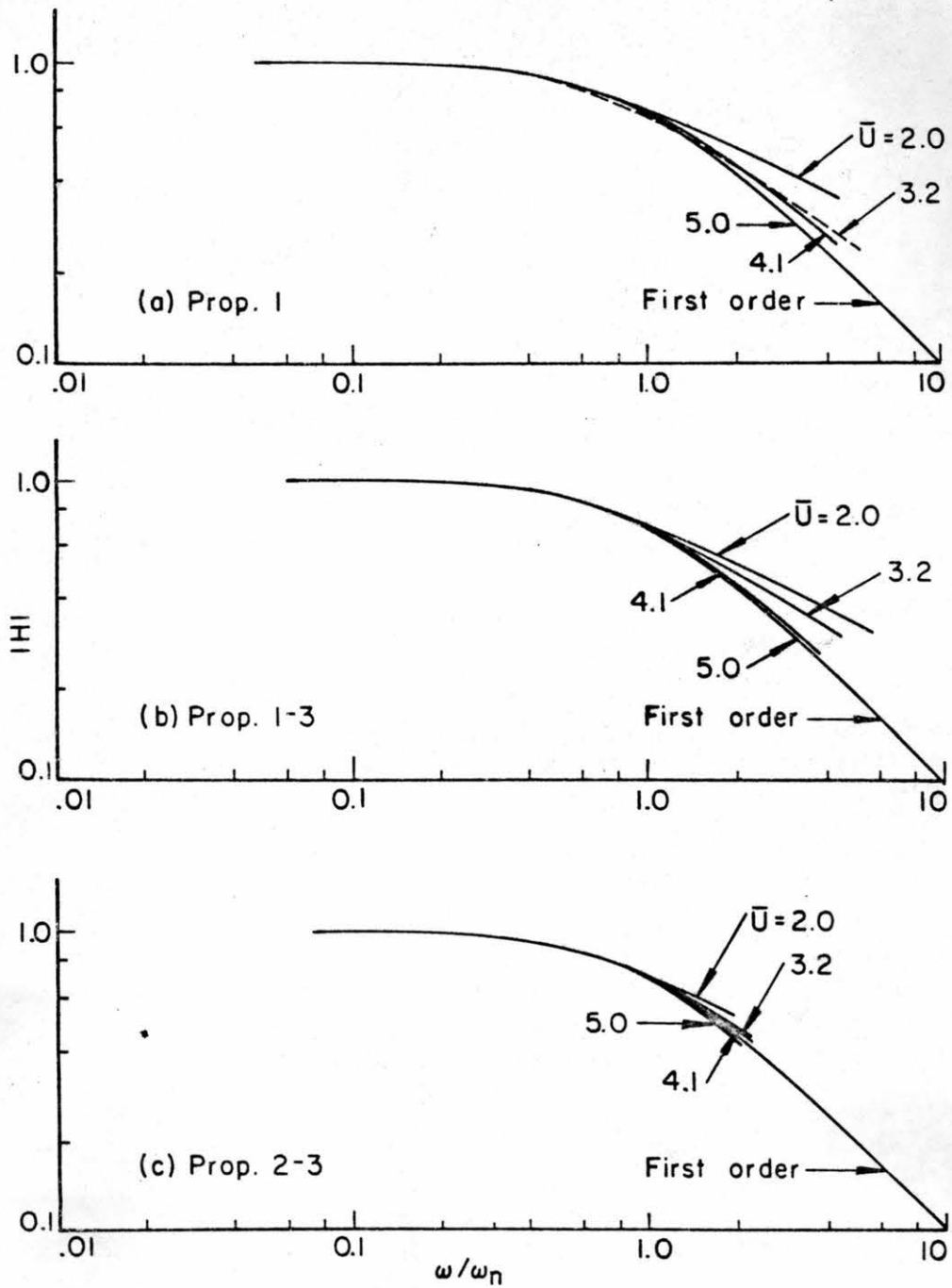


Fig. 17. Absolute value of the system function $|H(\omega)|$ as a function of frequency ratio ω/ω_n , all propellers.

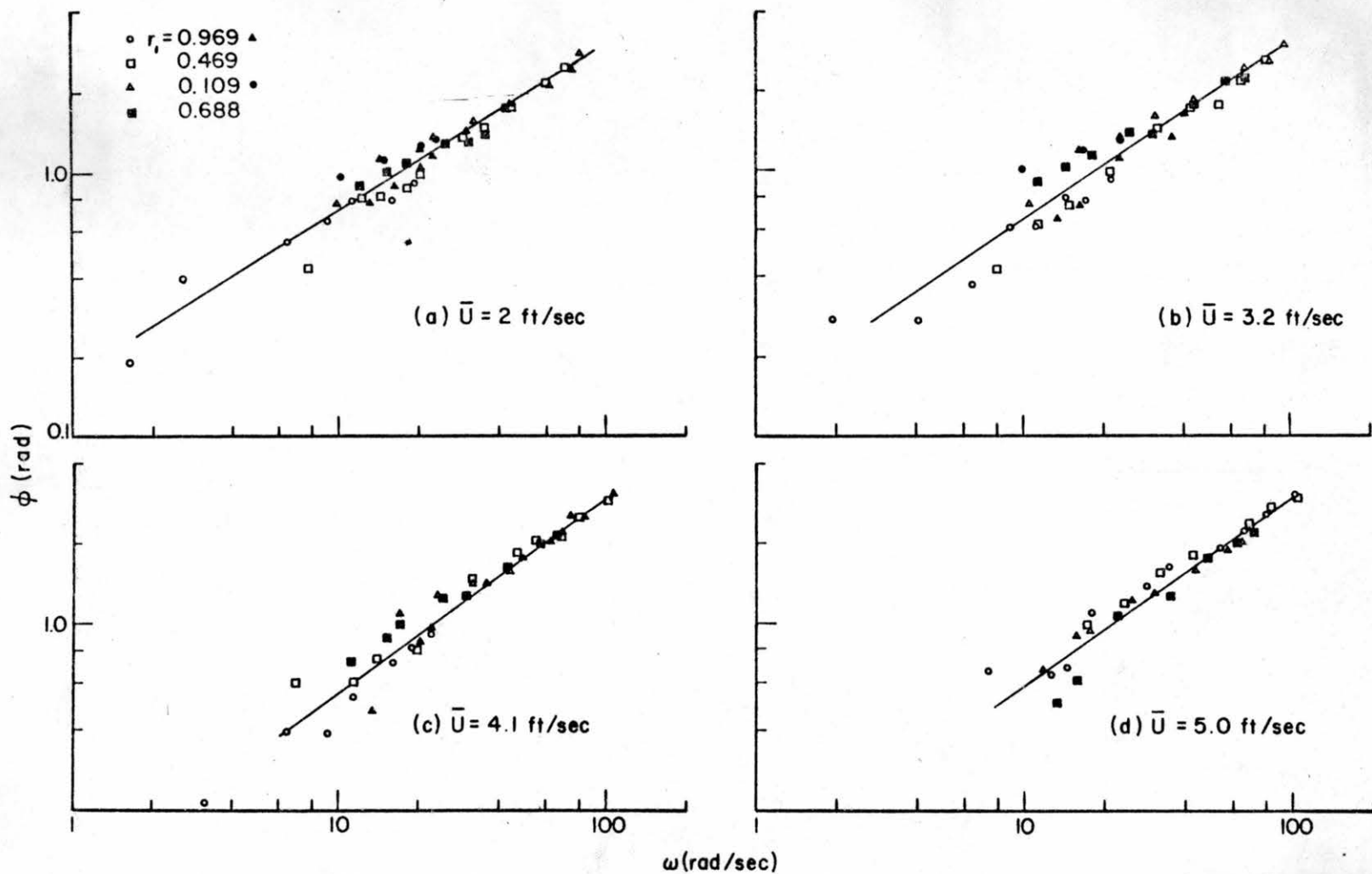


Fig. 18. Phase shift ϕ as a function of angular frequency ω , 1 propeller.

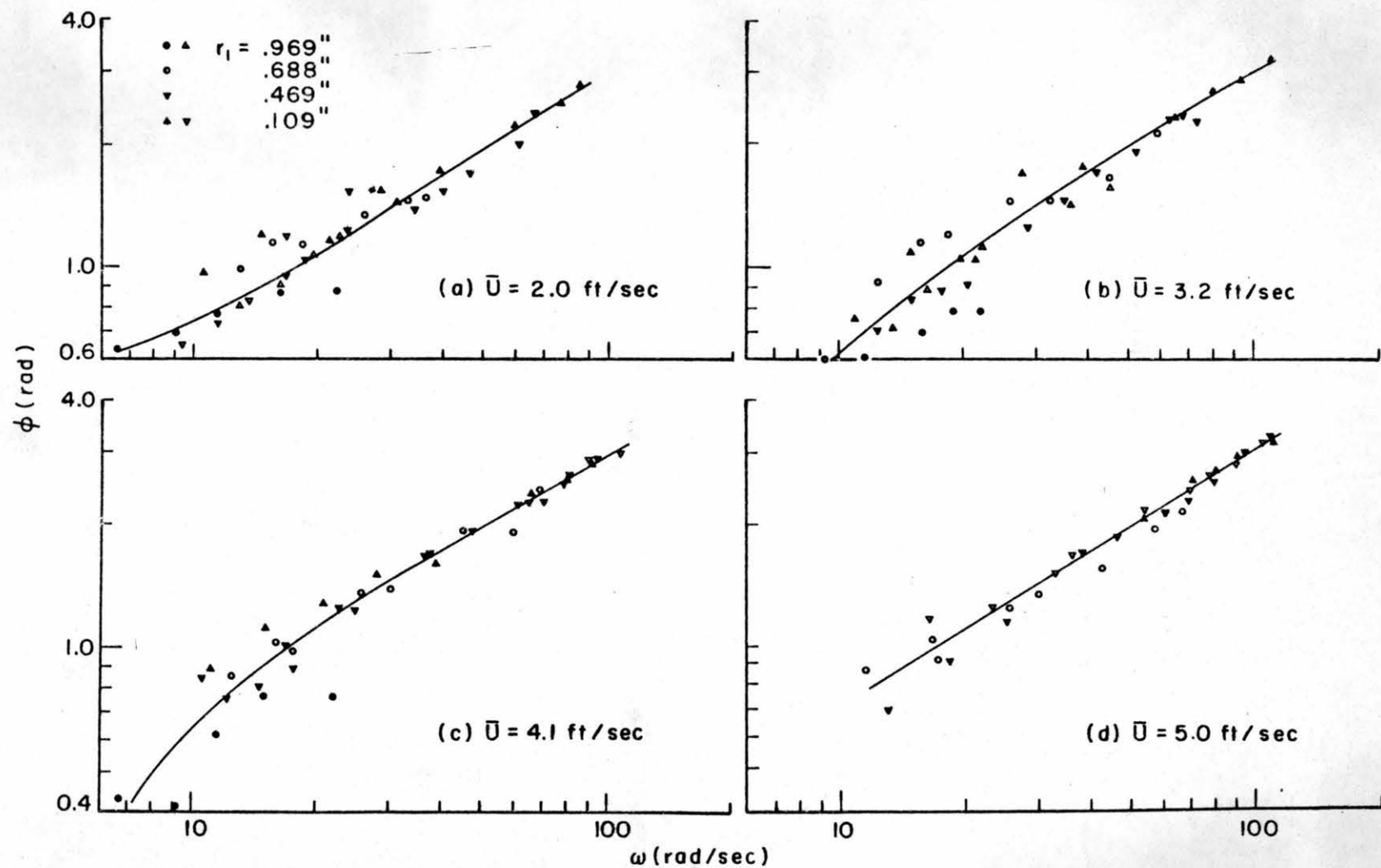


Fig. 19. Phase shift ϕ as a function of angular frequency ω , 1-3 propeller.

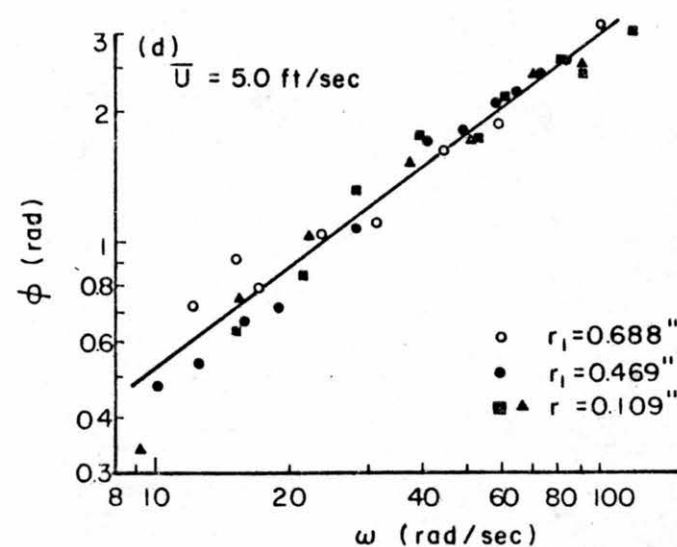
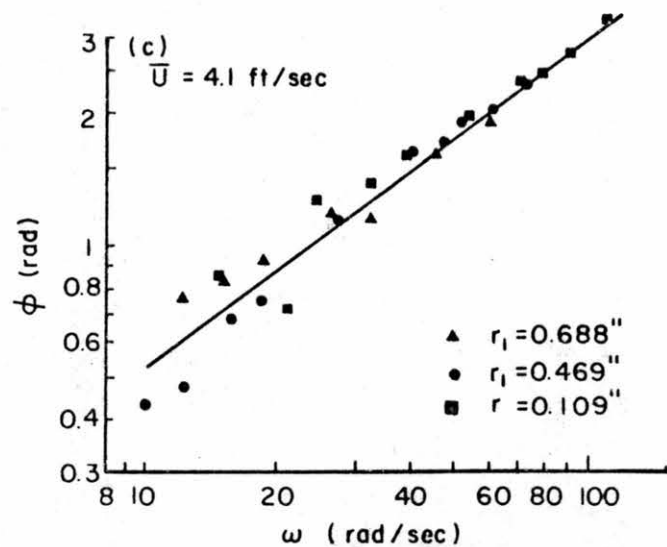
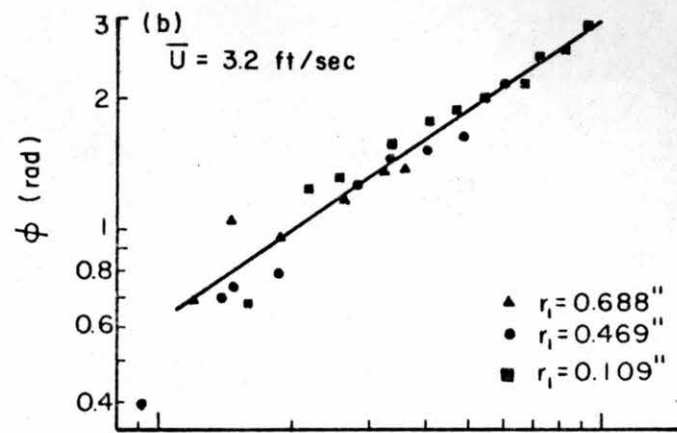
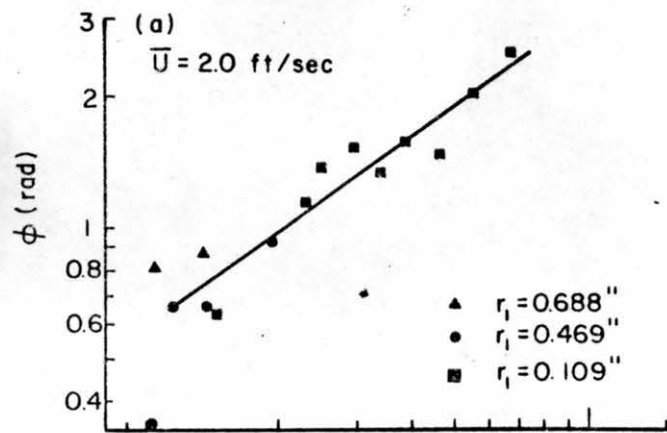


Fig. 20. Phase shift ϕ as a function of angular frequency ω , 2-3 propeller.

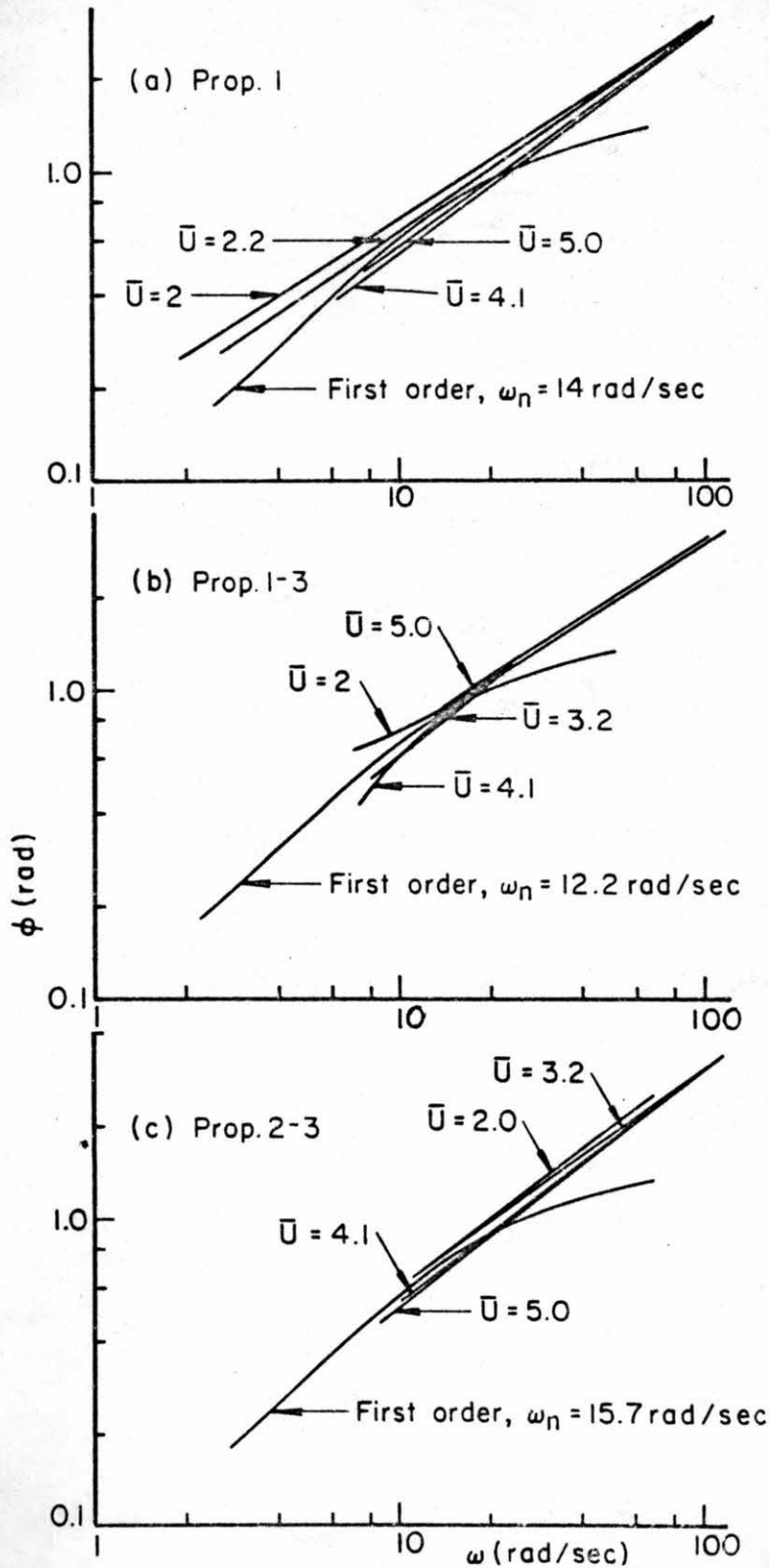


Fig. 21. Phase shift ϕ as a function of angular frequency ω , all propellers.

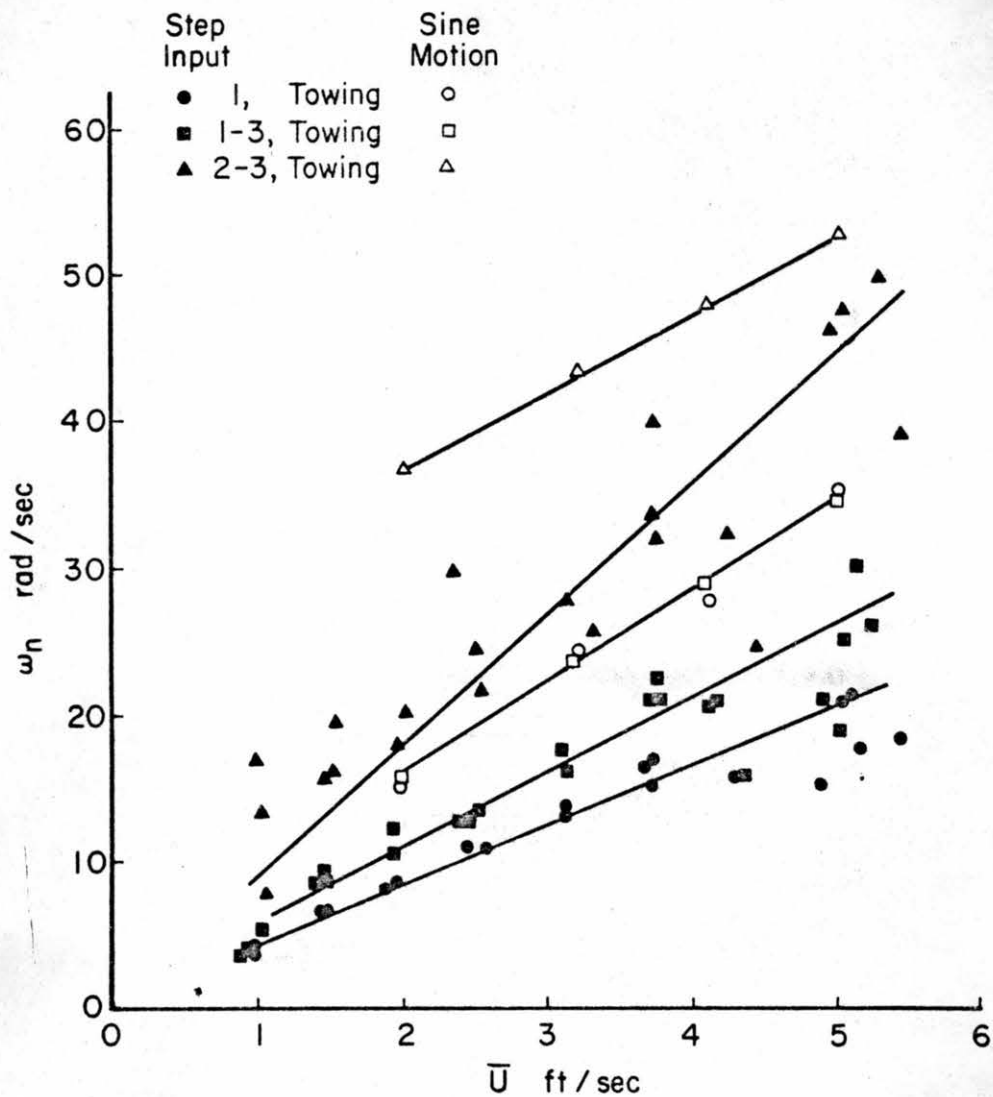


Fig. 22. Natural frequency ω_n as a function of mean velocity \bar{U} .

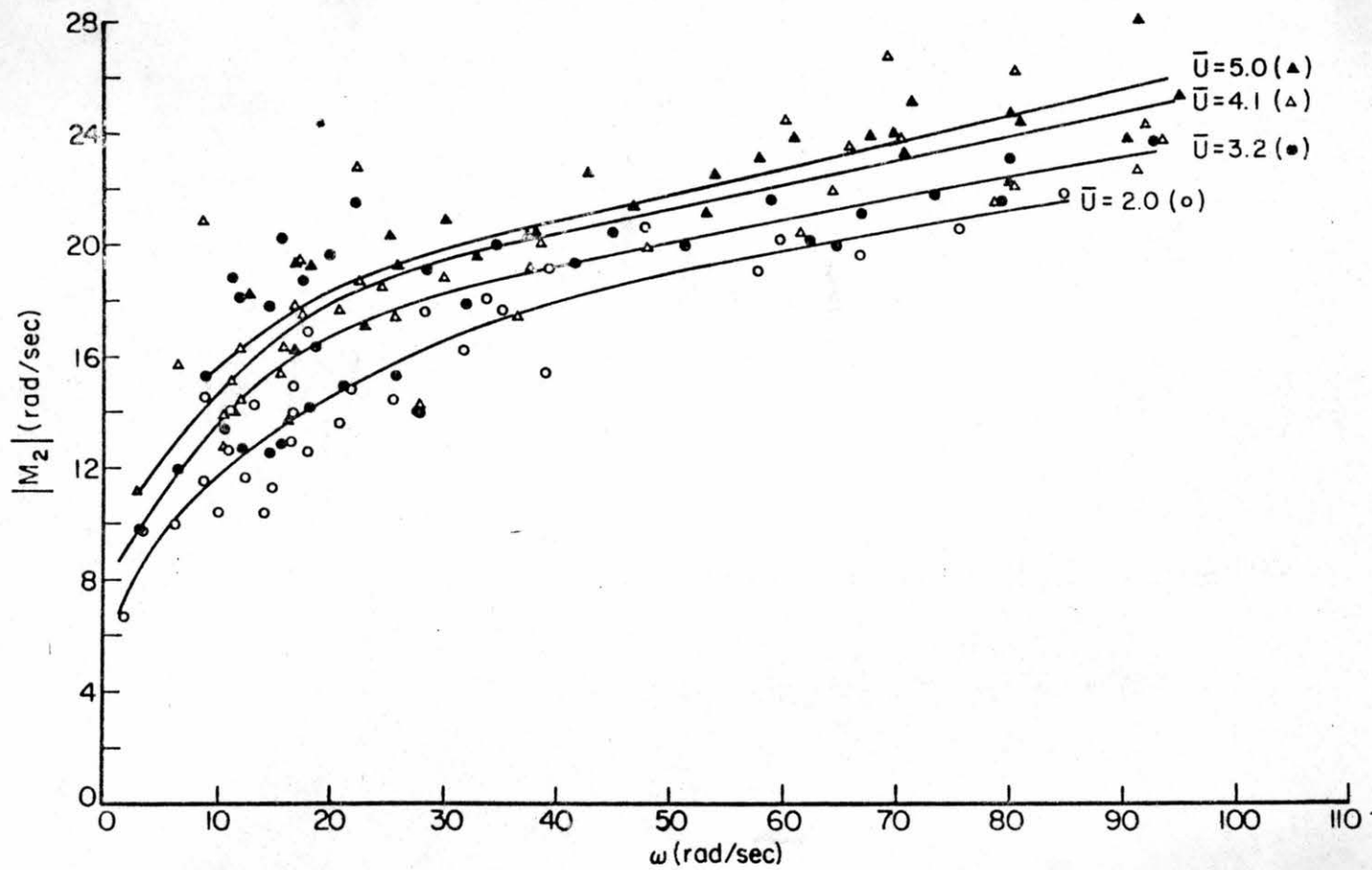


Fig. 23. $|M_2|$ as a function of angular frequency ω .

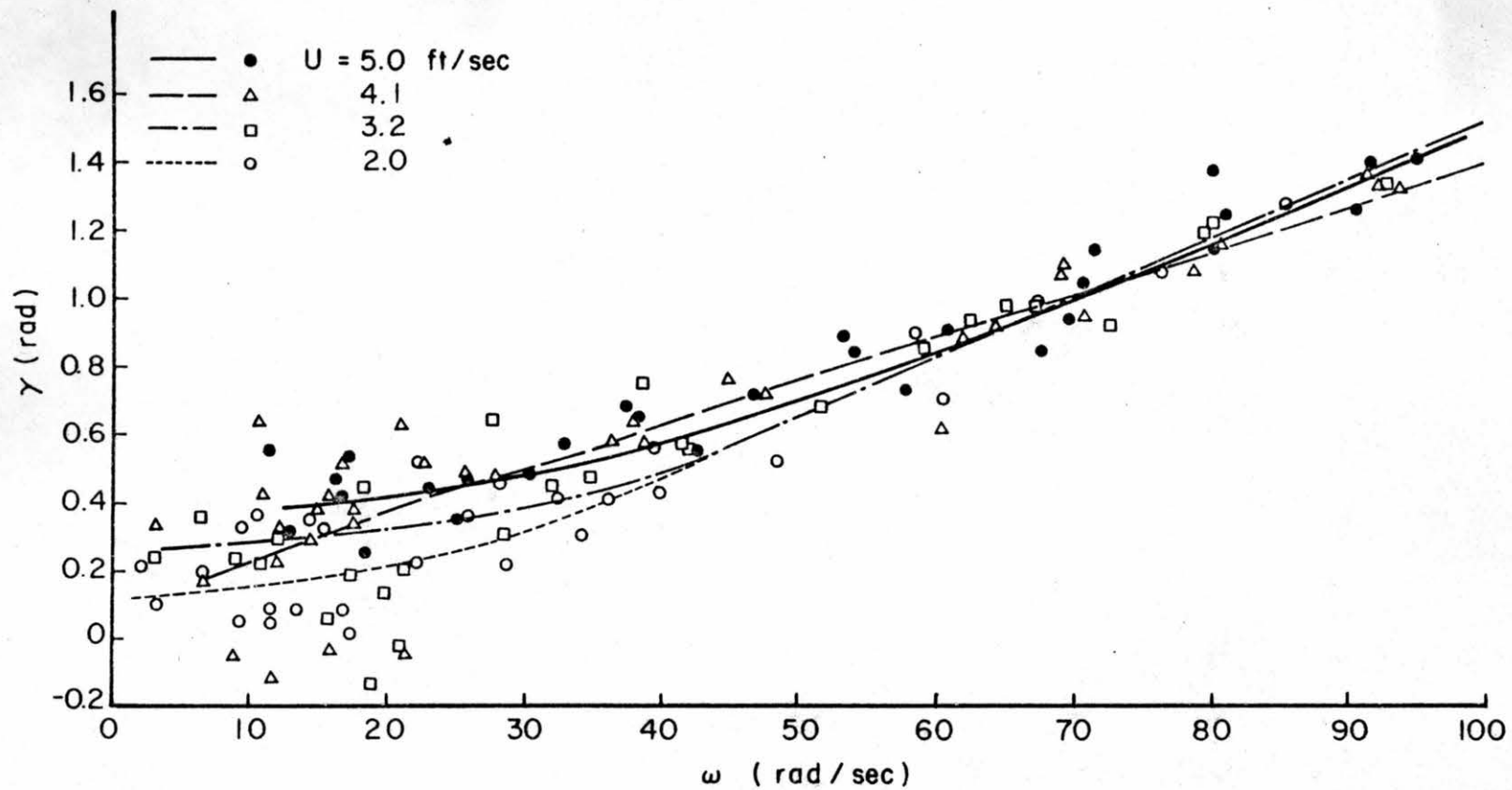


Fig. 24. Phase shift of the complex natural frequency γ as a function of angular frequency ω , 1-3 propeller.

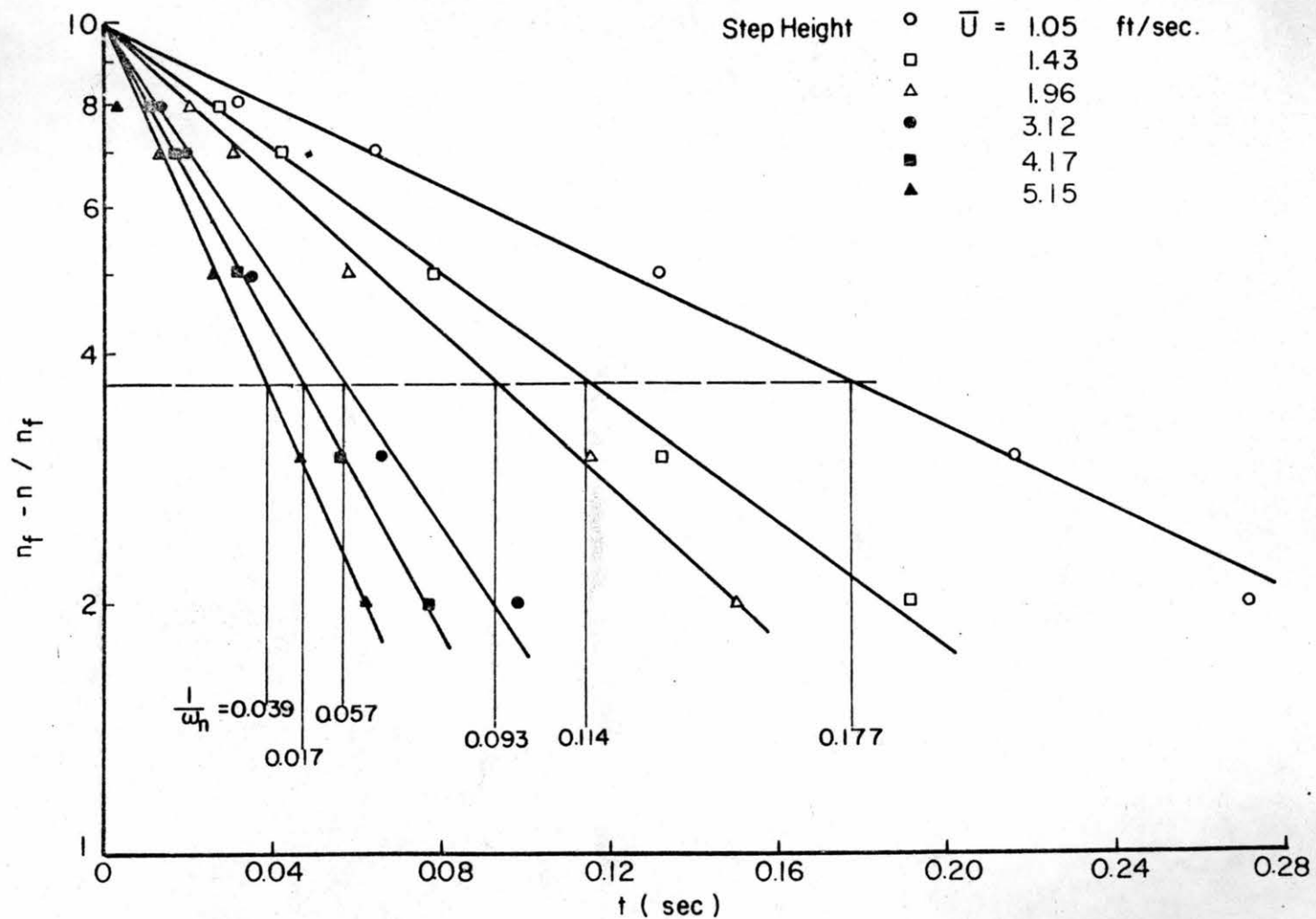


Fig. 25. Response of the propeller-flow system to a step input.

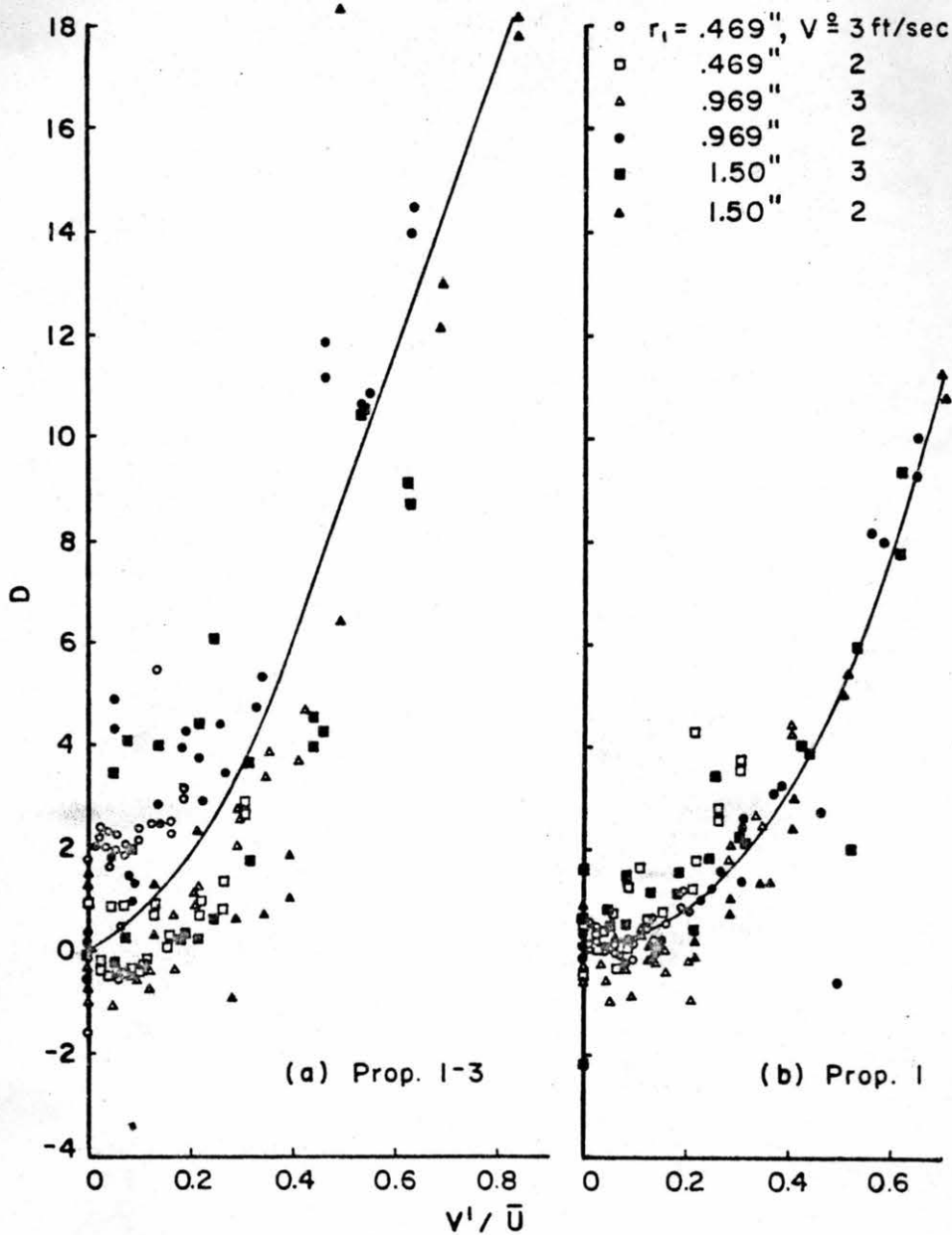


Fig. 26. D the output velocity percent deviation from true mean velocity as a function of the relative intensity v'/\bar{U} .

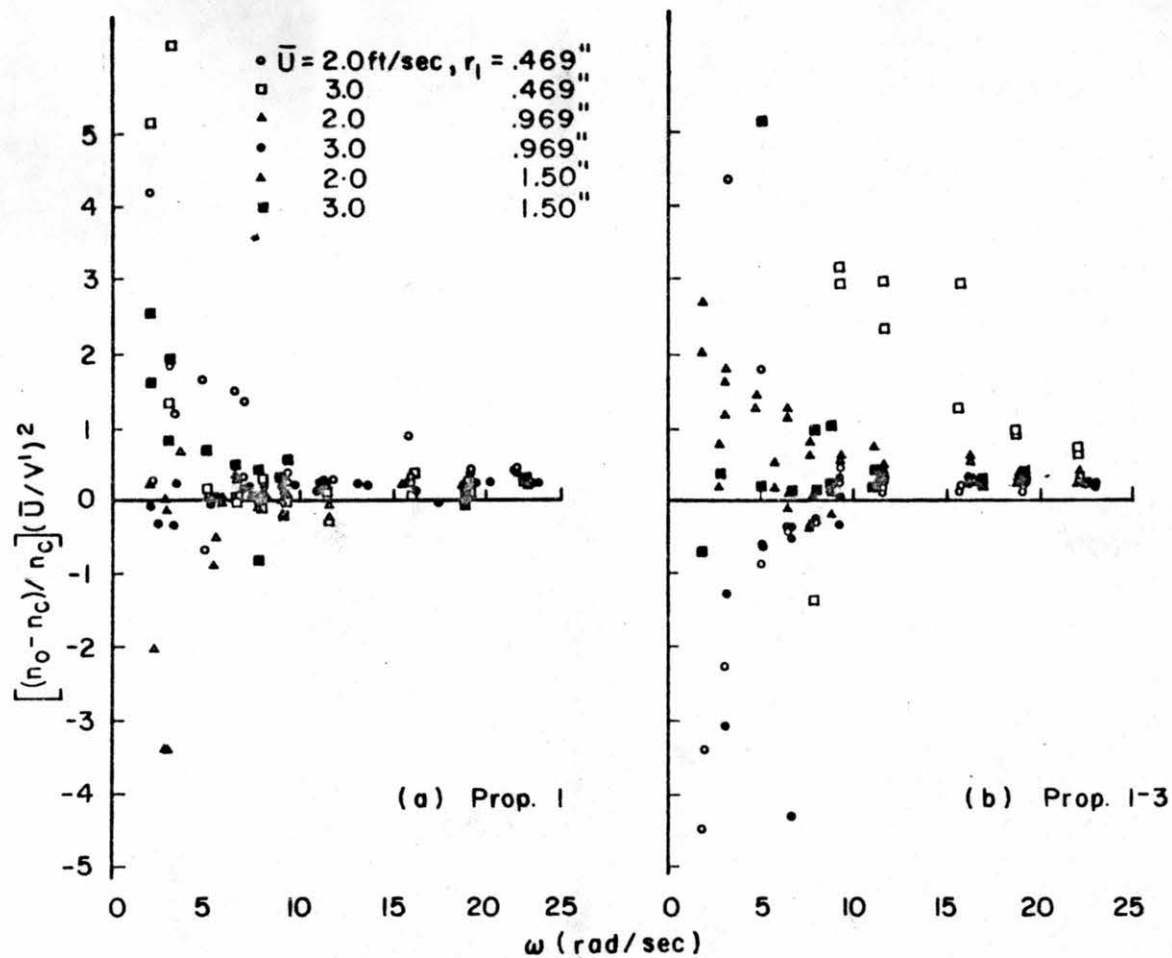


Fig. 27. Mean velocity misregistration function $g(\omega) = (\bar{U}/v')^2 (n_0 - n_c)/n_c$ as a function of angular frequency ω .

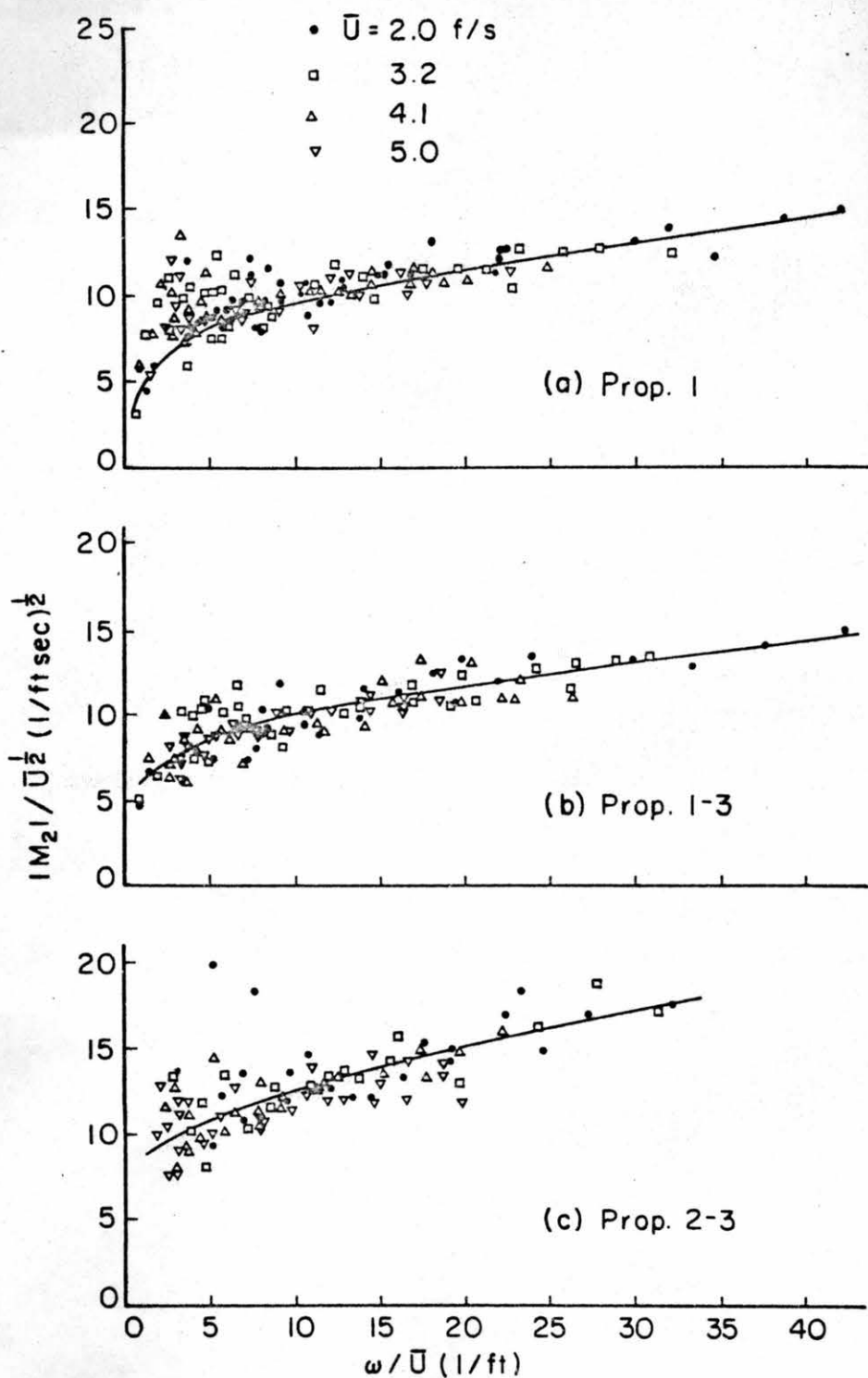


Fig. 28. Generalized magnitude function $|M_2|/\bar{U}^{1/2}$ as a function of ω/\bar{U} .

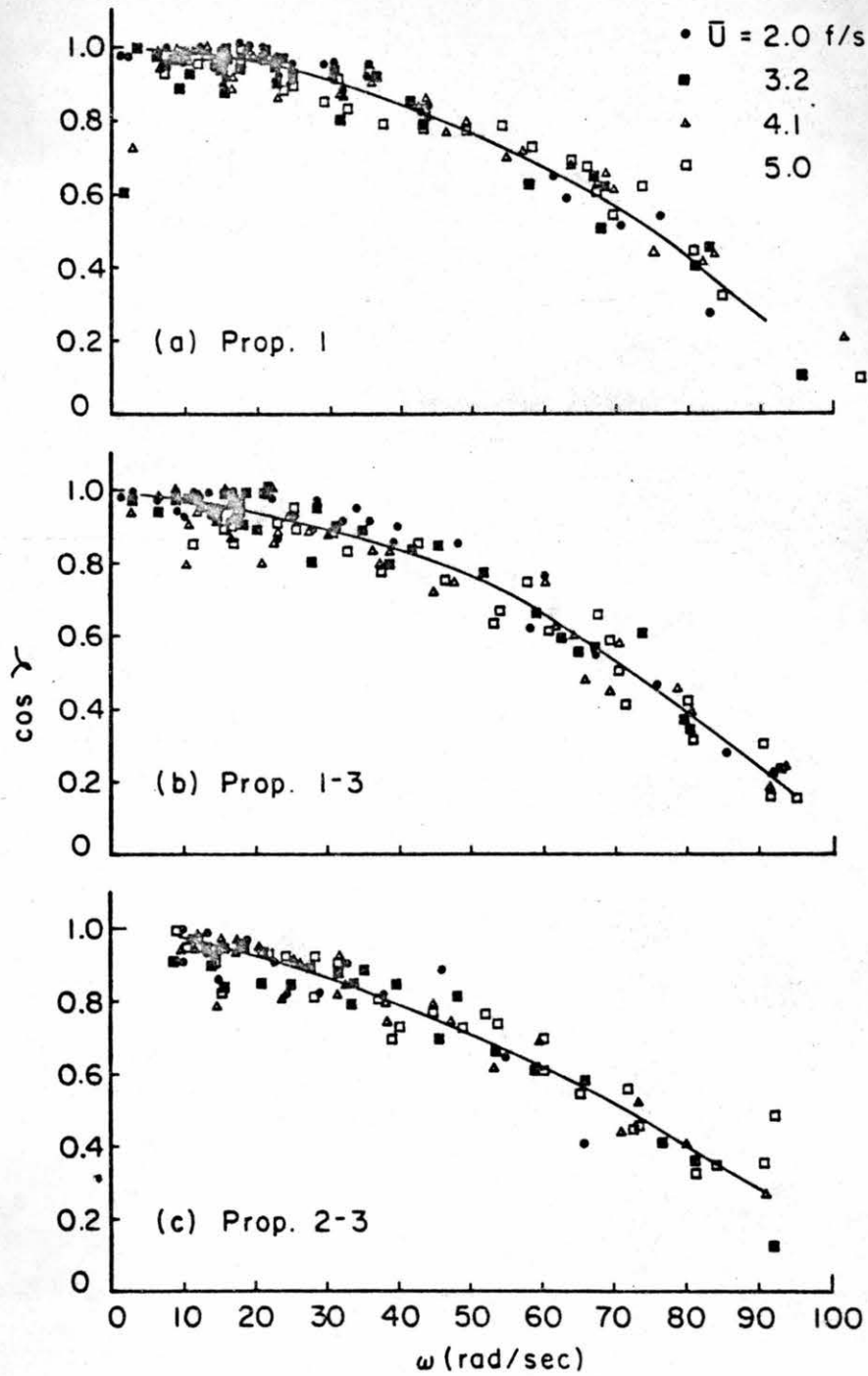


Fig. 29. Generalized phase function $\cos \gamma$ as a function of angular frequency ω .

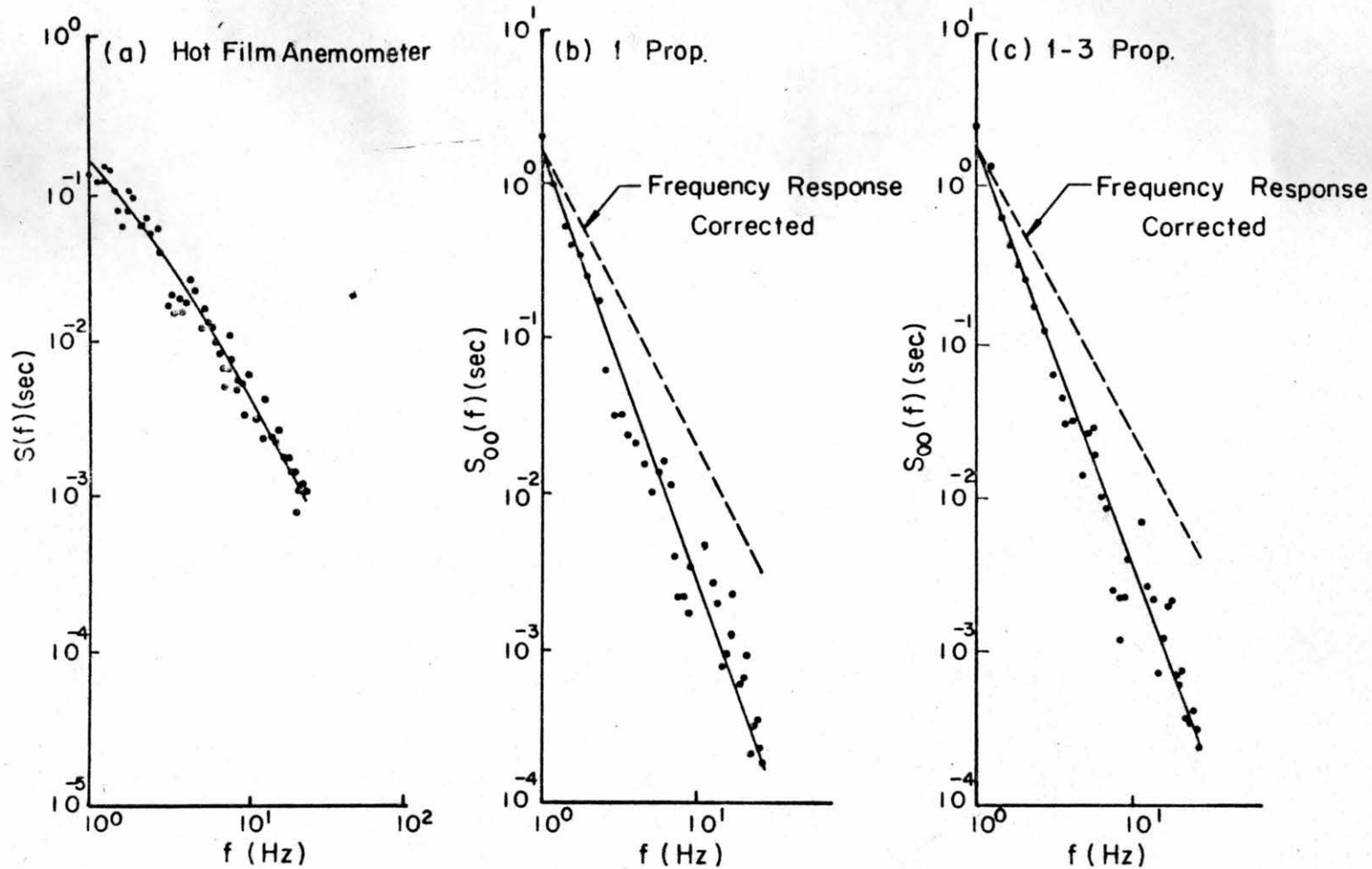


Fig. 30. Power spectral densities $S(f)$ and $S_{\infty}(f)$ as functions of frequency f , run 12.

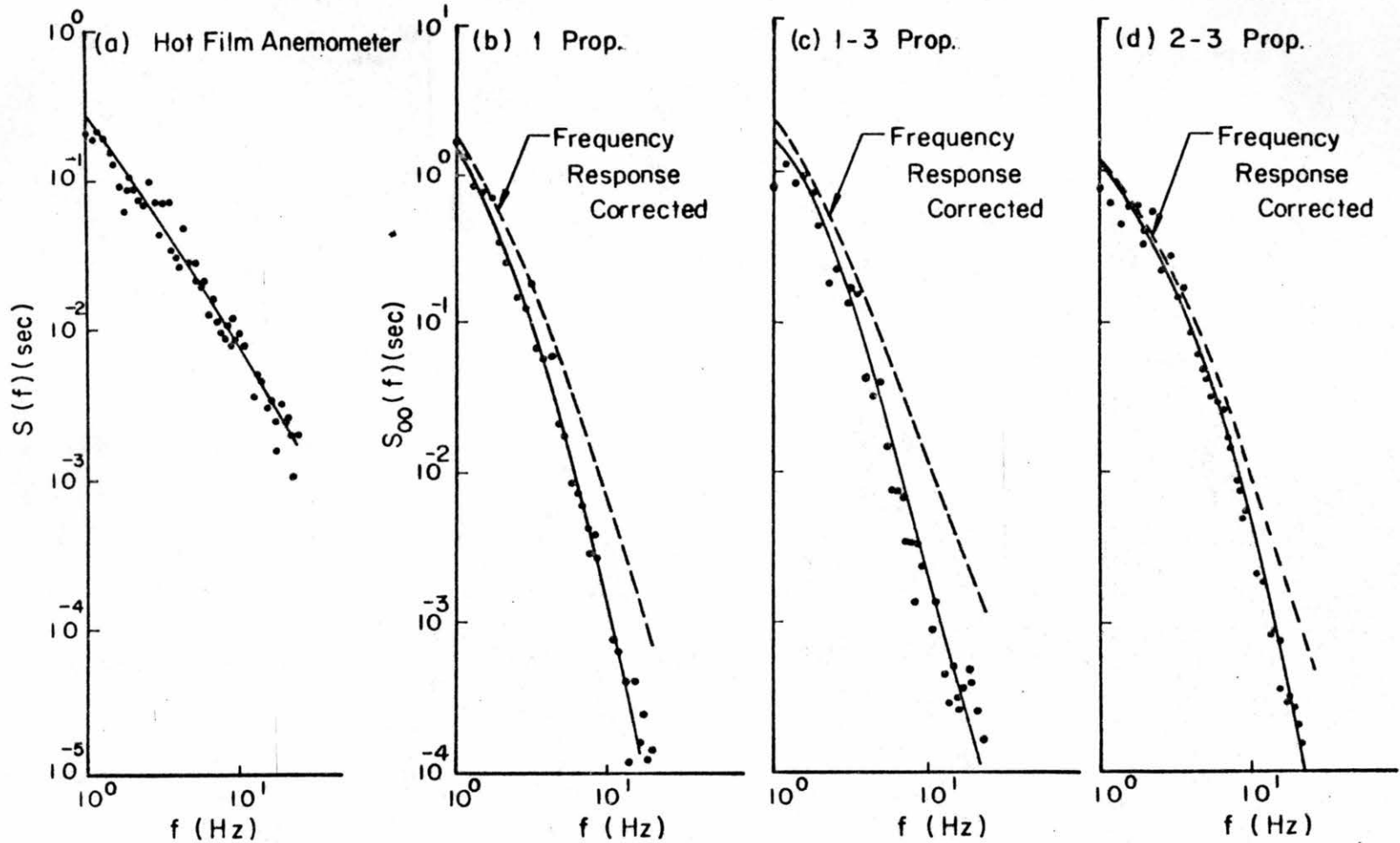


Fig. 31. Power spectral densities $S(f)$ and $S_{oo}(f)$ as functions of frequency f , run 16.

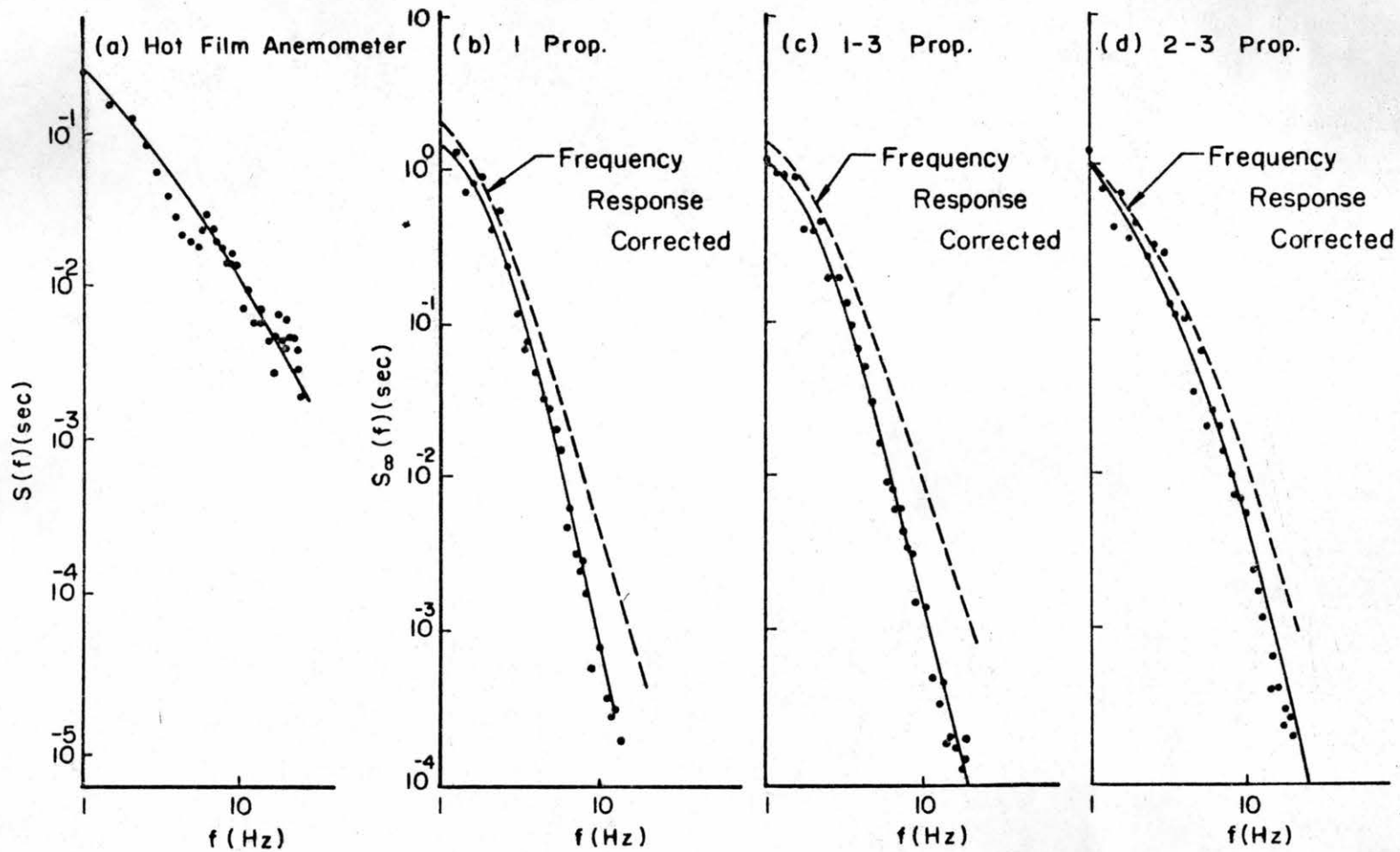


Fig. 32. Power spectral densities $S(f)$ and $S_{\infty}(f)$ as functions of frequency f , run 17.

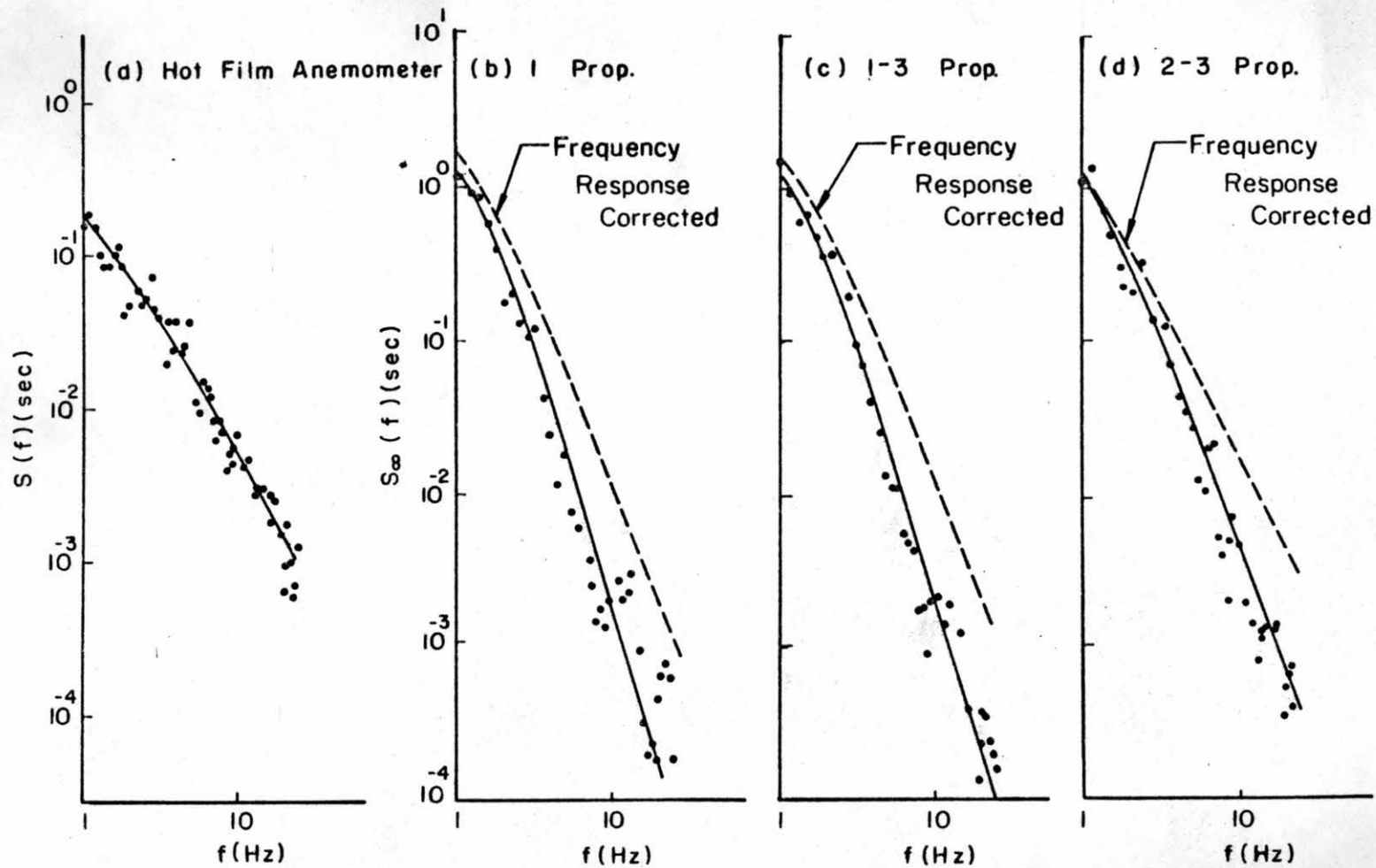


Fig. 33. Power spectral densities $S(f)$ and $S_{\infty}(f)$ as functions of frequency f , run 18.

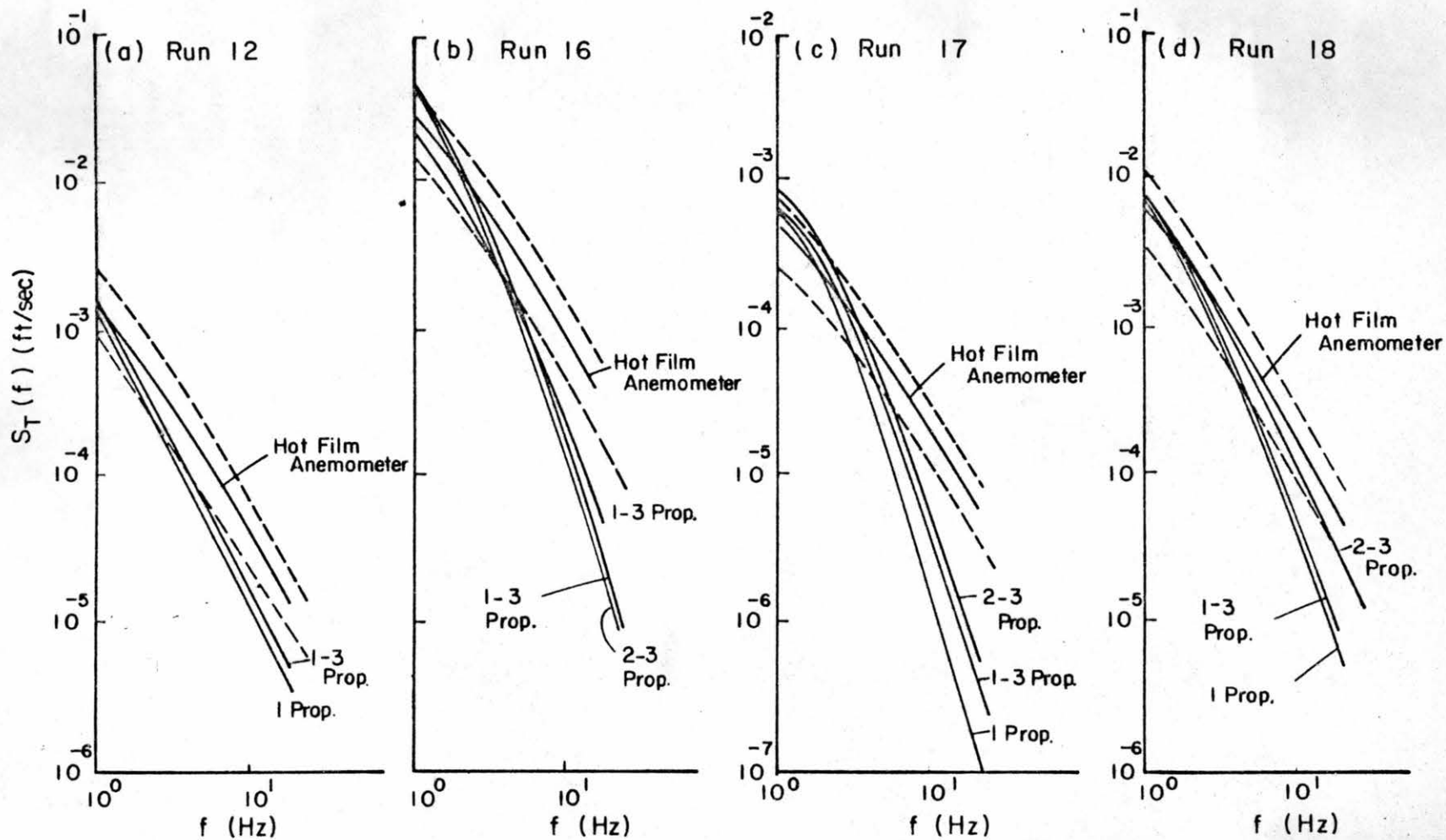


Fig. 34. Frequency response corrected power spectral densities $S_T(f)$ as functions of frequency f .

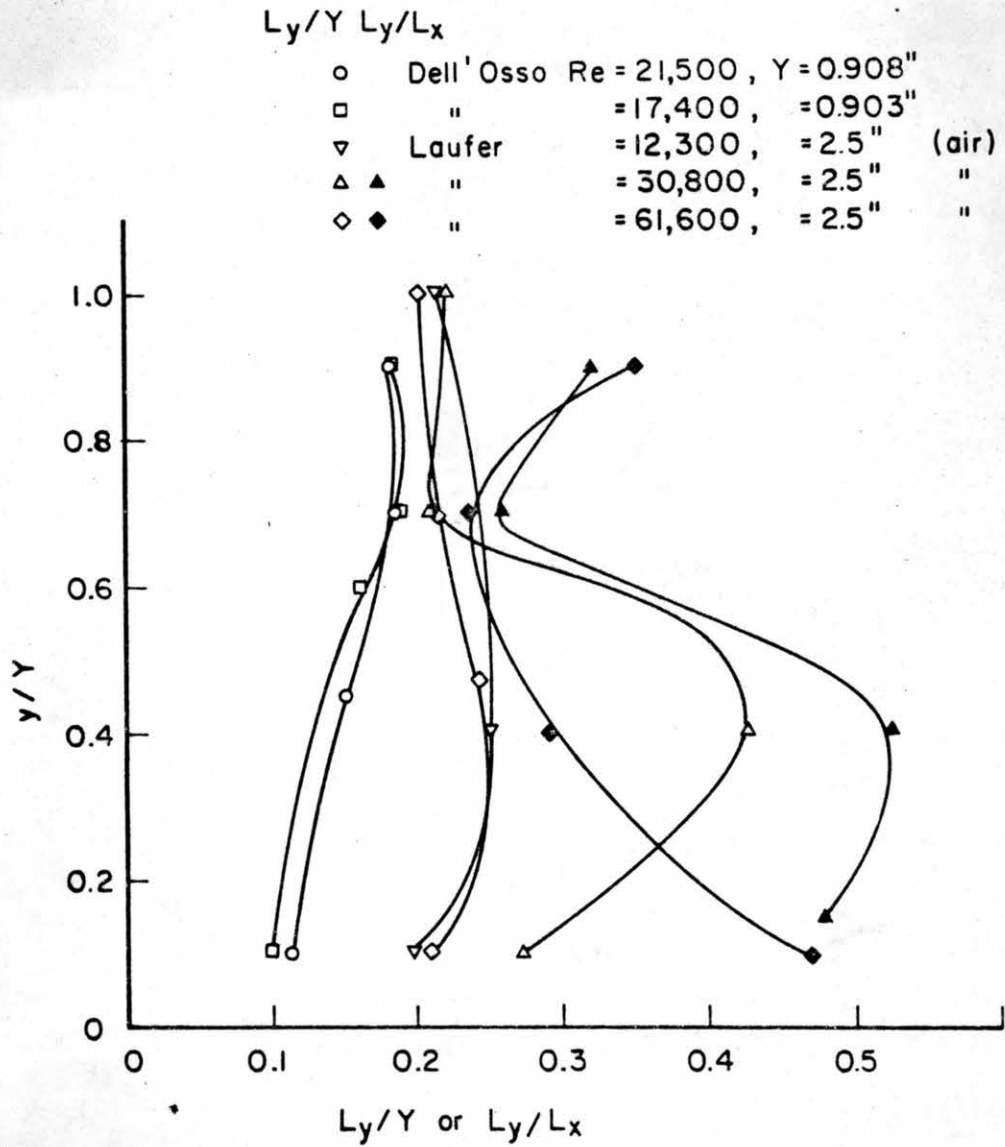


Fig. 35. Lateral scale ratio L_y/Y and eddy shape factor L_y/L_x as functions of relative depth y/Y .

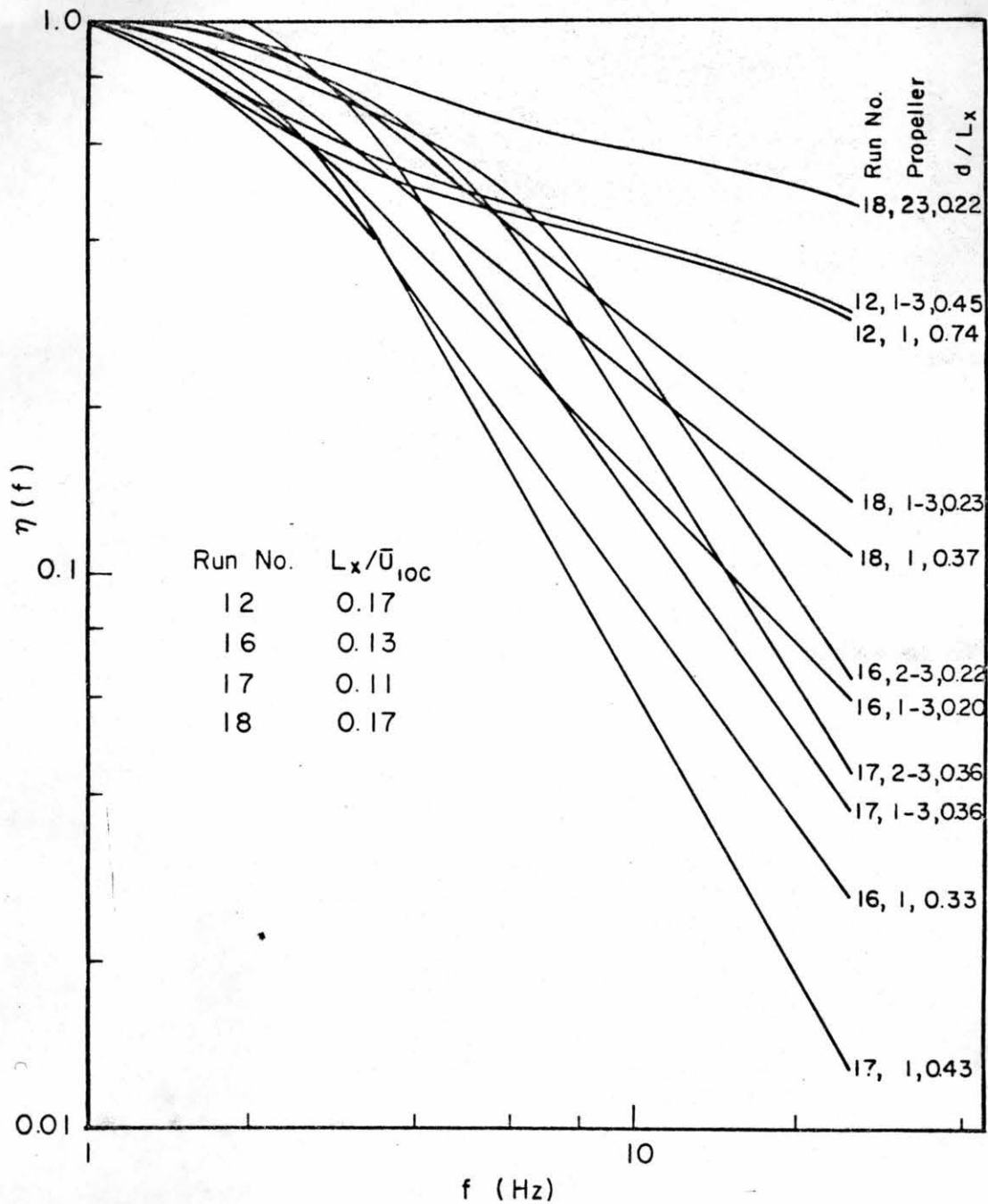


Fig. 36. Spectral recovery efficiency $\eta(f)$ as a function of frequency f .

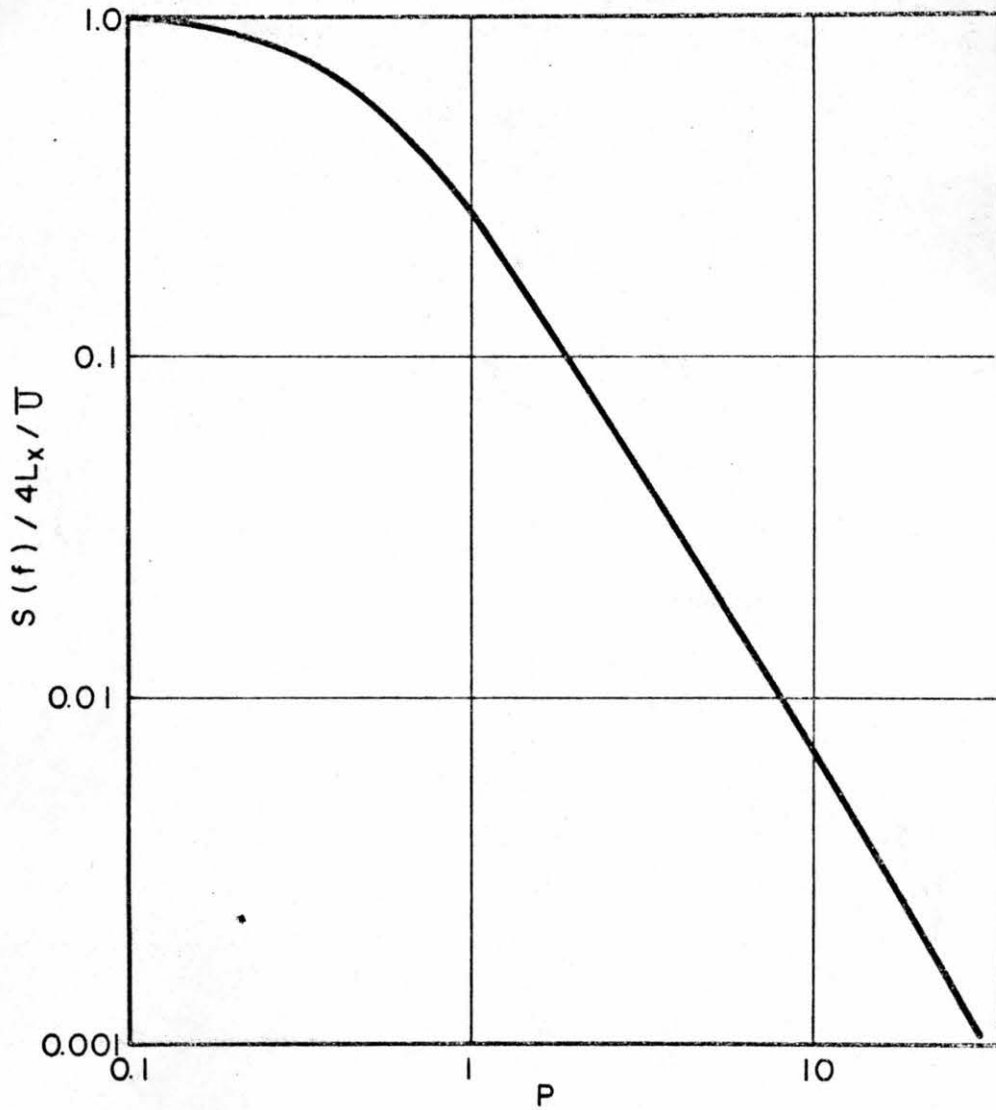


Fig. 37. Generalized empirical power spectral density $S(f)/(4L_x/\bar{U}_{loc})$ as a function of non-dimensionalized frequency P .

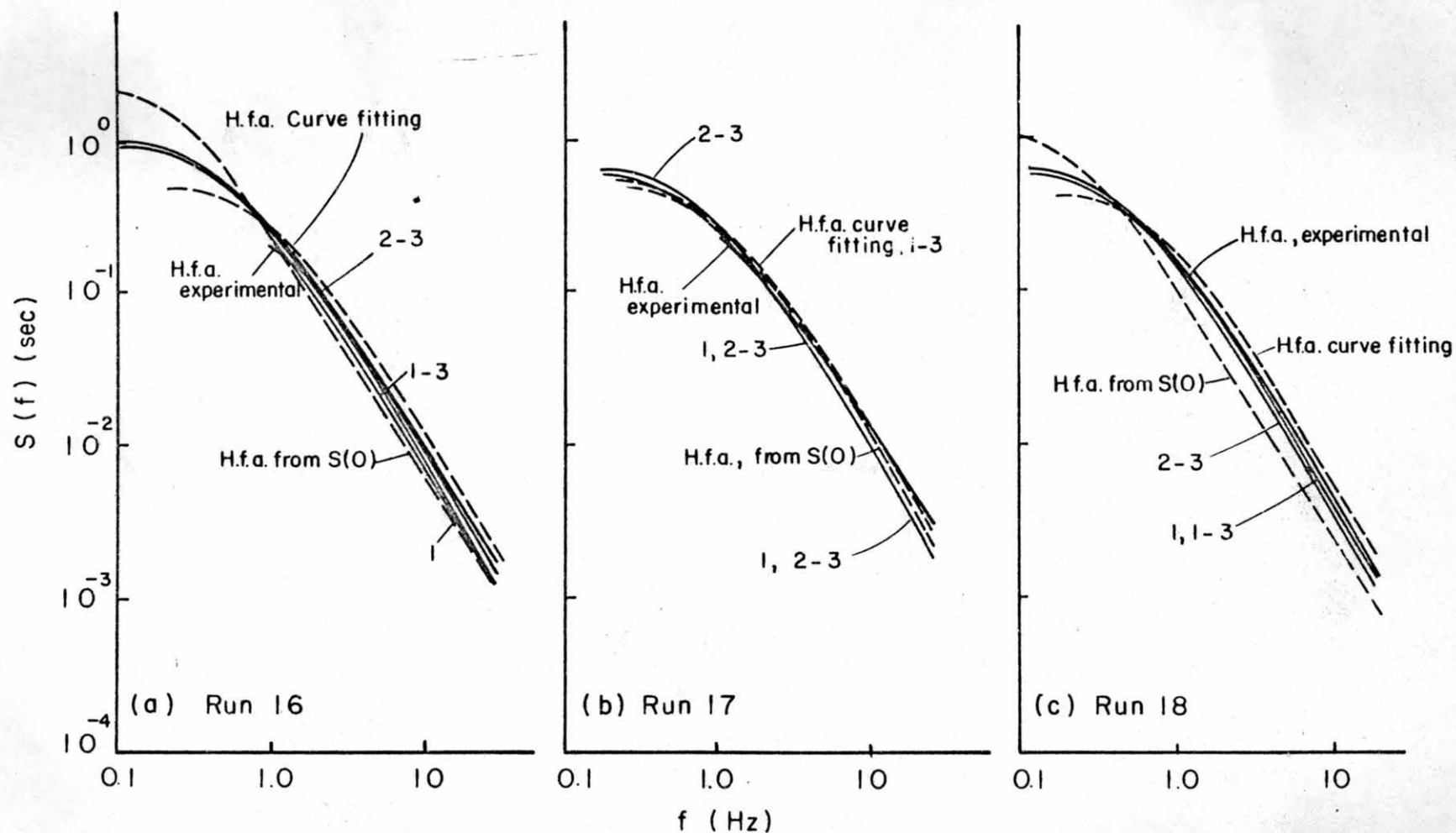


Fig. 38. Comparison of empirical power spectral densities with experimental power spectral densities.

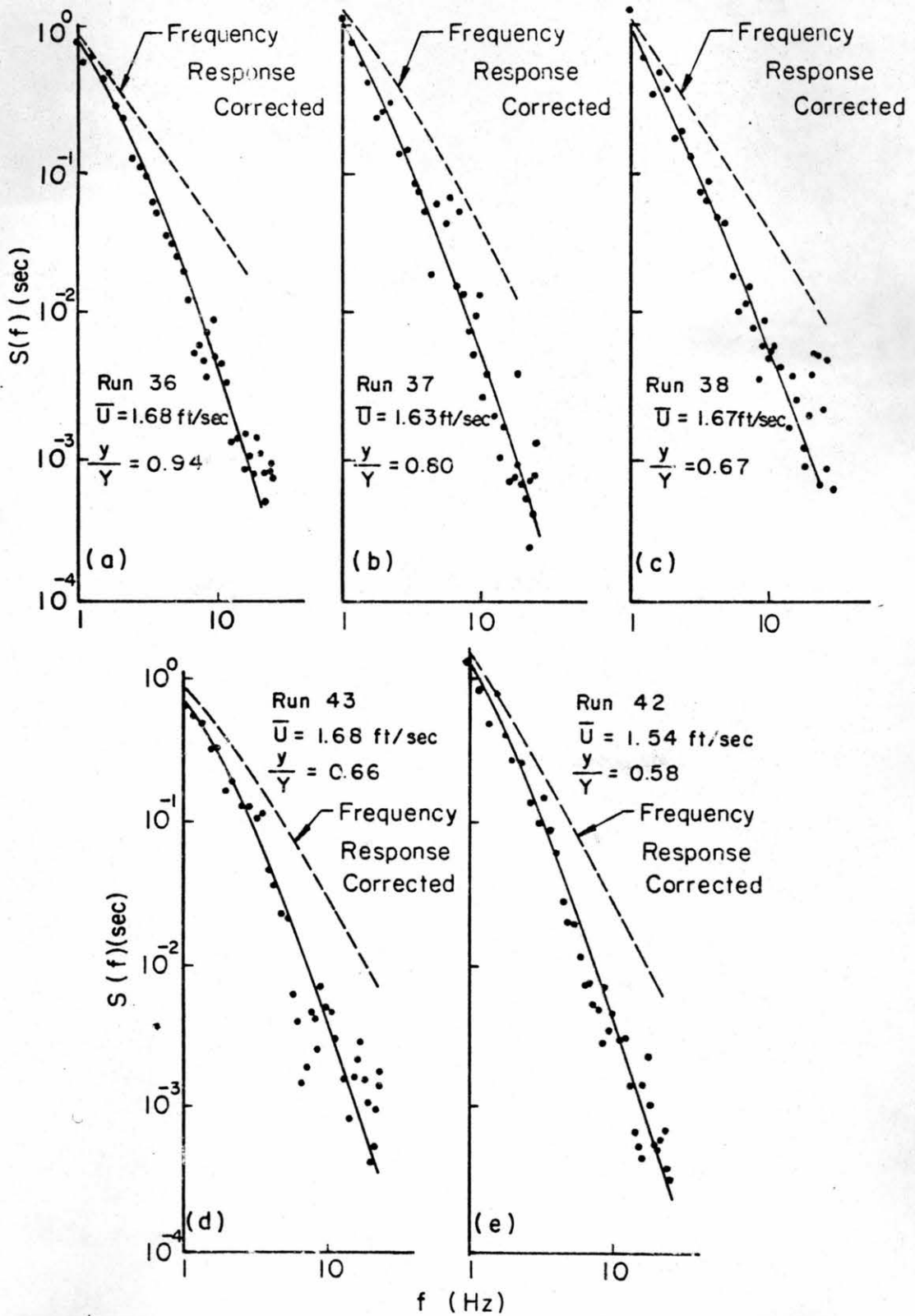


Fig. 39. Propeller output and frequency response corrected power spectral densities $S(f)$ as functions of frequency f , field measurements.

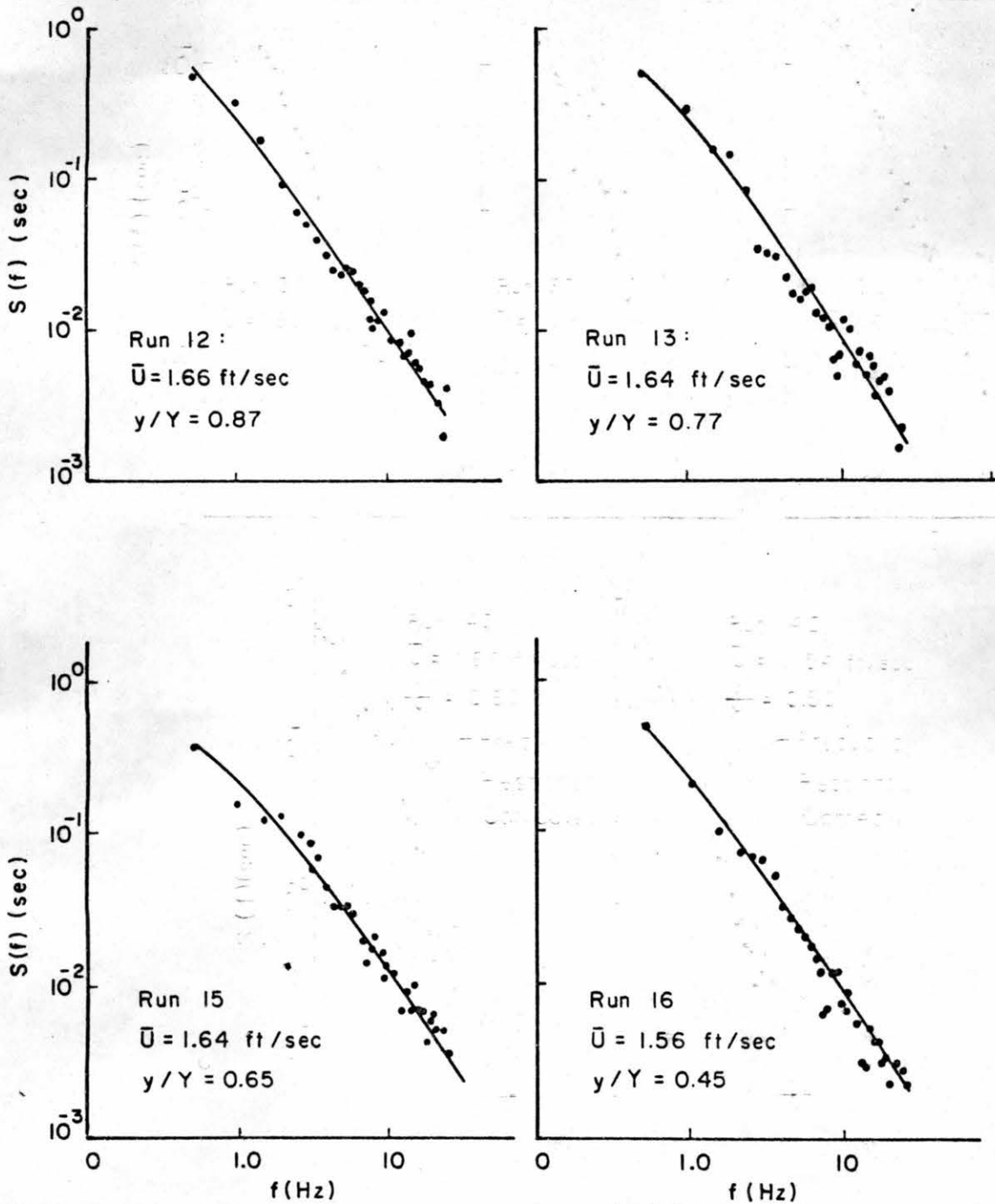


Fig. 40. Hot-film anemometer velocity power spectral densities $S(f)$ as functions of frequency f , field measurements.

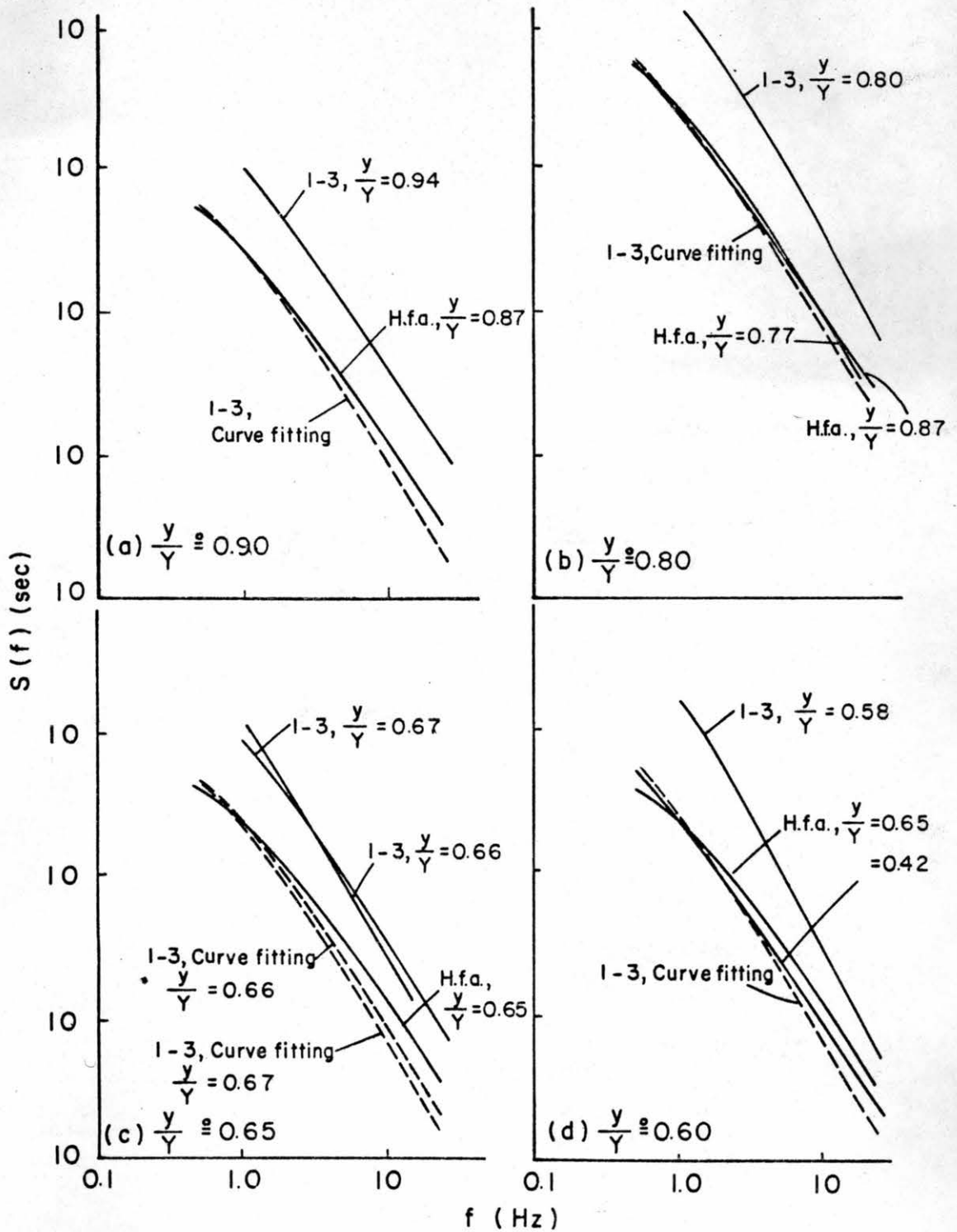


Fig. 41. Comparison of normalized power spectral densities, field measurements.

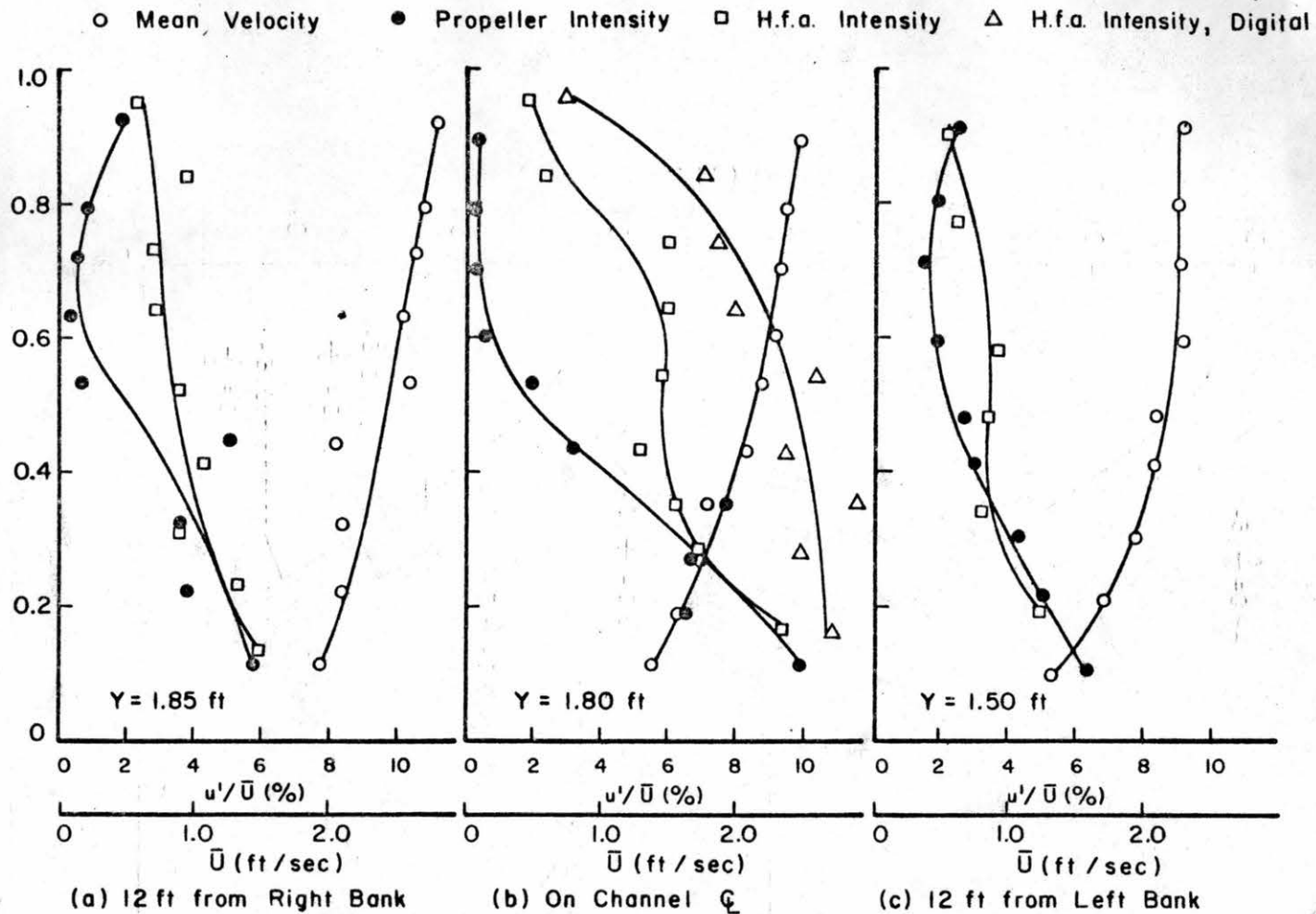


Fig. 42. Mean velocity \bar{U} and turbulent intensity \bar{u}'/\bar{U} as functions of relative depth y/Y , Atrisco runs.

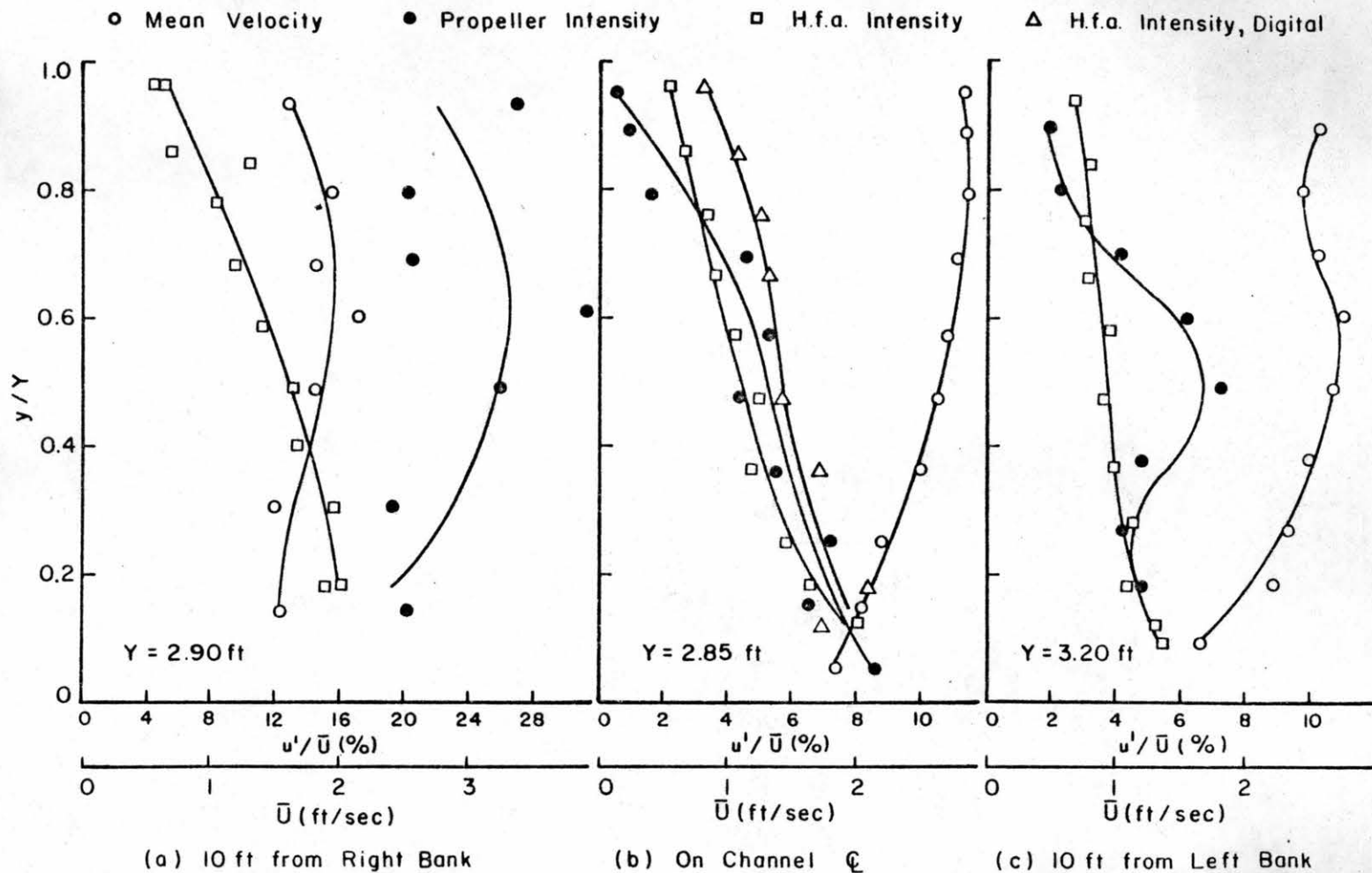


Fig. 43. Mean velocity \bar{U} and turbulent intensity \bar{u}'/\bar{U} as functions of relative depth y/Y , Bernardo runs.